Technische Universität München

Fakultät für Medizin

Lehrstuhl für Stoffwechselerkrankungen

Dietary interventions in C57BL/6 mice and their interplay with selected metabolic and genetic parameters

Ingrid Petra Kapser-Fischer

Vollständiger Abdruck der von der Fakultät für Medizin der Technischen Universität München zur Erlangung des akademischen Grades eines

Doktors der Naturwissenschaften (Dr. rer. nat.)

genehmigten Dissertation.

Vorsitzender: Prof. Dr. Radu Roland Rad

Prüfer der Dissertation: 1. Prof. Dr. Dr. h.c. Matthias H. Tschöp

2. Prof. Dr. Martin Klingenspor

Die Dissertation wurde am 08.10.2018 bei der Technischen Universität München eingereicht und durch die Fakultät für Medizin am 08.10.2019 angenommen.

Für Mama.

Abstract

Within the last three decades, the prevalence of obesity has doubled and the numbers of associated co-morbidities such as type 2 diabetes and non-alcoholic fatty liver disease have also risen. To study the etiology of obesity and novel pharmaceutical interventions for the cure of obesity, diet-induced obese mouse models are the preferred choice for many researchers worldwide. Yet, study protocols for the induction of diet-induced obesity (DIO) in mice vary with respect to numerous factors, which all affect the outcome of these studies themselves. Therefore, results of different DIO studies are often neither comparable, nor reproducible. For this thesis, it was examined how variations in the experimental design of DIO experiments, such as differences in strain and gender of the mice used as well as differences in feeding durations and dietary fat content of the (high fat) diets affect the phenotypical heterogeneity of C57BL/6 mice. In doing so, certain key parameters such as body weight and fat mass gain, as well as the development of hyperglycemia, glucose intolerance and hyperinsulinemia were compared. Undergoing a low-calorie diet is the most popular, non-invasive way to loose weight. Yet, the underlying molecular mechanisms following a diet-induced weight loss have not been fully understood. This thesis presents detailed transcriptional analyses of the molecular alterations in liver and adipose tissue of mice with a history of obesity. Briefly, male C57BL/6J mice with DIO underwent a switch from a high-fat diet to a low-fat diet *ad libitum* and displayed a "normalized" metabolic phenotype, comparable to age-matched never-obese mice, 7 weeks after the diet-switch. Yet, at this time point, signs of hepatosteatosis and fibrosis, together with increased pro-inflammatory gene expressions, were present in liver tissues of formerly obese mice. This was paralleled by depot-specific adipocyte hypertrophy and macrophage infiltration in the perigonadal adipose tissue of formerly obese mice. Microarray analyses of the perigonadal adipose tissue of formerly obese mice further revealed up-regulation of numerous, partly inflammatory genes and pathways. One of these up-regulated genes in perigonadal and brown adipose tissue (BAT) of obese and formerly obese mice was the Activating Transcription Factor 3 (ATF3). Thus, by creating an UCP1-specific conditional knockout of ATF3 in BAT of mice, the impact of BAT-derived ATF3 on the development of DIO was analyzed. Here, the conditional knockout of ATF3 in male and female mice displayed no significant impact on the susceptibility to DIO, regarding the onset of body weight and fat mass gain, glucose intolerance and hyperinsulinemia. Still, a hypertrophy of adipocytes in BAT and subcutaneous white adipose tissue from diet-induced obese $Atf3^{fl/fl}$;$Ucp1^{cre+}$ mice was identified, contributing first insights into the role of ATF3 in BAT. In summary, this thesis contributes to novel understandings on how different dietary interventions impact the pathogenesis and reversibility of DIO in mice and presents metabolic and genetic alterations due to a history of DIO. Moreover, the presented results indicate that the presence of ATF3 in brown adipocytes does not play a role for the development of DIO in mice.

Zusammenfassung

Innerhalb der letzten drei Jahrzehnte hat sich die Prävalenz von Adipositas verdoppelt und die Fallzahlen von assoziierten Begleiterkrankungen wie Typ 2 Diabetes mellitus und nichtalkoholischer Fettleber sind ebenso gestiegen. Um die Krankheitsursachen von Adipositas und neue pharmazeutische Interventionen zur Heilung von Adipositas zu erforschen, sind diätinduzierte adipöse Mausmodelle die bevorzugte Wahl für viele Wissenschaftler weltweit. Jedoch variieren Studienprotokolle für die Entstehung von diätinduzierter Adipositas (DIA) in Mäusen hinsichtlich zahlreicher Faktoren, die jeweils selbst Auswirkungen auf die Ergebnisse der Studien haben. Deshalb sind Ergebnisse verschiedener DIA-Studien oft weder vergleichbar noch reproduzierbar. Für diese Arbeit wurde untersucht wie Variationen in den Versuchsanordnungen von DIA Experimenten, wie beispielsweise Unterschiede im Stamm und Geschlecht der Mäuse sowie Unterschiede in der Fütterungsdauer und im Fettgehalt der (Hoch-) Fettdiäten, die phänotypische Heterogenität der C57BL/6 Mäuse beeinflussen. Dabei wurden Schlüsselparameter wie die Zunahme von Körpergewicht und Fettmasse sowie die Entstehung von Hyperglykämie, Glukoseintoleranz und Hyperinsulinämie verglichen. Sich einer kalorienarmen Diät unterziehen ist die populärste, nichtinvasive Methode um Gewicht zu verlieren. Die molekularen Mechanismen, die einer diätinduzierten Gewichtsabnahme zugrunde liegen, sind bisher nicht vollständig erfasst. Diese Arbeit präsentiert detaillierte Transkriptionsanalysen der molekularen Veränderungen in Leber und Fettgewebe von Mäusen mit einer Vorgeschichte von Adipositas. Mit wenigen Worten, diätinduziert-adipöse C57BL/6J Männchen wurden von einer Hochfettdiät auf eine Niederfettdiät *ad libitum* umgestellt und zeigten einen „normalisierten“ metabolischen Phänotyp, der vergleichbar war zu gleichaltrigen nie-ädipös gewesenen Mäusen, 7 Wochen nach der Diätumstellung. Dennoch waren zu diesem Zeitpunkt histologische Zeichen einer Fettleber und Fibrose zusammen mit erhöhten pro-inflammatorischen Genexpressionen im Lebergewebe von ehemals adipösen Mäusen vorhanden. Dies ging mit einer depot-spezifischen Fettzellhypertrophie und Makrophageninfiltration im perigonadalen Fettgewebe ehemals adipöser Mäuse einher. Microarrayanalysen vom perigonadalen Fettgewebe ehemals adipöser Mäuse zeigten weiterhin die Hochregulierung einer Vielzahl zum Teil inflammatorischer Gene und Signalwege. Eines dieser hochregulierten Gene im perigonadalen und braunen Fettgewebe von adipösen und ehemals adipösen Mäusen war der Transkriptionsfaktor Activating Transcription Factor 3 (ATF3). Indem ein UCP1-spezifischer konditioneller Knockout von ATF3 im braunen Fettgewebe von Mäusen geschaffen wurde, wurde der Einfluss von ATF3 aus dem braunen Fettgewebe auf die Entstehung von DIA untersucht.

Zusammenfassung

Hier zeigte der konditionelle Knockout von ATF3 in männlichen und weiblichen Mäusen keinen Einfluss auf die Suszeptibilität für DIA hinsichtlich der Zunahme von Körpergewicht und Fettmasse, der Entstehung von Glukoseintoleranz und Hyperinsulinämie. Dennoch wurde eine Fettzellhypertrophie im braunen und subkutanen weißen Fettgewebe von diätinduziert - adipösen $Atf3^{fl/fl}$;$Ucp1^{cre+}$ Mäusen gefunden, was zu ersten Einblicken hinsichtlich der Rolle von ATF3 im braunen Fettgewebe beiträgt. Zusammenfassend trägt diese Arbeit zu neuen Verständnissen bei, wie verschiedene Diätinterventionen die Pathogenese und Umkehrbarkeit von DIA in Mäusen beeinflussen und zeigt metabolische und genetische Veränderungen aufgrund einer Vorgeschichte von DIA auf. Des Weiteren weisen die in dieser Arbeit präsentierten Ergebnisse darauf hin, dass das Vorhandensein von ATF3 in braunen Adipozyten keine Rolle für die Entstehung von DIA spielt.

Table of Contents

Table of Contents

List of Figures

List of Figures

List of Tables

Abbreviations

Table 1 List of abbreviations

Abbreviation	Meaning
Acaca	Acetyl-coA-carboxylase
Afap1	Actin philament associated protein 1
Agrp	Agouti-related peptide
AP-1	Activator-protein 1
ATF	Activating transcription fatcor
AUC	Area under the curve
AV	Average
BAT	Brown adipose tissue
Bcl6b	B-cell lymphoma 6b
BMI	Body mass index
BSA	Bovine serum albumin
bZip	Basic leucine zipper domaine
C/ebp	CCAAT-enhancer-binding protein
cAMP	Cyclic adenosine monophosphat
Ccl	Chemokine (C-C motif) ligand 5
CD	Cluster of differentiation
CIDEA	Cell Death-Inducing DFFA-Like Effector A
CLS	Crown like structures
CNS	Central nervous system
COX	Cytochrome c-oxidase
Ct	Cycle threshold
Ctrl	Control diet
DIO	Diet-induced obesity
DNA	Deoxyribonucleic acid
DTT	Dithiothreitol
dWAT	Dermal white adipose tissue
ECM	Extra-cellular matrix
EDTA	Ethylenediaminetetraaceticacid
EGFR	Epidermal growth-factor receptor
EGTA	Ethyleneglycoltetraaceticacid
ER	Endoplasmatic reticulum
ERK	Extracellular signal-regulated kinase
FABP	Fatty acid binding protein
Fasn	Fatty acid synthase
FC	Fold change
FDR	False-discovery rate
Foxo1	Forkhead box protein O1
FTO	Fat mass and obesity associated protein

Glut4	Glucose transporter 4
GTT	Glucose tolerance test
gWAT	Perigonadal white adipose tissue
H&E	Hematoxylin and eosin
HFD	High-fat diet
HIF1-α	Hypoxia-inducible factor 1 alpha
Hprt	Hypoxanthine-guanine phosphoribosyltransferase
i.p.	Intraperitoneal
IF	Impact fatcor
IFNy	Interferon gamma
IKMC	International Knockout Mouse Consortium
IL	Interleukine
Iso	Isoproterenol
ko	Knockout
Ldlr	Low-density lipoprotein receptor
Lepr	Leptin receptor
LFD	Low-fat diet
MAT	Bone marrow adipose tissue
MIF1	Macrophage inflammation factor 1
MRI	Magnetic resonance imaging
mRNA	Messenger ribonucleic acid
NAC	N-acetyl-l-cystein
NAFLD	Non-alcoholic fatty liver disease
NASH	Non-alcoholic steatohepatitis
NEFA	Non-esterified free fatty acids
NIH	National Institute of Health
NK	Natural killer cells
NMR	Nuclear magnetic resonance
NNT	Nicotinamide nucleotide transhydrogenase
PBS	Phosphate-buffered saline
PCR	Polymerase chain reaction
Pdx-1	Pancreatic and duodenal homebox1
Pepck1	Phosphoenylpyruvate carboxykinase
PFA	Paraformaldehyde
PGC1a	Peroxisome proliferator-activated receptor gamma coactivator 1-alpha
PI3K	Phosphatidylinositol-4,5-bisphosphate 3-kinase
Pomc	Proopiomelanocortin
PPARy	Peroxisome proliferator-activated receptor y
Ppp1r10	Protein phosphatase 1
PRDM16	PR domain 16
RIN	RNA integrity number
RNA	Ribonucleic acid
RT	Room temperature

Abbreviations

RT-PCR	Reverse transcription polymerase chain reaction
Scd1	Steaoryl-CoA desaturase 1
scWAT	Subcutaneous white adipose tissue
SD	Standard deviation
SEM	Standard error of the means
SNP	Single-nucleotide polymorphism
SREBP	Sterol-regulating element binding factor
SVF	Stromal vascular fraction
Tbp	Tata-box protein
T1DM	Type 1 diabetes mellitus
T2DM	Type 2 diabetes mellitus
TBS	Tris-buffered saline
TG	Triglycerides
TNF	Tumor necrosis factor
UCP1	Uncoupling protein 1
VAT	Visceral adipose tissue
WAT	White adipose tissue

1. Introduction

The section 1.3 of this chapter contains in parts text and figures, which were published by the author of this dissertation together with Dr. Theresa Schöttl and Dr. Siegfried Ussar in the review article "Heterogeneity of adipose tissue in development and metabolic function", Schöttl, T., Fischer, I.P. and Ussar, S., Journal of Experimental Biology (2018) [1].

1.1 Obesity - causes and consequences

Obesity, which can be defined as the abnormal and excessive accumulation of fat that results in a body mass index (BMI) $\geq 30 kg/m^2$ [2], has become a major health problem of the modern society since its prevalence has doubled in more than 70 (westernized) countries over the past three decades [2, 3]. In 2015, 603.7 million adults and 107.7 million children were obese and especially childhood obesity is on the rise [3]. Interestingly, this problem represents a greater burden for female adults than male adults, whereas the opposite is true for children [3]. Occurring due to an imbalance of energy intake and energy expenditure, excessive fat accumulation, specifically in the visceral part of the body, is known to deregulate systemic lipid- and glucose- homeostasis [4]. Obesity is therefore considered as a major risk factor for the development of type 2 diabetes mellitus, non-alcoholic fatty liver disease (NAFLD), cardiovascular and other, neoplastic diseases [4]. The most relevant epidemiological factors causing obesity are excessive dietary intake of saturated fatty acids, in combination with lack of activity and a sedentary lifestyle [1]. Throughout multiple genome-wide association studies (GWAS) mono - or polygenic predispositions to obesity have been recognized. Prominent examples of monogenic mutations, associated with obesity, are for instance the melanocortin 4 receptor [5, 6], leptin [7] or leptin receptor [8]. Most of the known genetic predispositions are apparent as single nucleotide polymorphisms (SNPs) and were identified via GWAS. Among other genes, multiple widespread SNPs were identified in the alpha-ketoglutarate-dependent dioxygenase (FTO) gene [9, 10], which encodes for an enzyme, which oxidxatively demethylates single-stranded DNA and RNA. Mutations in the FTO gene have been therefore frequently studied but only proven to attribute to 22% of the risk of becoming obese [10]. Newer studies even question the direct involvement of SNPs in FTO gene in the obesity development, as obesity-associated SNPs have been functionally associated with two FTO-neighboring genes: Iroquois-class homeodomain protein (IRX3) and Protein Phosphatase 1, Regulatory Subunit 134 (RPGRIP1 L) [11, 12] [13]. Indicating that in general, novel candidate genes, identified from metabolically relevant GWAS studies may have to be treated with caution. In total, estimates of heritability of increased BMI approximately vary around 40% to 70% [14, 15]. Therefore, epigenetic modifications, caused by a variety of environmental factors such as parental high fat diets (HFD), as well as changes in gut microbiota additionally contribute to the

development of obesity [16-18].

1.2 Obesity related co-morbidities

1.2.1 Non alcoholic fatty liver disease

If the capacity to store triglycerides in (visceral) adipose tissues is exhausted, ectopic lipid accumulation takes place, due to a spillover of lipids, preferably to near metabolic organs such as the liver, pancreas or muscle. Thereby, the accumulation and storage of triglycerides in the liver, the so-called process of hepatosteatosis, is an early event occurring in the development of nonalcoholic fatty liver disease (NAFLD) and is one of the most prominent obesity-related co-morbidity with approximately 51% of prevalence [19, 20]. NAFLD describes the excessive accumulation of triglycerides within the hepatocytes, without the presence of inflammation, fibrosis or hepatocellular ballooning [20, 21]. NAFLD has a global prevalence of estimated 25% and is closely associated with other metabolic co-morbidities, such as e.g. type 2 diabetes, as 23% of patients suffering from NAFLD were estimated to suffer from type 2 diabetes [19]. Untreated NAFLD can progress to non-alcoholic steatohepatitis (NASH), hepatic fibrosis, cirrhosis, hepatocellular carcinoma and, in the last consequence, lead to death [22, 23]. Therefore, NAFLD is considered an important complication of obesity, which should be targeted for instance by lifestyle interventions such as dieting [24].

1.2.2 Type 2 diabetes mellitus (T2DM)

Glucose homeostasis is highly regulated in the body by a variety of factors, but primarily the pancreatic hormone insulin. Shortly, upon postprandial increase of glucose in the blood, insulin is being secreted from the pancreatic β-cells and travels through the blood stream to peripheral tissues to initiate glucose-uptake. Diabetes mellitus can be defined as a group of metabolic disorders, which are all characterized by chronically elevated blood glucose levels (hyperglycemia). Symptoms occur as polydypsia, polyuria, fatigue and peripheral neuropathy often present in feet or the eyes [25]. Therefore, long-term complications include blindness, renal failure and cardiovascular diseases. In 2014, around 366-422 million people were estimated to suffer from either type 1or type 2 diabetes mellitus (T1DM, T2DM) or, its closely related disease, gestational diabetes. Thereby, patients suffering from T2DM accounted for over 90% of the mentioned causes [26, 27]. Moreover, 3.7 million deaths were estimated to be caused by diabetes and hyperglycemia in 2014 [26]. T1DM is a chronic disease characterized by the absence of insulin production, due to an autoreactive immune system, attacking and destroying the insulin producing β-cells and resulting in constant hyperglycemia. Known mechanisms causing insulitis and β-cell-loss include, among others, hyperactive CD8+ T-cells, auto-antigen production and T-effector cell resistance to T-regulatory cells

[28, 29]. This abberant immune responsiveness is believed to be partly caused by genetic predispositions, as approximately 40 risk loci are known for the development of T1DM, so far [29]. Treatment options for T1DM comprise different insulin-replacement therapies and require a lifelong application. Delineating from this, T2DM, is a multifactorial disease, which is caused by a combination of risk factors such as genetic predispositions as well as environmental factors, including obesity, nutrient excess and a sedentary lifestyle. So far, over 100 gene loci have been identified for the development of T2DM [30-32]. The predominant manifestation of T2DM varies between less insulin production, due to β-cell dysfunction, and insulin resistance in peripheral tissues, in both cases leading to hyperglycemia. Insulin resistance in metabolically active organs, such as liver, muscle and adipose tissue can be triggered, e.g. by accumulation of lipids in the cell and local tissue inflammation. Insulin resistant cells cannot recognize insulin and thus cannot take up glucose. The accumulating glucose in the blood therefore triggers a feedback loop to the pancreas to produce more insulin, eventually leading to a state of hyperinsulinemia. Chronic elevation of insulin production can induce exhaustion of the β-cell and β-cell dysfunction [30, 33]. Treatment options comprise a healthy lifestyle, physical activity and a variety of pharmaceutical drugs, aiming to restore insulin sensitivity [30].

1.3 Adipose tissue is a heterogeneous organ

1.3.1 Adipose tissue depots in mice and men

The primary location to store energy varies between different species: While vertebrates, such as amphibians and reptiles preferentially store energy intra-abdominal, mammals accumulate fat within the abdomen but also subcutaneously (anterior and posterior) [1, 34, 35] (Figure 1). In humans, the subcutaneous depots comprise cranial, facial, abdominal and gluteal accumulation of fat and serve as protection against heat loss and mechanical damage. In contrast, intra-abdominal storage of triglycerides takes places in the omentum as well as retroperitoneal and visceral, and shields vital organs. Of note, the individual distribution of subcutaneous and visceral adipose tissue varies due to several factors such as genetics, age, sex, nutrition and the energy homeostasis of the specific depots [36-38]. In mice, subcutaneous adipose tissue (scWAT) includes the posterior subcutaneous, so called, inguinal and anterior subcutaneous adipose tissue. Murine visceral adipose tissue comprises mesenteric, retroperitoneal, perirenal and perigonadal adipose tissue (gWAT) [1, 39] (Figure 1). In the majority of above-mentioned adipose depots, white adipocytes are the predominant type of cells, yet, brown and brown-like adipocytes can be sporadically found in the visceral and subcutaneous depots of mice under normal conditions, which can be augmented under certain stimuli, as explained later

(1.3.3). Still, the primary location of BAT is in the inter- and subscapular, axillary and cervical areas of the subcutaneous anterior depot in mice [1, 35, 40]. BAT was firstly described in hibernating small mammals undergoing torpor and its main function was attributed to maintaining body temperature in cold environments [41, 42]. This process is specifically important for small mammals that cannot undergo shivering thermogenesis. Its function is explained in more detail in section 1.3.3.

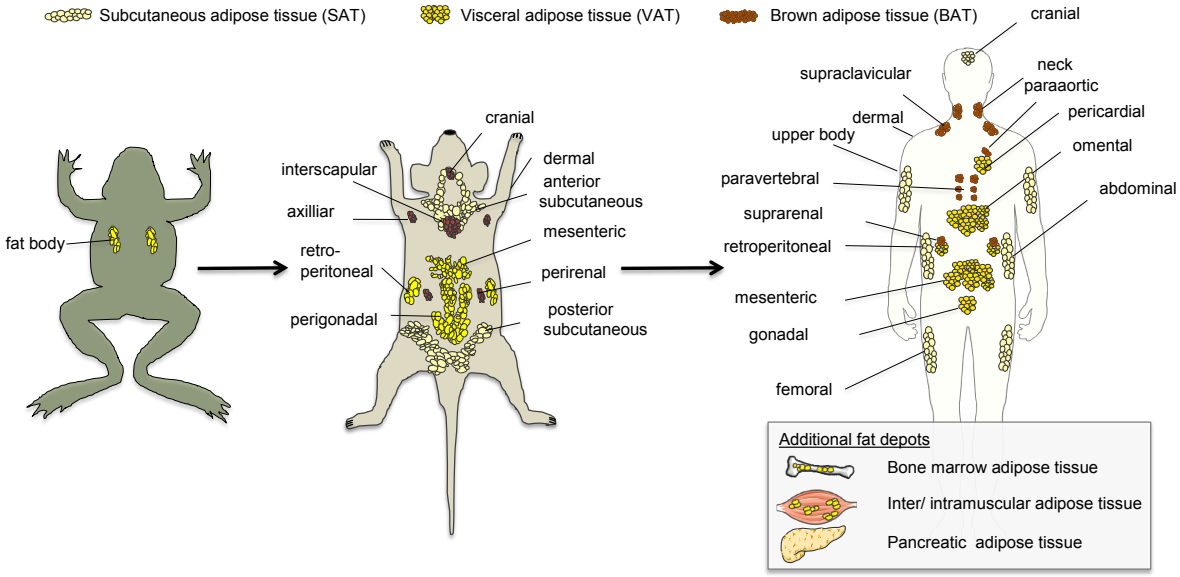

Figure 1 Adipose tissue depots in different species.
Reptiles and amphibians store fat in the intra-abdominal cavity, as so-called fat bodies. In contrast, mammals such as mice and humans store fat in distinct adipose depots within the abdomen, but also under the skin (subcutaneous). These adipose compartments can be grouped into subcutaneous white adipose tissue (SAT), visceral white adipose tissues (VAT), dermal adipose tissue (dWAT), bone marrow adipose tissue (MAT) and brown adipose tissue (BAT) and hold individual metabolic functions and risks. This graphic was produced by using Servier Medical Arts templates, which are licensed under a Creative Commons Attribution 3.0 Unported License; https://smart.servier.com and is adapted with permission from [1].

1.3.2 White adipose tissue exhibits depot-specific plasticity and metabolic function in obesity

Latest since the discovery of leptin in 1994 [7, 43], the adipose tissue is considered as a metabolically active organ, which has important endocrine and immunological functions [44, 45]. Among other factors, the anatomic location of each (white) adipose tissue depot itself impacts the endocrine profile. It was for instance shown that subcutaneous adipose depots secrete and express higher rates of leptin than visceral depots of lean and obese subjects [46, 47]. In contrast, adiponectin expression has been shown to be oppositely regulated. Leptin has pro-inflammatory functions as it increases the recruitment of monocytes and production of pro-inflammatory cyto- and chemokines

[44, 48, 49]. Increased adiponectin levels in the plasma and adipose tissue are associated with high insulin sensitivity and a decreased risk for T2DM and cardiovascular diseases [44]. The administration of adiponectin for instance resulted in a decline in body and fat mass [50] and reduced hyperglycemia and restored insulin sensitivity in obese mice [51]. In obese states, adiponectin expression and secretion is decreased, therefore past research targeted to increase the expression of insulin-sensitizer adiponectin by activation through e.g. peroxisome proliferator-activated receptor y (PPARy) agonists [52]. Moreover, also deviating from most adipose-secreted hormones, adiponectin exhibits anti-inflammatory properties as it suppresses pro-inflammatory cytokine production and remodels macrophage function [44]. In line, production of adiponectin is curtailed by pro-inflammatory cytokines such as tumor necrosis factor (TNF) and interleukine 6 (IL6) [44, 53]. Moreover, while adipokines derived from visceral adipose tissue are secreted into the portal system and have direct access to the liver [54], adipokines secreted by the subcutaneous depots enter the system circulation [1]. Therefore, severe accumulation of fat in the visceral part directly impacts hepatic metabolic function, and is moreover associated with an overall higher (cardio)-metabolic risk [1, 37].

1.3.2.1 Hypertrophy vs. Hyperplasia and metabolic dysfunction in obesity

Accompanying excessive weight gain, obesity is marked by enlarged adipocyte cell size (hypertrophy) due to increased triglyceride storage as well as augmented adipocyte numbers (hyperplasia) [55]. While hypertrophy already occurs with moderate weight gain, adipocyte hyperplasia primarily occurs in severely obese humans [56, 57] and mice [58] [59]. Still, some studies report the subcutaneous depot to be the primary site for hyperplasia [60]. In humans, lean subjects show larger adipocytes in the subcutaneous adipose tissue than in visceral adipose tissue [61]. Yet in mice, the opposite is the case, as multiple mouse studies showed smaller adipocytes in the subcutaneous than in the visceral depots (Figure 2). Recently, a rodent study by van Beek and colleagues demonstrated that the gWAT had a limited capacity to store lipids, which was reached at an average body weight of 40g [62]. Therefrom, prolonged HFD-feeding caused crown-like structure (CLS) formation, and ectopic lipid accumulation in the liver, promoting the development of hepatic steatosis and insulin resistance [62]. In contrast, scWAT and mesenteric WAT initially displayed a slower rate in expanding, but continued to increase lipid accumulation throughout 34 weeks of HFD-feeding [62]. In contrast, hypoplasia in subcutaneous adipose tissue seems to be largely driven by an overall reduction of stored triglycerides within individual adipocytes and is associated with increased insulin sensitivity [1, 63, 64]. Rapid adipose tissue expansion is associated with detrimental metabolic alterations accumulating in tissue insulin resistance (Figure 2) [65]. In particular, hypoxia, occurring due to the incapability of the neovasculature to meet the requirements of oxygen supplementation to the expanding tissue, was shown to be an early hallmark of adipose tissue dysfunction [65, 66]. Already a few days of HFD-challenge rapidly boost adipocyte expansion [67, 68], which is paralleled

by an induction of hypoxia-inducible factor 1 (HIF1-α). In adipose tissue, HIF1-α thereby activates the transcription of extra cellular matrix (ECM) components eventually leading to fibrosis, instead of having beneficial angiogenic effects [67]. Yet, contradictory results on the genetically and pharmacologically ablation of HIF1-α suggest both an amelioration [69] but also aggravation of DIO and associated glucose intolerance [70].

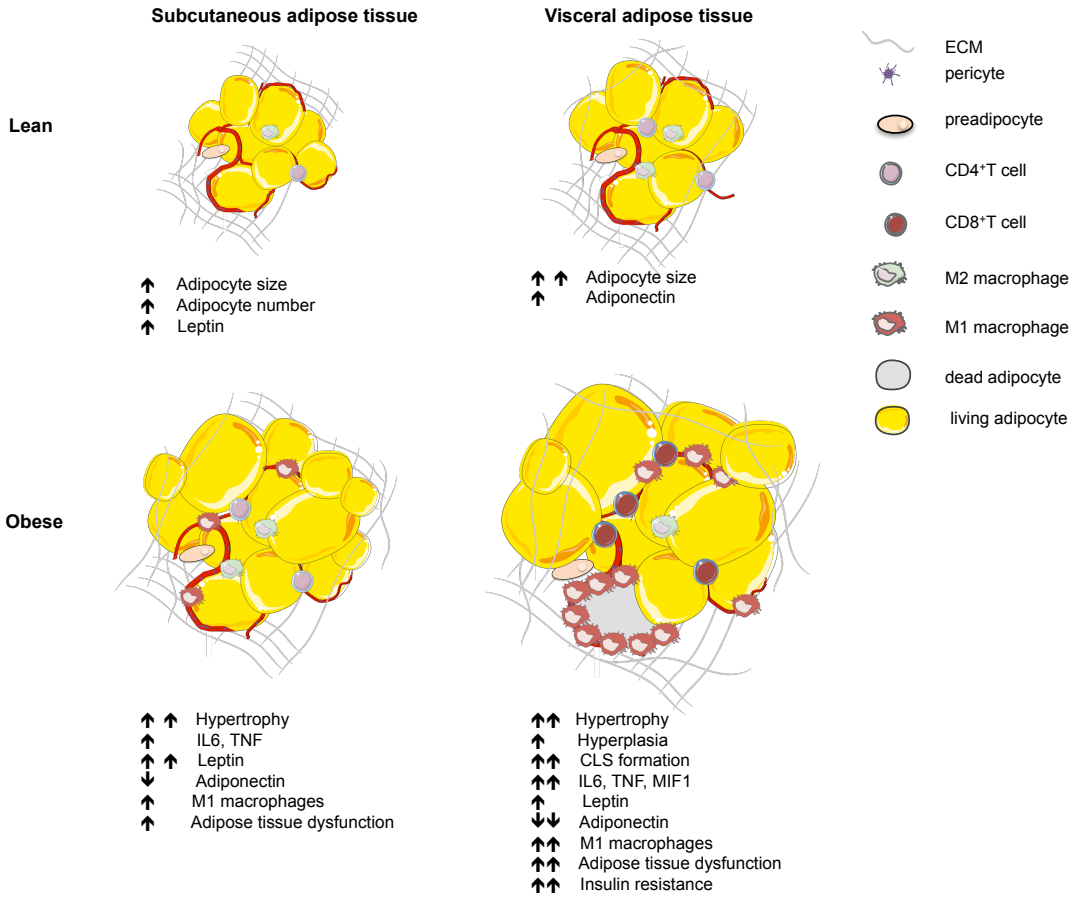

Figure 2 Heterogeneity of white adipose tissue in lean and obese states.
In the lean state, murine subcutaneous adipose tissue is characterized by smaller but increased number of adipocytes. Weight gain triggers adipocyte hypertrophy, with visceral adipocytes increasing their cell sizes more rapidly. This associates with reduced adiponectin expression in visceral adipose tissue. In subcutaneous adipose tissue, hypertrophy results in lower expression of pro-inflammatory cytokines and less M1 macrophage infiltration. Visceral adipose tissue expansion triggers pro-inflammatory cytokine expression as well as recruitment of immune cells and contributes to adipose tissue dysfunction and insulin resistance. This graphic was produced by using Servier Medical Arts templates, which are licensed under a Creative Commons Attribution 3.0 Unported License; https://smart.servier.com and is adapted with permission from [1].

1.3.2.2 Obesity - a state of low-grade inflammation giving rise to insulin resistance

Around 10-15% of the glucose uptake after a meal is mediated by adipocytes, thus adipose tissue plays an important role in the glucose homeostasis [71, 72]. Glucose itself contributes to lipid metabolism, as 50% of the up-taken glucose is used to synthesize glycerol and fatty acids in adipocytes [73].

In adipose tissue, glucose is taken-up by the insulin-dependent glucose transporter 4 (GLUT4 or SLC2A) [74]. In basal states, GLUT4 is stored in intracellular vesicles. Upon binding of insulin to its specific receptor, GLUT4 carrying vesicles are being incorporated into the plasma membrane via exocytosis and GLUT4 is released and freed to mediate the glucose uptake. Increased lipid influx from nutrition together with glucose-induced lipogenesis create a constant lipid overload in obese states, which decreases the anti-lipolytic effect of insulin and promotes insulin resistance. The full mechanisms causing the development of local insulin resistance are currently not known [37, 75, 76]. Yet, the presence of a low-grade inflammatory state in obesity is strongly associated with the development of a (local) insulin resistance. Accompanying adipose tissue expansion upon obesity, the increase in hypoxia and HIF1-α mediates the up-regulation of pro-inflammatory cytokines such as IL-6 and macrophage inflammation factor (MIF1), contributing to the low-grade inflammatory state (Figure 2) [66]. There are two types of macrophages residing in the stromal vascular fraction (SVF) of adipose tissue, M1 type macrophages and M2 type macrophages. M1 are pro-inflammatory, activated cells promoting cytotoxicity and tissue damage, induced by pro-inflammatory cytokines, such as IFNy and TNF. In contrast, M2 type macrophages are unactivated cells, or alternatively-activated by IL-4, IL-13 and express arginase-1, the mannose receptor/CD206 and macrophage galactose-type C lectin/CD301 [44]. In lean adipose tissue, M2 macrophages predominate the presence of M1 macrophages with a ratio 4:1. M2 macrophages are promoting immune suppression and are expressing anti-inflammatory cytokines (Figure 2). Yet, with advancing obesity, hypertrophic adipocytes secrete increased amounts of pro-inflammatory adipokines (leptin, IL-6, TNF) and decreased amounts of anti-inflammatory adipokines such as adiponectin, enhancing the recruitment of immune and vascular cells, such as $CD8^+$cells and natural killer cells (NK cells) to the adipose tissue [44]. This in turn accelerates the production of pro-inflammatory cytokines, creating a state of mild metabolic dysfunction [44]. In severely obese conditions, M1 macrophages are predominantly surrounding necrotic adipocytes, forming CLS, fueling the pro-inflammatory environment but also contributing to tissue remodeling (Figure 2) [44, 66, 77]. Thereby, cellular lipid overload is suspected to cause the formation of CLS [77]. Providing one possible scenario of how adipose tissue expansion causes insulin resistance. Yet, recently, Shimobayashi et al reported that insulin resistance even precedes macrophage accumulation and adipose tissue inflammation. Therefore the exact mechanisms of the hierarchy of adipose tissue inflammation and insulin resistance have to be further investigated [78].

1.3.3 Brown and beige adipocytes and their thermogenic function

WAT is mainly composed of unilocular cells, with a high capacity to store triglycerides, while BAT contains multilocular adipocytes, rich in mitochondria, which possess a lower capacity to store

energy. Most importantly, brown adipocytes hold the unique feature to dissipate energy in form of heat, upon noradrenergic stimulation. This process is mediated by uncoupling protein 1 (UCP1), a protein residing in the inner mitochondrial membrane, which uncouples the proton motive force of the respiratory chain, thereby combusting energy as heat. BAT activity can be increased upon cold exposure and nor-adrenergic stimulation, which can be initiated pharmacologically [79] and by fasting [80]. In humans, for a long time it had been believed that active BAT was only present in the neck and shoulder of newborns and small children, where its function was attributed to the defense of body temperature upon cold exposure, in order to compensate for the lack of shivering-thermogenesis [1, 81]. Further, it was believed that BAT activity would decrease during aging and would be vanished by reaching adulthood. However, in 2009, multiple studies finally manifested the presence of metabolically active BAT in adult humans, using F^{18}-FDG PET/CT Scans [1, 82-84]. Active BAT was identified ranging from the anterior neck to the thorax [82] yet, the highest localization of active BAT was found in the paracervical and supraclavicular region [1, 83, 84] (Figure 1). The presence of metabolically active BAT in humans varies due to several intrinsic factors such as the individual age, sex, and body mass, but also due to seasonal changes, and is estimated to be prevalent in between 1-10% of humans [1, 85, 86]. Thereby, higher presence of active BAT was detected in young, lean women than in men. Batches of brown-like adipocytes with thermogenic function can also accumulate in WAT upon cold exposure, noradrenergic – and various other endocrine stimuli [87]. These beige or alternatively termed brite (brown in white) [88, 89] adipocytes have the characteristics of brown adipocytes, as they possess the same morphology and express most of the brown adipocyte specific genes, such as *Ucp1*, Cell Death-Inducing DFFA-Like Effector A *(Cidea)* and proliferator-activated receptor gamma coactivator 1-alpha (*Pgc1α),* p2x purino receptor 5 (*P2rx5)* and *Pat2* [87, 90]. Yet, it has been shown that beige and brown adipocytes cannot be considered as identical, as they emerge from different embryonic precursor cells [89] and are individually transcriptionally regulated [91]. Due to their favorable function of dissipating energy in form of heat, instead of storing it as fat, recent research aims to target the activation of brown adipocytes and the conversion of white to brown or beige adipocytes, in order to increase ways of energy expenditure as a cure for the obesity epidemic [1, 87, 92-95].

1.4 Animal models of DIO

To analyze the etiology of obesity *in vivo*, animal models have become very helpful. Over the years, various monogenic and polygenic knock-out mouse lines for specific obesity related loci have been made available to study the causes and consequences of obesity. Prominent examples are the leptin or leptin receptor deficient *ob/ob* [7] or *db/db* [96] mice. Yet, since the genetic contribution to

the development of obesity is estimated only between 40-70% [14, 15], different diet-induced obesity (DIO) animal models have been generated to determine the progression and outcome of this multifactorial disease [97, 98]. When exploring environmental factors affecting weight gain, DIO models are more representative of the human pathogenesis and, thus, remain the preferable choice in obesity and diabetes research [97]. The phenotypes of the DIO mice are known to vary with the specific environment of the animal facility (e.g. ambient temperature, humidity and light/dark cycle), the experimental study design (e.g. duration of feeding, endpoints), utilized diets (caloric value, composition, source of fat) and involved animals (age, gender, strain) [99]. Specifically, the genetic background of the mice has been found to impact the susceptibility to DIO. Inbred strains such as C57BL/6, 129X1/SvJ, DBA/2 and FVB/N were shown to be susceptible in varying degrees to HFD induced adiposity, glucose intolerance and insulin resistance [100]. Among those, and due its high affinity to obesity and impaired glucose tolerance, the C57BL/6 strain has been most commonly used in metabolic studies [101]. The C57BL/6 mouse line was first established by C.C. Little in the 1920s and is one of the most frequently used genetic inbred mouse line [102]. Over the years, distinct sub-strains of the C57BL/6 mouse have evolved as the result of genetic drifts, occurring at different breeding facilities [101]. In the last years, a great variety of genetic differences between the Jackson Laboratory derived C57BL/6J strain and strains derived from other breeders, such as the National Institute of Health (NIH) C57BL/6N strain, were elucidated [102, 103]. A frequently discussed, in-frame, five-exon deletion was discovered in the nicotinamide nucleotide transhydrogenase (*Nnt*) gene of the C57BL/6J strain 2005 [104]. The *Nnt* encodes for an enzyme, residing in the inner mitochondrial membrane, which is responsible for the proton coupling and hydride transfer from NADH to $NADP^+$ and malfunction of the enzyme is associated with oxidative stress [105]. The five-exon deletion in the *Nnt* has been made responsible for the more obesogenic phenotype of C57BL/6J mice, as this mutation was shown to cause mitochondrial dysfunction [106], associated with insulin resistance [100, 107]. Further, a loss of the *Nnt* gene aggravated high-fat diet induced gain in total body mass, fat mass and non-fasting glucose levels of C57BL/6J mice [108, 109]. Therefore, the functional *Nnt* possessing C57BL/6N strain is currently considered to be the model of interest for future metabolic research, e.g. by the International Knockout Mouse Consortium (IKMC) [101]. Broad evidence of a sexual dimorphism of obesity in rodents, displayed by divergent kinetics of HFD induced weight gain, adipose tissue plasticity and insulin sensitivity is given nowadays [110-112]. Thus, some studies claim that female mice are protected against obesity and its associated dysregulation of glucose- and insulin homeostasis [113, 114]. Therefore, special notice should be taken when planning DIO studies, concerning the gender of the mice involved.

1.5 Strategies and challenges overcoming DIO

Today, there are multiple ways to overcome obesity, by either increasing energy expenditure through enhanced physical activity and/or decreasing energy intake [4, 115]. Among these, bariatric surgery is the most efficient in reducing body mass, with a long term reduction of > 50% of pre-operative body mass [18, 116]. Moreover, concurrent co-morbidities as type 2 diabetes, hypertension and dyslipidemia have been shown to be mitigated by bariatric surgery [18, 117]. Still, surgical-based weight loss approaches can induce post-operative adverse effects, such as the dumping syndrome, consequent malabsorption and impaired nutritional status, bowl injuries and ulcera [18, 118, 119]. A popular, and less effective way to lose weight and eventually overcome obesity is dieting. Unfortunately, many obese patients struggle to maintain a stable body weight after dieting and regain weight to an even greater extent [120, 121], giving rise to a new and higher body set point [122]. Maintenance of a reduced body weight in formerly obese patients was shown to be affected by compensatory mechanisms, including a reduction in resting energy expenditure [123]. This decrease in energy expenditure was further shown to be paralleled by an increase in hunger, which was hypothesized to cause the rebound to obesity of over 95% of formerly obese American patients [124]. Furthermore, evidence is given by multiple rodent studies that weight loss, induced by caloric restriction, reprograms orexigenic pathways [125] and promotes hyperphagia [126, 127]. Upon weight loss, adipocyte cell sizes, but not numbers are decreasing. This suggests that the individual number of adipocytes is set during childhood and adolescence, while the expansion of adipocytes is adaptable to the nutritional status [128, 129]. Among the adipokines, especially leptin, plays a major role in body weight regulation [130, 131]. Circulating leptin levels are directly proportional to fat mass and adipocyte size [132] and act as afferent satiety signals to the central nervous system (CNS) [133]. In lean individuals, increased levels of leptin stimulate receptors in the hypothalamus and other brain regions to decrease food intake and increase energy expenditure [134, 135]. In contrast, most obese individuals have exacerbated levels of circulating leptin, but do not exhibit the regulation of appetite and energy metabolism upon it. This term has been often called “leptin resistance” and is studied frequently [136, 137]. Moreover, reduction of fat mass and paralleled decrease in circulating leptin, has been discussed to be the cause for the impaired regulation of hunger and increased rate of body weight rebound in formerly obese men and mice [138, 139]. However, the molecular and functional underpinnings of a history of obesity and body mass rebound have not been fully understood, yet.

Another approach of resetting the energy balance and overcoming obesity, by increasing the rate of energy expenditure, is through pharmacological targeting the activation of BAT. Therefore, activation of adaptive thermogenesis in humans is currently one of the focuses of obesity research [94, 95] [18].

1.6 Activating Transcription Factor 3 - a regulator of metabolism?

Activating transcription factor 3 (ATF3) is part of the mammalian ATF/CREB family of transcription factors and also known by its alternative names LRF-1, LRG-21, CRG-5 and TI-241 [140]. All members of the ATF-family share the consensus cAMP responsive element (CRE) binding site TGACGTCA and a bZip DNA binding domain (Figure 3). It is known that ATF/CREB proteins regulate gene expression by forming-selective heterodimers with each other or other bZip proteins such as AP-1 and C/EBP and thereby acting as transcriptional repressors or activators [140]. Among the protein family members, especially ATF2, ATF4 and ATF6 are of relevance. While ATF4 and ATF6 are predominantly involved in unfolded protein response and endoplasmatic reticulum (ER) stress regulation, [141, 142] ATF2 has been shown to be involved in regulation of BAT adaptive thermogenesis [143, 144].

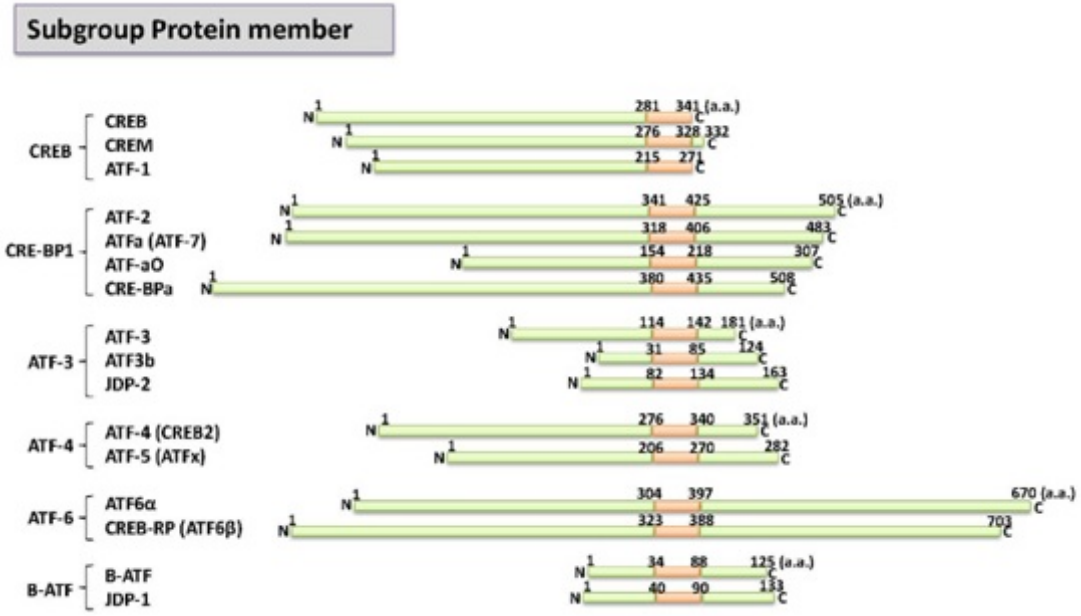

Figure 3 Members of the ATF/CREB transcription factor family.
ATF family members can be divided into 6 subclasses according to their sequence homology, all sharing a consensus bZIP sequence (marked in orange). This figure was taken with permission from [145].

ATF3 homodimers function as transcriptional repressors, while heterodimers of ATF3 with e.g. c-Jun or ATF2 act as transcriptional activators [140]. Over the past years, ATF3 has been shown to be of clinical interest, as it is highly expressed in the livers of patients with type 2 diabetes or non-alcoholic fatty liver disease (NAFLD) [146] as well as in pancreatic islets of type 1 and type 2 diabetics [147, 148]. Additionally, ATF3 is identified to be up-regulated in endothelial cells of patients suffering from atherosclerosis [149]. Moreover, in rodents, ATF3 expression was shown to be induced by various conditions such as ischemia, cancer, seizures, obesity and diabetes. *In vitro* experiments further showed up-regulation of ATF3 upon stress signals such as hypoxia [150], radiation [151], ER stress

[152] and inflammation [140] as well as in cases of pancreatomy, ischemia-perfusion and streptozotocin treatment [147]. Moreover, ATF3 expression was exacerbated in isolated β-cells under H_2O_2 treatment, mimicking oxidative stress, which could be rescued by dosage of n-acetyl-L-cystein (NAC), a known antioxidant [147]. From rodent studies we know that ATF3 whole body knockout mice are protected from cytokine-induced β-cell apoptosis [148]. Moreover, it has been proposed that ATF3 directly regulates insulin transcription in the β-cells [153]. Thereby, both detrimental as well as protective roles have been attributed. For instance, whole body knockout of ATF3 ameliorated HFD-induced hyperinsulinemia in mice [153]. *In vivo* overexpression of ATF3 in murine β-cells was associated with growth retardation and a high rate of perinatal death, decreased expression of hepatic gluconeogenic genes, abnormal distribution of insulin producing cells and in severe cases β-cell loss [148]. Yet, some of the mice overexpressing ATF3 in β - cells showed a more liver-specific phenotype, exhibiting reduced serum glucose levels. Still, the effects within the pancreas positively correlated with ATF3 expression. Overall, suggesting that stress-induced expression of ATF3 positively controls insulin transcription, before enhancing β-cell apoptosis, due to constant β-cell overwork [153]. Newer studies demonstrate that ATF3 is also regulating glucagon production in α-cells [154, 155]. In addition, mice depleted from ATF3 in the hypothalamus and pancreas exhibit better glucose tolerance, higher insulin sensitivity and decreased energy intake in lean and obese states [155]. In regard to adipose tissue, an adipocyte-specific overexpression of ATF3 was shown to induce mitochondrial dysfunction and decreased glucose tolerance in DIO mice [156]. In line, in DIO as well as *ob/ob* and *db/db* mice, *Atf3* was found to be up-regulated in WAT [157]. Moreover, ATF3 has been described as a negative regulator of the insulin-sensitizing adipokine adiponectin [157], linking obesity-induced mitochondrial dysfunction to reduced adiponectin levels and hyperinsulinemia [158]. In cases of cellular or ER stress, caused for instance by hypoxia, it was further reported that ATF3 counteracts adipocyte differentiation by transcriptionally repressing CCAAT/enhancer binding protein α (C/EBPα), peroxisome proliferator activated receptor y (PPARy) [159, 160], and its co-activator fatty acid-binding protein 4 (FABP4) *in vitro* [161]. In line, knockout of ATF3 in 3T3-L1 cells was shown to ameliorate mitochondrial dysfunction in obesity-mimicking hypoxic states [156] (Figure 4).

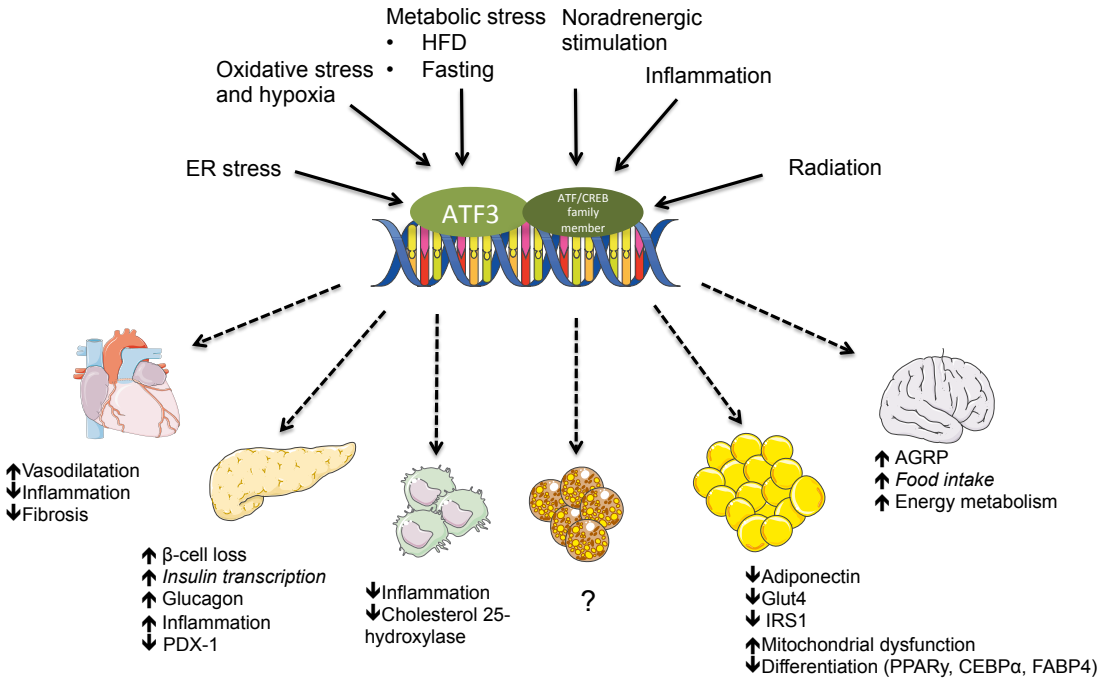

Figure 4 Targets of ATF3 in metabolic regulation.
ATF3 is induced by various stress factors and acts as a hetero- or homodimer and controls transcription of genes involved in various metabolic processes in the heart, pancreas, macrophages,WAT and the hypothalamus. The function of ATF3 in BAT has not been elucidated yet. Scheme was adapted from [162] and made by using Servier Medical Arts templates, which are licensed under a Creative Commons Attribution 3.0 Unported License; https://smart.servier.com.

Hasin and colleagues showed that ATF3 expression on gene as well as protein level can be induced by pharmacological doses of α- and β-adrenergic stimuli in all heart chambers (phenylepinephrine and isoproterenol both 2.5mg/kg) [163]. The biggest effect however was found upon angiotensin II injection, where ATF3 expression was particularly found in the left chamber, after which EGFR-dependent pathways via ERK and PI3K-Akt were activated [163]. Moreover, it was presented that ATF3 plays a protective role in cardiac fibroblasts under an angiotensin II stimulus. Consistently, cardiac specific ATF3ko mice exhibited increased hypertensive ventricular remodeling and heart failure, which could be rescued by ATF3 overexpression [164] (Figure 4).

Previous studies performed by Dr. Carola Meyer, Jana Schäfer and myself identified ATF3 as a noradrenergic response gene in BAT *in vivo* and *in vitro (Master Thesis Jana Schäfer)* [165]. In BAT, *Atf3* was one of the strongest up-regulated genes ($p< 0.01$ and FC 10.33) among 855 differentially regulated genes ($p<0.01$, FDR<10%, FC >1.2) 2.5h after noradrenalin stimulation.

This finding was validated in primary or immortalized differentiated brown adipocytes from wildtype mice stimulated with isoproterenol or the specific β_3- receptor agonist CL-316,243, indicating that *Atf3* might be a β-adrenergic response gene [165]. Despite the known functions of ATF3 in the regulation of white adipose tissue, relatively little is known about the function of ATF3 in BAT. Therefore studying the function of ATF3 in more detail is of great interest, especially with respect to the favorable BAT function of activating thermogenesis.

1.7 Aims of the work

The obesity epidemic has rapidly grown the last decades and represents a health threat for all age groups, since it is associated with the development of, e.g. T2DM and cardiovascular diseases. Thus, the need for personalized medicine is growing and most of the pre-clinical studies for anti-obesity drugs depend on rodent DIO models. Yet, DIO studies are often not comparable as they vary in experimental set ups and outcomes. **Therefore, the aim of this work was to identify how different dietary interventions influence the outcome of DIO studies and which metabolic and genetic underpinnings could be observed due to a history of DIO in C57BL/6 mice.** In detail, one aim was to elucidate how the experimental set up impacts the development of HFD-induced obesity in C57BL/6 mice. **Specifically asking the question how variations in mouse strains, gender, diet composition and feeding durations affect body weight and fat mass gain as well as the development of glucose intolerance.** Consuming a low-fat diet is a well-liked method for overcoming obesity. Thus, it was aimed to see whether DIO could be reversed in C57BL/6 mice by *ad libitum* switch from a HFD to a low-fat diet. **In particular, it was aimed to uncover metabolic underpinnings of diet-induced weight loss in peripheral tissues of C57BL/6J mice.** Since many formerly obese subjects regain body mass after dieting, it was aimed to see whether formerly obese mice were more susceptible to recurring weight gain upon re-exposure to a hypercaloric environment for 48h. **Moreover, the question was asked if candidate genes could be identified, which were up-regulated in adipose tissue of obese and formerly obese mice, when compared to age-matched never-obese mice.** In this context Activating Transcription Factor 3 (ATF3) was identified to be an interesting candidate gene in white and brown adipose tissue of obese and formerly obese mice. **Thus, the impact of BAT derived -ATF3 on the development of DIO was analyzed using an UCP1-specific ATF3 knockout model.**

2. Material & Methods

2.1 Material

2.1.1 Laboratory equipment

Table 2 List of laboratory equipment

Equipment	Supplier
Cell culture hood Safe 2020	Thermo Fisher Scientific Inc., Waltham, MA, USA
Centrifuge Mikro 200R	Hettrich Zentrifugen, Tuttlingen, Germany
CO_2 incubator	Thermo Fisher Scientific Inc., Waltham, MA, USA
Nuclear magnetic resonance measurement device	EchoMRI®LLC, Houston, TX, USA
Glucometer	Abbott GmbH & Co. KG, Wiesbaden, Germany
Heating magnetic stirrer	VELP scientifica, Usmate, Italy
Shaking incubator	Thermo Fisher Scientific Inc., Waltham, MA, USA
Mice weighing scale (Ranger 4000)	OHAUS Europe GmbH, Greifensee, Switzerland
Microscope AxioScope	Zeiss, Oberkochen, Germany
Nanodrop 2000 UV-Vis spectrophotometer	Thermo Fisher Scientific Inc., Waltham, MA, USA
Oroboros, Oxygraph 2k	Oroboros Instruments GmbH, Innsbruck, Austria
Pherastar FS	BMG Labtech, Ortenburg, Germany
PH-meter Lab 850	SI Analytics GmbH, Mainz, Germany
Scale M-prove	Sartorius, Goettingen, Germany
Table centrifuge perfect spin mini	PeQ Lab, Erlangen, Germany
Taqman cycler Viia7	Applied biosystems, Foster City, USA
Tissue lyzer II	Qiagen, Hilden, Germany
VapoProtect Mastercycler	Eppendorf, Hamburg, Germany
Water bath	Thermo Fisher Scientific Inc., Waltham, MA, USA

Table 3 List of consumables

Consumable	Supplier
Histological casettes 500	Carl Roth GmbH + Co. KG, Karlsruhe, Germany
Pipettes 5ml	Greiner Bio-One GmbH, Frickenhausen Germany
Pipettes 25ml	Greiner Bio-One GmbH, Frickenhausen Germany
Pipettes 10ml	Greiner Bio-One GmbH, Frickenhausen Germany
Einmalspritzen 1ml	B.Braun, Melsungen, Germany
FilterTips TipOne 1-200	Starlab GmbH, Hamburg, Germany
FilterTips TipOne 0.1-10	Starlab GmbH, Hamburg, Germany
FilterTips TipOne 0.5-20	Starlab GmbH, Hamburg, Germany
FilterTips TipOne 100-1000	Starlab GmbH, Hamburg, Germany

Glucose stripes	Abbott GmbH & Co. KG, Wiesbaden, Germany
MicroAmp Optical 384-Well Reaction Plate	Gibco/Life Technologies/Thermo Fisher Scientific Inc., Massachusetts MA, USA
Superfrost Plus slides	Menzel GmbH & co KG Braunschweig, Germany
Optical adhesive covers	Gibco/Life Technologies/Thermo Fisher Scientific Inc., Massachusetts MA, USA
PCR 8ER-SOFTSTRIPS 0.2ml 5X25	Biozym Scientific GmbH, Oldendorf, Germany
Reaction tubes 2.0ml	Sarstedt, Nümbrecht, Germany
Reaction tubes 1.0ml	Sarstedt, Nümbrecht, Germany
TC-Platte 12 Well,Standard,F	Sarstedt, Nümbrecht, Germany
TC-Platte 6 Well,Standard,F	Sarstedt, Nümbrecht, Germany
10cm cell culture dish	Thermo Fisher Scientific, Nunc AG, Roskilde, Denmark
15cm cell culture dish	Thermo Fisher Scientific, Nunc AG, Roskilde, Denmark

2.1.2 Mouse diets

Table 4 List of used mouse diets

Name	**Chow**	**Ssniff Ctrl**	**Ssniff 45%**	**Ssniff 60%**	**RD Ctrl**	**RD 58%**	**RD 60%**
Number	Altromin 1318	E15745-04	E15744-34	E15742-34	D 12329	D 12331	D 12492
Protein (kcal%)	27.00	20.00	20.00	19.00	16.40	16.40	20.00
Carbohydrate (kcal%)	59.00	70.00	35.00	21.00	73.10	25.60	20.00
Fat (kcal%)	14.00	10.00	45.00	60.00	10.50	58.00	60.00
Total (kcal%)	100.00	100.00	100.00	100.00	100.00	100.00	100.00
Metabolizable energy (kcal/g)	3.47	3.66	4.59	5.11	4.07	5.56	5.24

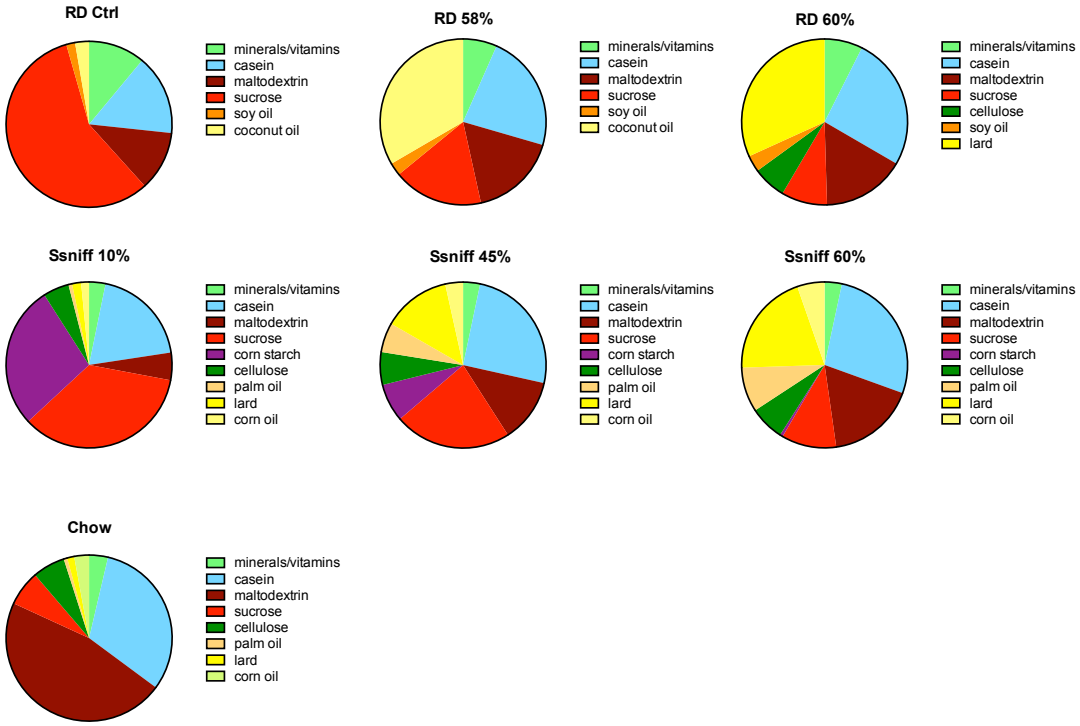

Figure 5 Composition of used mouse diets.

2.1.3 Chemicals

Table 5 List of chemicals

Product	Supplier
2 - Mercapethanol	Carl Roth GmbH + Co. KG, Karlsruhe, Germany
Acetic Acid	Carl Roth GmbH + Co. KG, Karlsruhe, Germany
Agarose	Sigma-Aldrich Chemie GmbH, Taufkirchen, Germany
Ascorbate	Carl Roth GmbH + Co. KG, Karlsruhe, Germany
Bovine serum albumin (BSA), fatty acid free TG	Sigma-Aldrich Chemie GmbH, Taufkirchen, Germany
Bradford Reagent	Sigma-Aldrich Chemie GmbH, Taufkirchen, Germany
Chloroform	Applichem GmbH, Darmstadt, Germany
Collagenase IV	Life Technologies/Thermo Fisher Scientific Inc., MA, USA
Cytochrom C	Sigma-Aldrich Chemie GmbH, Taufkirchen, Germany
Dexamethason	Sigma-Aldrich Chemie GmbH, Taufkirchen, Germany
Dimethyl sulfoxide (DMSO)	Carl Roth GmbH + Co. KG, Karlsruhe, Germany
DNTP Set	Gibco/Life Technologies/Thermo Fisher Scientific Inc., Massachusetts MA, USA
DTT	Applichem GmbH, Darmstadt, Germany
EDTA	Carl Roth GmbH + Co. KG, Karlsruhe, Germany
EGTA	Carl Roth GmbH + Co. KG, Karlsruhe, Germany
Eosin (Chromotrope II)	Alfa (Aesar), Thermo Fisher (Kandel) GmbH, Karlsruhe, Germany
Ethanol (denatured)	Brenntag GmbH, Essen, Germany

Ethanol, absolute	Merck KGaA, Darmstadt, Germany
Glucose (20%)	B.Braun, Melsungen, Germany
HEPES	Carl Roth GmbH + Co. KG, Karlsruhe, Germany
Hematoxilin (Mayer's Hämalaunsolution)	Merck KGaA, Darmstadt, Germany
IBMX	Sigma-Aldrich Chemie GmbH, Taufkirchen, Germany
Indomethazin	Sigma-Aldrich Chemie GmbH, Taufkirchen, Germany
Insulin	Sigma-Aldrich Chemie GmbH, Taufkirchen, Germany
Isoproterenol hydrochloride	Sigma-Aldrich Chemie GmbH, Taufkirchen, Germany
Isopropanol	Sigma-Aldrich Chemie GmbH, Taufkirchen, Germany
KCl	Carl Roth GmbH + Co. KG, Karlsruhe, Germany
KFl	Carl Roth GmbH + Co. KG, Karlsruhe, Germany
KH_2PO_4	Carl Roth GmbH + Co. KG, Karlsruhe, Germany
$MgCl_2$	Applichem GmbH, Darmstadt, Germany
NaCl	Carl Roth GmbH + Co. KG, Karlsruhe, Germany
Na-Desoxychelat	Carl Roth GmbH + Co. KG, Karlsruhe, Germany
NaOH	Carl Roth GmbH + Co. KG, Karlsruhe, Germany
Noradrenalin	Carl Roth GmbH + Co. KG, Karlsruhe, Germany
Nu-PAGE LDS sample buffer	Gibco/Life Technologies/Thermo Fisher Scientific Inc., Massachusetts MA, USA
Nuclease free water	Qiagen GmbH, Hilden, Germany
PFA	Carl Roth GmbH + Co. KG, Karlsruhe, Germany
PCR-Puffer without MgCl2 10x	Sigma-Aldrich Chemie GmbH, Taufkirchen, Germany
Protease Phosphatase inhibitor cocktail	Thermo Fisher Scientific Inc., Massachusetts MA, USA
Proteinase K	VWR International GmbH, Ismaning, Germany
PMSF	Carl Roth GmbH + Co. KG, Karlsruhe, Germany
Qiazol	Qiagen GmbH, Hilden, Germany
Rnase free Water	Qiagen GmbH, Hilden, Germany
Rosiglitazone	Santa Cruz Biotechnology, Dallas, (TX), USA
SDS - 20%	Applichem GmbH, Darmstadt, Germany
SERVA DNA Stain Clear G	SERVA Electrophoresis GmbH, Heidelberg, Germany
T3	Sigma-Aldrich Chemie GmbH, Taufkirchen, Germany
Triton X	VWR International GmbH, Ismaning, Germany
TRIS	Carl Roth GmbH + Co. KG, Karlsruhe, Germany
TRIS HCL	Carl Roth GmbH + Co. KG, Karlsruhe, Germany
Tween 20	Gibco/Life Technologies/Thermo Fisher Scientific Inc., Massachusetts MA, USA
Xylol	Carl Roth GmbH + Co. KG, Karlsruhe, Germany

2.1.4 Media and buffers

Table 6 List of cell culture media

Product	Supplier
DMEM, high glucose, GlutaMAX	Gibco/Life Technologies/Thermo Fisher Scientific Inc., (MA), USA
DPBS	Gibco/Life Technologies/Thermo Fisher Scientific Inc., (MA), USA
Fetal bovine serum (FBS)	Gibco/Life Technologies/Thermo Fisher Scientific Inc., (MA), USA
Penicillin-Streptomycin (10,000 U/ml)	Gibco/Life Technologies/Thermo Fisher Scientific Inc., (MA), USA
Trypsin-EDTA (0.05%)	Gibco/Life Technologies/Thermo Fisher Scientific Inc., (MA), USA

Table 7 Composition of digestion mix

Reagent	Final concentration
DMEM (pure)	100%
Collagenase IV	1%
BSA	0.1%

Culture medium (DMEM/10%FBS/1%P/S):

500 ml DMEM with 50 ml FBS and 5 ml Penicillin-Streptomycin

Induction medium:

Induction medium was prepared by supplementing culture medium with the in Table 8 described compounds.

Table 8 Induction medium compounds

Reagent	Final concentration
IBMX/ 0.5M KOH	0.5mM
Dexamethason/100% Ethanol	5µM
Indomethazin/DMSO	125µM
T3/0.1% DMSO (H_2O)	1nM
Insulin	100nM
Rosiglitazone (optional)	*1µM*

Differentiation medium:

Differentiation medium was prepared by supplementing culture medium with the in Table 9 described compounds.

Table 9 Differentiation medium compounds

Reagent	Final concentration
T3/0.1% DMSO (H_2O)	1nM
Insulin	100nM

10x PBS (pH 7.4):
1000ml ddH_2O with
- 80g NaCl
- 2.0g KCl
- 14.4g Na_2HPO_4
- 2.4g KH_2PO_4

10x TBS (pH 7.4)
1000ml ddH_2O:
- 12.1g Tris
- 85g NaCl

10x TRIS (pH 7.6)
900ml ddH_2O:
- 87.6 NaCl
- 60.5 g TRIS
- Set pH-value to 7.6 with 1M HCl
- Adjust volume to 1000l

50x TAE buffer (pH 8.5):
750ml ddH_2O:
- 242g Tris-Base
- 57.1ml acetic acid
- 100ml 0.5M EDTA
- Adjust volume to 1000ml

2%Agarose gel:
2g agarose in 100ml 1xTAE buffer

4% PFA (pH 7.4):
800ml 1xPBS:
- 4g PFA
- 1M NaOH dropwise until clear
- Adjust to 1000ml with 1xPBS

RIPA (pH 7.2):
250ml ddH_2O:
- 1.97g Tris-HCl
- 2.19g NaCl
- 93.05g EDTA
- 0.62g Na-Deoxychelat
- 2.5ml Triton-X

COX assay buffer (pH 7.4):
250ml ddH_2O:

- 1.7g Kh_2Po_4 (50mM)
- 0.19g EGTA (2mM)
- 440mg Ascorbate (10mM)

COX tissue buffer:
50ml ddH_2O:

- 0.12g HEPES (10mM)
- 0.15g KCl (40mM)
- 0.04g EGTA (2mM)
- 0.03g KFl (10mM)
- 5ml Tween (20)
- 0.5µl PMSF (2µM)

2.1.5 Primers

Table 10 List of qPCR primers

Gene-name	Forward (5'<3')	Reverse (3'<5')
Acaca	GATGAACCATCTCCGTTGGC	GACCCAATTATGAATCGGGAGTG
Adiponectin	TGTTCCTCTTAATCCTGCCCA	CCAACCTGCACAAGTTCCCTT
Agrp	GGCCTCAAGAAGACAACTGC	GCAAAAGGCATTGAAGAAGC
Asc1	AGTGTTCCAGGACACCCTTG	GGGTGGCACTCAAGAAAGAG
Atf3	GAGGATTTTGCTAACCTGACACC	TTGACGGTAACTGACTCCAGC
Cd11b	TGACCTGGCTTTAGACCCTG	ACCTCTGAGCATCCATAGCC
Cd11c	CTGGATAGCCTTTCTTCTGCTG	GCACACTGTGTCCGAACTCA
Cd206	TGATTACGAGCAGTGGAAGC	GTTCACCGTAAGCCCAATTT
Cd301	CTCTGGAGAGCACAGTGGAG	ACTTCCGAGCCGTTGTTCT
Cd68	TGTCTGATCTTGCTAGGACCG	GAGAGTAACGGCCTTTTTGTGA
Cidea	AATGGACACCGGGTAGTAAGT	CAGCCTGTATAGGTCGAAGGT
F4/80	CATAAGCTGGGCAAGTGGTA	GGATGTACAGATGGGGGATG
Fasn	AGAGATCCCGAGACGCTTCT	GCTTGGTCCTTTGAAGTCGAAGA
Foxo1	CGCCTCCTACTACTGAGC	TGTCTGTACTTAGGCGCACA
Glut4	CCGCGGCCTCCTATGAGATACT	AGGCACCCCGAAGATGAGT
Hprt	CAGTCCCAGCGTCGTGATTA	AGCAAGTCTTTCAGTCCTGTC
Il1β	GCAACTGTTCCTGAACTCAACT	ATCTTTTGGGGTCCGTCAACT
Il6	TAGTCCTTCCTACCCCAATTTCC	TTGGTCCTTAGCCACTCCTTC
Ldlr	TCAGACGAACAAGGCTGTCC	CCATCTAGGCAATCTCGGTCTC
Lepr	CGTGGTGAAGCATCGTACTG	GGGCCATGAGAAGGTAAGGT
Leptin	GGGCTTCACCCCATTCTGA	TGGCTATCTGCAGCACATTTTG
P2rx5	CTGCAGCTCACCATCCTGT	CACTCTGCAGGGAAGTGTCA
Pat2	GTGCCAAGAAGCTGCAGAG	TGTTGCCTTTGACCAGATGA
Pepck1	CTGCATAACGGTCTGGACTTC	CAGCAACTGCCCGTACTCC
Pgc1α	AGCCGTGACCACTGACAACGAG	GCTGCATGGTTCTGAGTGCTAAG
Pomc	CATTAGGCTTGGAGCAGGTC	TCTTGATGATGGCGTTCTTG
Pparγ	CCCTGGCAAAGCATTTGTAT	GAAACTGGCACCCTTGAAAA

Prdm16	CCGCTGTGATGAGTGTGATG	GGACGATCATGTGTTGCTCC
Scd1	TCCAAGCGCAGTTCCGCCAC	TGGAGATCTCTTGGAGCATGTGG
Srebp1c	GGAGCCATGGATTGCACATT	GGCCCGGGAAGTCACTGT
Srebp2	CATTCTCCAGCAGTTCCGTG	GCCCTCTCACAGTGACAGAA
Tbp	GAAGCTGCGGTACAATTCCAG	CCCCTTGTACCCTTCACCAAT
Tnfα	CAGGCGGTGCCTATGTCTC	CGATCACCCCGAAGTTCAGTAG
Ucp1	GGCCTCTACGACTCAGTCCA	TAAGCCGGCTGAGATCTTGT

2.1.6 Kits

Table 11 List of used Kits

Kit	Supplier
Adiponectin ELISA	Merck KGaA, Darmstadt, Germany
Cholesterol	WAKO Chemicals GmbH, Neuss, Germany
Leptin ELISA	Alpco Diagnostics, Salem, NH, USA
Masson's Trichrome Stain	Sigma-Aldrich Chemie GmbH, Taufkirchen, Germany
Mouse Ultrasensitive Insulin ELISA Kit	Alpco Diagnostics, Salem, NH, USA
NEFA	WAKO Chemicals GmbH, Neuss, Germany
PeqGreen	VWR Life Science Competence, Erlangen, Germany
PCR Taq Polymerase	Qiagen GmbH, Hilden, Germany
QuantiTect Reverse Transcription Kit	Qiagen GmbH, Hilden, Germany
RNA 6000 Pico Kit	Agilent, Santa Clara, CA, USA
RNeasy Mini Kit	Qiagen GmbH, Hilden, Germany
SYBR Green PCR Master Mix, 2-Pack	Gibco/Life Technologies/Thermo Fisher Scientific Inc., Massachusetts MA, USA
Triglyceride (used for plasma measurements)	WAKO Chemicals GmbH, Neuss, Germany
Triglyceride (used for tissue measurements)	BioVision Inc., Milpitas, CA, USA

2.2 Methods

2.2.1 In vivo measurements

2.2.1.1 Mouse Strains

Wild type male and female C57BL/6NCrl and C57BL/6JCrl mice were purchased from Charles River (Germany) at the age of 6 weeks. The colony of $Atf3^{fl/fl}$ and $Atf3^{fl/fl}$;$Ucp1^{cre+}$ mice was generated by crossing male C57BL/6J mice, carrying heterozygous Atf3 flox alleles ($Atf3^{fl/+}$) [166], to C57BL/6N mice with a knockin of the cre-recombinase under the UCP1 locus [167]. Tsonwin Hai, from the Ohio State University, generously provided the two founder $Atf3^{fl/+}$ mice and $Ucp1^{cre+}$ mice were kindly provided by Dr. Timo Müller, from the Institute of Diabetes and Obesity at the Helmholtz Zentrum München and were originally described in [167, 168].

2.2.1.2 Housing conditions

All mice were maintained in a conventional animal facility of the Helmholtz Zentrum München (Neuherberg, Germany) at constant ambient temperature of 22± 2°C, with 45-65% humidity and a 12h light-dark cycle. All mice received a standard chow diet (Altromin 1318, Lage, Germany) and water *ad libitum* until further dietary interventions or death (Figure 5 and Table 4). *In vivo* animal experiments were performed upon approval of the Bavarian Animal Care and Use Committee (AZ 55.2-1-54-2532-36-2012, 55.2-1-54-2532-152-13, 55.2-1-54-2532-33-2014 and 55.2-1-54-2535-172-14).

2.2.1.3 Dietary intervention studies

2.2.1.3.1 Diet-induced obesity (DIO) protocols

For the comparison of different DIO protocols regarding their potency to induce obesity, in a first step, 7 weeks old male C57BL/6JCrl and C57BL/6N wildtype mice were randomly assigned to different low-fat diets (LFD) and HFDs: 'Ssniff 60%' (60% kcal from fat (lard), E15742-34 Ssniff GmbH, Soest, Germany), 'RD 60%' (60% kcal from fat (lard), D 12492 Research Diets, New Brunswick (NJ), USA) or 'Ssniff Ctrl' (10% kcal from fat, E15745-04, Ssniff GmbH, Soest, Germany) for 16 weeks (Figure 5 and Table 4). During the further DIO protocols, 7 weeks old male and female C57BL/6N wildtype mice were randomly assigned to one of three experimental diet groups (n=6): 'Ssniff 60%' (60% kcal from fat (lard), E15742-34 Ssniff GmbH, Soest, Germany), 'Ssniff 45%' (45% kcal from fat (lard), E15744-34, Ssniff GmbH, Soest, Germany) or the LFD 'Ssniff Ctrl' (10% kcal from fat (lard) E15745-04, Ssniff GmbH, Soest, Germany) and received respective diets for 3 days up to 140 days *ad libitum*. Regarding the 3, 14, 84 and 140 days cohorts,

the experimental feeding started in October 2015 and ranged until February 2016, whereas the 56 days cohort was run from April 2016 to June 2016 (Figure 6).

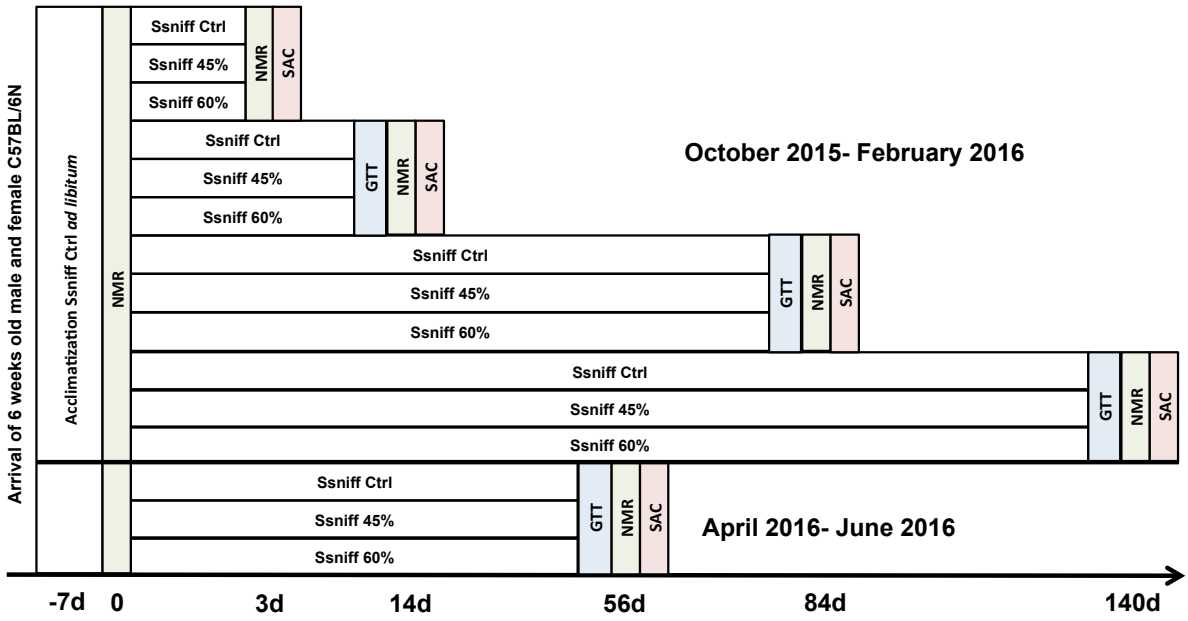

Figure 6 Scheme of cohorts running in the DIO phenotyping study.
Upon arrival, all male and female C57BL/6N mice were acclimatized to the Ssniff Ctrl diet (10%kcal from fat) for one week. Prior to starting the experimental feedings with either one of the three diets: Ssniff Ctrl, Ssniff 45% or Ssniff 60% , body composition was determined of all mice via NMR. Body mass was determined in a weekly manner. Prior to sacrificing the mice at indicated time points (3 days–140days) i.p. GTTs and NMR measurements were performed. Except the 56 days cohort, all feeding experiments took place during October 2015 and February 2016.

For the HFD-characterization of the $Atf3^{fl/fl}$;$Ucp1^{cre+}$ mice, male and female $Atf3^{fl/fl}$ (n=6 and n=10) and $Atf3^{fl/fl}$;$Ucp1^{cre+}$ (n=6 and n=10) littermates were given the RD 58% HFD (D12331, Research diets, New Brunswick (NJ), USA) for a duration of 13 weeks (Figure 5 and Table 4**).** During all the DIO studies, body weight was determined in a weekly manner, using ranger 4000 scale from OHAUS (Greifensee, Switzerland).

2.2.1.3.2 Diet induced weight-loss

8 week old male C57BL/6JCrl mice were distributed into weight-matched pairs and were randomly assigned to either the RD 58% HFD (D12331, Research diets, New Brunswick (NJ), USA, 'obese', n=47) or a LFD 'RD Ctrl' (10.5% kcal from fat, D12329, USA Research diets, New Brunswick (NJ), USA, 'lean', n=23). After 20 weeks of feeding, a group of HFD-fed mice was switched to the LFD (formerly obese**,** n=23) *ad libitum* for 7 subsequent weeks. A sub-group of the diet-switched (formerly obese) mice and age-matched lean mice were (re-) introduced to the RD 58% HFD *ad libitum* for 48h (formerly obese- HFD and lean-HFD, n=12).

2.2.1.4 NMR-Analysis

Body composition was assessed by nuclear magnetic resonance measurements (EchoMRI ®LLC, Houston, USA) before the onset of dietary interventions and prior to sacrificing the mice (Figure 6).

2.2.1.5 Glucose Tolerance Test (GTT)

Mice were fasted for six hours during the light phase and basal glucose levels (0min) were determined 6h postprandial, using a FreeStyle Freedom Lite Glucometer (Abbot, Wiesbaden, Germany). Thereafter, 2g/kg body weight glucose (20% glucose in saline) was injected intraperitoneally and blood glucose was assessed at 15, 30, 60 and 120 min past injection.

2.2.1.6 Sacrifice and tissue collection

All mice were sacrificed in the same manner with respect to the individual projects. Regarding the DIO-phenotyping study, mice were euthanized by Ketamin (100mg/kg) / Xylazin (7mg/kg), blood was taken from the vena facialis for plasma isolation and organs were isolated for further molecular and histological analysis. The $Atf3^{fl/fl}$;$Ucp1^{cre+}$ mice were sacrificed by cervical dislocation and the diet-induced weight loss mice were killed via CO_2, following a 3h fast. Blood was withdrawn from the interior vena cava and put in EDTA-coated cups on ice until further use. Blood was centrifuged (4000g, 4°C, 10min). Plasma was collected and stored at -20°C until further use. Tissues were rapidly dissected, weighed, snap-frozen on dry ice, and stored at -80°C until further analysis.

2.2.2 Ex vivo measurements

2.2.2.1 Genotyping

Tissue specimen, e.g. ear clips, were digested with 1M NaOH in a thermocycler at 95°C for 30 min under vigorous shaking (1000rpm). Subsequently, the pH was readjusted, using 50mM Tris-HCl. For genotyping the Atf3 floxed allelles, a PCR Mastermix was prepared Table 13. 21.5µl oft he *Atf3*-PCR Mastermix was added to 1µl of digested DNA and amplified following the protocol given in Table 14.

Table 12 List of primers used for genotyping.

Primer	Forward (5'<3')
Atf3 Oligo 956	TTCACTGCTAATAGCTCCTG
Atf3 Oligo 845	TTCATAGCTCAGGGAACATCGG
Atf3 Oligo 916	CAACTCCCTCTCCTCAAGTC
Ucp1cre F1	CAAGGGGCTATATAGATCTCCC
Ucp1cre R1	ATCAGAGGTGGCATCCACAGGG
Ucp1cre R2	GTTCTTCAGCCAATCCAAGGG

Table 13 *Atf3*-PCR Mastermix for genotyping

Reagent	Volume (µl)
10x PCR buffer	2
25mM MgCl2	1.5
5mM dNTP's	0.4
Primer Mix (20µM)	1
Taq Polymerase	0.2
ddH_2O	14.4
10x Coral Red Dye	2
Total	**21.5**

Table 14 *Atf3*-PCR protocol

PCR steps	Temperature (°C)	Time	Number of cycles
Denaturation	94	4 min	1
Melting	94	20 sec	35
Annealing	64	20 sec	35
Polymerisation	72	1 min	35
Polymerisation	72	2 min	1
Cooling	12	Infinite	1

For the *Ucp1*cre genotyping, 9.5µl of *Ucp1*cre-PCR Mastermix (Table 15) was added to 0.5µl of DNA and amplified in a PCR cycler, following the protocol given in Table 16.

Table 15 *Ucp1* cre-PCR Mastermix

Reagent	Volume (µl)
10x PCR Mix Platinum Green	5
Primer (10µM)	0.5
ddH_2O	4
Total	**9.5**

Table 16 *Ucp1* cre PCR protocol

PCR steps	Temperature (°C)	Time	Number of cycles
Denaturation	95	5 min	1
Melting	95	45 sec	35
Annealing	58	45 sec	35
Polymerisation	72	45 sec	35
Polymerisation	72	10 min	1
Cooling	12	Infinite	1

Amplified DNA was loaded on a 2% agarose gel containing DNA stain clear and run at 150V for 45min. *Atf3* floxed alleles were detected at a size of 347bp and wildtype bands observed at a size of 189bp. Sometimes, recombination was visible with an additional band showing up at 242bp (Figure 7). *Ucp1*cre+ bands were detected at a size of 336bp and *Ucp1*cre- bands were observed at a size of 554bp **(**Figure 7).

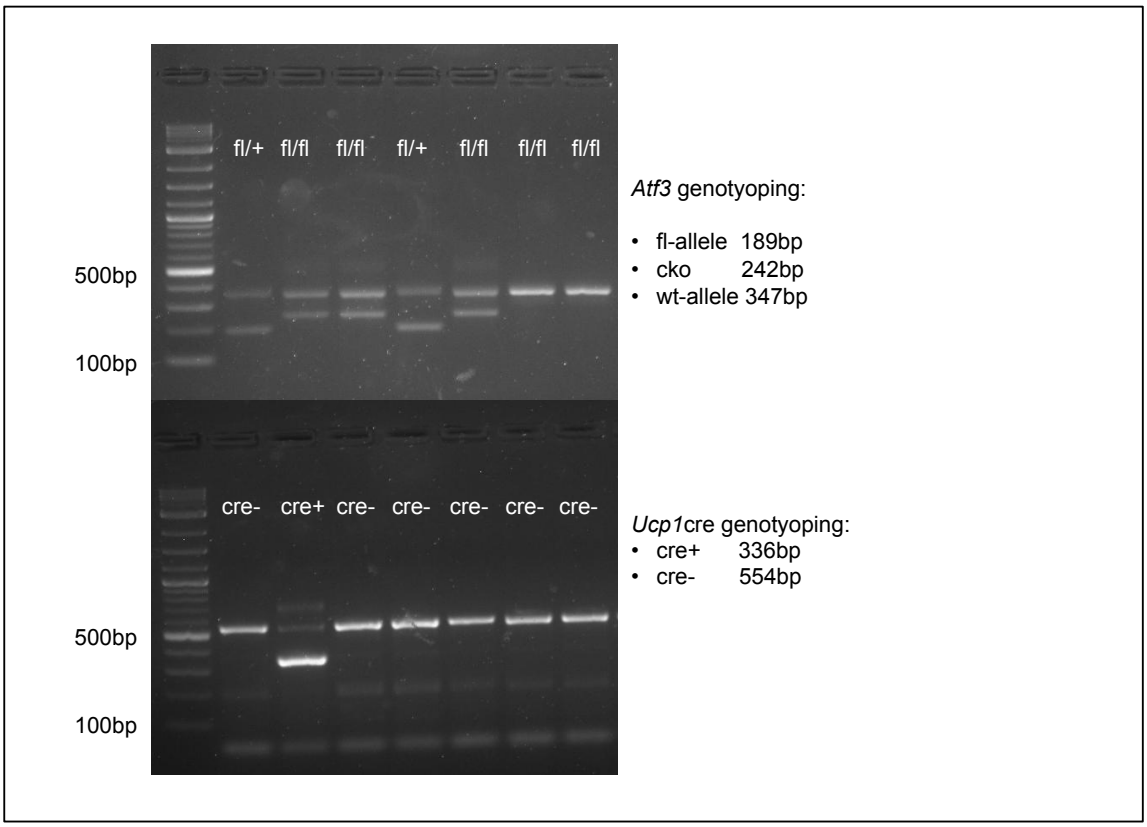

Figure 7 Example of *Atf3* flox and *Ucp1*cre genotyping loaded on a 2% agarose gel.

2.2.2.2 Metabolic measurements

Plasma and liver triglycerides, cholesterol and non-esterified free fatty acids (NEFA) were determined via the LabAssay™ kits (WAKO Chemicals, Neuss, Germany), according to the manufacture's instruction. Plasma insulin and leptin were measured using the Ultrasensitive insulin and leptin ELISA Kits (ALPCO Diagnostics, Salem, USA). Plasma adiponectin was determined using the MOUSE Adiponectin ELISA Kit (Merck Millipore, Darmstadt, Germany) according to the manufacture's instructions.

2.2.2.3 Hepatic triglyceride content

Hepatic triglyceride content was determined in 40mg of grinded liver tissue and extracted using the LabAssay™ Triglyceride Kit from WAKO Chemicals GmbH and BioVision (Milpitas, USA) according to the manufacturer's instructions.

2.2.2.4 Cytochrome C Oxidase (COX)- activity measurements

30mg of BAT was homogenized in COX-tissue buffer (2.1.1), using a Potter-type homogenizer and subsequently sonicated with several short bursts, following previous publication [169]. 2ml of COX-Assay buffer was transferred to the O2k Oxygraph chambers and suspended with 40µM Cytochrome C, 5mM ADP and 2µM oligomycin. Tissue homogenate was added in steps of 2.5µl and oxygen consumption as recorded in the Oroboros instruments (Innsbruck, Austria) at 37°C. Protein content of the homogenized BAT was determined via Bradfordassay (Sigma Aldrich, Taufkirchen, Germany) and COX activity was determined from 120µg of homogenized BAT and normalized to mg BAT tissue.

2.2.2.5 Histology

For histological analysis, pieces of scWAT, gWAT and liver were taken and fixed in 1ml of 4% PFA (Carl Roth, Karlsruhe, Germany) in PBS at room temperature for 24h and restored in 1ml 70% ethanol until further analysis. Ethanol fixed tissues were dehydrated in an ascending row of ethanol and xylene (90% ethanol, 2x 100% ethanol, each for 1h and subsequently 3x xylene, each for 10min). Subsequently, tissues were saturated with paraffin (2x 1h and overnight at 65°C) and embedded with paraffin (Leica, Germany) on the next day. Embedded tissues were cut into 5µm sections using a microtome (Leica, Germany). Sections were floated into a water bath (37°C; Thermo Haake, Germany), taken up on microscopic slides and oven-dried (60°C, 10min, Binder GmbH, Germany).

2.2.2.5.1 H&E staining

Tissue sections were stained with Hematoxylin and Eosin. The sections were cleared in xylene (2x 2min) and deparaffinized in a descendent row of ethanol (100%-70% each 2min). After washing with ddH_2O (2min), the sections were stained with Hematoxylin and Eosin (30sec.) and subsequently washed under running tap water (2min). Thereafter, the tissue sections were dehydrated through an ascendant row of ethanol (96%-100% each 2min) and cleared in xylene (2x 5min). Immediately after staining the sections were mounted using Roti-Histokit (Carl Roth, Germany), coverslipped (Medite Medizintechnik, Germany) and air-dried.

2.2.2.5.2 Masson's trichrome staining

To assess the level of hepatic fibrosis, Masson's trichrome stainings were performed on 5µm thick, paraffin embedded liver tissue sections (n=5) using the trichrome stain (Masson)-Kit (HT15) from Sigma Aldrich according to the instructions.

2.2.2.5.3 Grading of fibrosis and steatosis

Fibrosis (0=no fibrosis, 6=cirrhosis) and steatosis grading (1=<5% of liver cells involved, 4=>66% liver cells involved) were performed according to standard guidelines [170]. The histological score was calculated by summing up the assessed fibrosis score and histological score.

2.2.2.5.4 Adipocyte size measurements

H&E stained sections of scWAT and gWAT were examined under a light microscope (Zeiss Axioscop 40, Germany, 200x magnification). Per tissue, pictures from three different areas were taken (Zeiss AxioCam MRC, 200 x magnifications). Adipocyte cell size was determined by measuring the scope of 20 to 25 randomly picked adipocytes per area of the respective adipose tissue using AxioVision Rel.4.8. Mean adipocyte cell sizes ± SD (μm^2) were calculated for each area, tissue, animal and experimental group. Adipocyte cell size distributions are presented as relative % per BIN ($2000\mu m^2$).

2.2.3 In vitro analysis

2.2.3.1 Isolation of primary cells

2.2.3.1.1 Digestion of adipocytes

7 week old $Atf3^{fl/fl}$ and $Atf3^{fl/fl}$;$Ucp1^{cre+}$ were sacrificed by cervical dislocation and BAT and scWAT were excised and subsequently stored in 10cm dishes with ice cold PBS. The tissues were cut into tiny pieces, using two razor blades. Cut tissues were digested in 5ml (BAT) or 10ml (scWAT) of in Table 7 described digestion mix, using a thermocycler at 1000rpm, 37°C, 30min.

2.2.3.1.2 Isolation of BAT adipocytes

Digested BAT was filtered through a 250µm mash into a 50ml falcon and washed with 5ml of ice cold PBS. The digested mix was left to stand for 15min, to allow adipocytes floating to the top. Subsequently, the layer of adipocytes was removed with a cut 1ml pipette tip and added to 1ml of Qiazol (Qiagen, Hilden, Germany) for subsequent RNA-isolation.

2.2.3.1.3 Isolation of preadipocytes

Digested BAT and scWAT was filtered through a 100µm yellow gauche into a 15ml falcon and the filter was washed with 5ml of ice cold PBS. The suspension was centrifuged (800g, RT, 5min). The supernatant was removed and the pellet was re-suspended in 5ml of culture medium and once more centrifuged (800g, RT, 5min). The supernatant was again removed and the pellet re-suspended in 3ml of culture medium and eventually plated on a 6-well plate.

2.2.3.2 Culturing of preadipocytes

Preadipocytes were maintained in culture medium (see chapter 2.1.4) at 37°C in a humified 5% CO_2, 95% air environment. The culture medium was changed every other day and cells were sub-cultured when reaching a confluence of 80-90%. For the latter, cells were washed with PBS, detached during a 3min incubation with trypsin and re-suspended in DMEM. After removal of the supernatant, the cells were re-suspended with fresh culture medium and splitted in a desired ratio.

2.2.3.3 Differentiation of preadipocytes

For the differentiation into mature adipocytes, $1x10^4$ preadipocytes were seeded to 12-well plate and the medium was changed every two days, until a confluence of 90%. The differentiation was induced by adding 1ml of induction mix (Table 8) to each well (Day 0). For the induction of subcutaneous preadipocytes, additionally, 1µM rosiglitazone was added. After two days, the induction medium was replaced by freshly prepared differentiation medium (Table 9) and this medium was changed every other day until the cells were fully differentiated.

2.2.3.4 Isoproterenol stimulation

Fully differentiated brown adipocytes were stimulated with 0.5µM isoproterenol for 2h. The medium was not changed in control treated cells. After 2h, the cells were washed with PBS, lyzed and frozen until further analysis.

2.2.4 Standard molecular biological techniques

2.2.4.1 Protein isolation

Tissues were roughly grinded in liquid nitrogen, aliquoted and stored at -80°C until further use. 20mg (BAT, liver) to 100 mg (gWAT, scWAT) of grinded tissue were homogenized in 1ml of freshly prepared RIPA-buffer, containing protease- and phosphatase inhibitor cocktail, by using the tissue lyzer (Tissue Lyzer II, Qiagen) two times for 1.5min at 28HZ. Supernatants were taken after two subsequent rounds of centrifugation (18600g, 4°C, 30min). Isolated protein homogenates were quantified using Bradfordassay and stored at -20°C until further use.

2.2.4.2 RNA isolation

In liquid nitrogen grinded tissues of BAT (20mg), WAT (80-100mg), and liver (20mg) were homogenized in 1ml of Qiazol and whole, isolated hypothalami and hearts were grinded in RPE buffer containing 2M β-mercaptoethanol for two times (1.5min at 28HZ) using the tissue lyzer. After an incubation (RT, 5min), tissue homogenates were centrifuged (2500g, 4°C, 5min) and the supernatant was transferred into a new RNAse-free cup. Subsequently, phase separation of the supernatant was induced by adding 200µl chloroform, vortexing and centrifugation (4°C, 18400g, 20min). 350µl of the RNA containing clear phase was further added to 70% Ethanol, mixed well and pipetted to a spin column of the RNeasy Mini Kit (Qiagen, Germany) and RNA isolation was further processed according to the manufacture's instruction. RNA yield was determined using the Nanodrop (Nanodrop 2000, Thermo Scientific).

2.2.4.4 cDNA-Synthesis and qPCR

1µg of RNA was reversely transcribed in to cDNA using QuantiTect Reverse Transcription Kit (Qiagen) according to the manufacture's protocol. Real-time quantitative poly chain reaction (RT-qPCR) was performed using SYBRgreen reagents and run on ViiA^{TM} 7 Real-Time PCR System from Applied Biosystems. Primer sequences are enlisted in Table 10. Differential expression levels were calculated via the ΔΔct method and are expressed as relative mRNA levels to the housekeeping-gene or fold change (FC) to the control group [171].

2.2.4.5 RNA integrity measurements

The integrity of the isolated RNA (RNA integrity number (RIN)) was determined using the Agilent RNA 6000 Pico kit in the Agilent 2100 Bioanalyzer, according to the manufacturer's instructions. Briefly, a previously prepared gel was mixed with 65µl of the blue RNA 6000 pico dye. After centrifugation (13000g, RT, 10min), a RNA 6000 pico chip was loaded at a priming station with 27µl of the gel-dye mix. Subsequently, the chip was loaded with 9µl of conditioning solution and 60µl

of the RNA 6000 Pico marker. Finally, 1µl of the ladder and each sample (2ng/µl) was applied to the gel. After vortexing the chip (2400rpm, RT, 1min), it was run in the bioanalyzer Agilent 2100 (AlphaMetrix Biotech, Germany), according to the manufacturer's instruction. Only high quality RNA (RIN > 7) was used for the microarray analysis and RNA-sequencing [18].

2.2.4.6 Expression profiling

Microarrays were performed by Dr. Martin Irmler from the Institute of Experimental Genetics at the Helmholtz Zentrum München. Total RNA (30ng) was amplified using the Ovation PicoSL WTA System V2 in combination with the Encore Biotin Module (Nugen, San Carlos, USA). Amplified cDNA was hybridized on Affymetrix Mouse Gene ST 2.0 arrays containing about 35,000 probe sets. Staining and scanning (GeneChip Scanner 3000 7G) was done according to the Affymetrix expression protocol including minor modifications as suggested in the Encore Biotion protocol [18].

2.2.4.7 RNA seq analyses

RNA seq analyses were performed by Dr. Elisabeth Graf and Thomas Schwarzmayr from the Institute of Human Genetics of the Helmholtz Zentrum München and were evaluated by Dr. Dominik Lutter from the Institute of Diabetes and Obesity, using DESeq2 analyses, as previously described [172]. Thereby, the default settings were used and the adjusted p value was <0.01.

2.2.5 Statistical analyses

Microarrays were analyzed by Dr. Martin Irmler from the Institute of Experimental Genetics, by using the Expression Console (v.1.4.1.46, Affymetrix) for obtaining annotated normalized RNA gene-level data (standard settings including median polish and sketch-quantile normalisation). Statistical analyses were performed by utilizing the statistical programming environment R [173], implemented in CARMAweb (CARMAweb version 1.5.18 - uses R version 2.11.0 together with Bioconductor version 2.6; [174]). Genewise testing for differential expression was done employing the limma *t*-test and Benjamini-Hochberg (BH) multiple testing correction (FDR<10%). Sets of regulated genes were defined by p<0.01 (limma *t*-test) or FDR<10% (BH) and further filtered for fold-change (>1.2x for liver and >1.3x for gWAT) and average expression in at least one group of the dataset (>8 for liver and >16 for gWAT). Heatmaps were generated with the R script pheatmap. In case of several probe sets for the same gene, only the one with the highest ratio is shown. The pathway analyses were generated through the use of QIAGEN's Ingenuity Pathway Analysis (IPA®, QIAGEN Redwood City, www.qiagen.com/ingenuity). The Fisher's Exact Test was used to define sets of enriched canonical pathways (p<0.05) or biological functions (p<0.01) [18]. Data are presented as mean ± standard error of the means (SEM), unless stated differently in the figure legend. Normality was tested by D'Agostino & Pearson omnibus, Shapiro-Wilk and KS normality test. For normally distributed

data, statistical significance was determined by unpaired Student's t-test or, for multiple comparisons, using One- or Two-Way ANOVA, followed by Tukey's Multiple Comparison's Test, if not stated otherwise in the respective figure legends. Nonparametric data was tested for statistical significance by using Kruskall-Wallis test followed by Dunn's Multiple Comparison's Test. Differences reached statistical significance with $p<0.05$(*), $p<0.01$(**), $p<0.001$ (***) and $p<0.0001$(****).

2.2.6 Literature survey

Prior to planning the experimental designs for the DIO phenotyping studies, a small literature survey was performed, reviewing at that time high-impact journal publications for used DIO protocols. Searching the "pubmed.gov" database from the National Center for Biotechnology Information (https://www.ncbi.nlm.nih.gov/) for 2013's publications, filtered by the terms "diet-induced obesity" AND "high-fat diet" AND "2013" AND "mice" AND "obesity" in total 472 publications were found, from which 402 were actually published in the year 2013. Restricting the identified results to high-impact journal publications (impact factor >10 according to the 2013 *Thompson Reuters Impact Factor*), in total 19 reports (Appendix) were analyzed regarding their methodology. Key parameters were age, gender and strains of the mice as well as feeding durations and composition of the HFDs used.

3. Results

3.1 The phenotype of diet-induced obesity (DIO) is variable

To extend the knowledge of factors impacting the onset and development of DIO, HFD- feeding experiments, differing in feeding durations and (high fat) diets, were performed in male and female mice from the C57BL/6N and C57BL/6J background.

3.1.1 DIO experimental set ups are heterogeneous

Prior to performing HFD-feeding studies in the year 2014, a small literature research was carried out in order to learn about at that time used DIO protocols. According to this literature research, in 2013, the C57BL/6 mouse was the most commonly used model in metabolic research (Figure 8A). Often, studies failed to indicate sub-strains of the C57BL/6 mice or even did not state the background, at all. However, when indicated, there was a clear preference of the C57BL/6J sub-strain, while only few studies performed their DIO experiments with C57BL/6N mice (Figure 8A). Another main finding of this small literature survey was that females were generally underrepresented in DIO studies (Figure 8B). Strikingly, despite the well-known interaction of sex hormones and metabolism, 29% of the studies did not indicate the gender of the mice used (Figure 8B). In most of the analyzed studies, the age of the mice at the onset of feeding varied between 6 to 8 weeks (Figure 8C). Moreover, the duration of high fat feeding was highly variable, ranging from 8 to 182 days, with a peak at 84 and 98 days of feeding (Figure 8D). Concerning the diet, the 60% kcal from fat HFD emerged as the most popular food to induce obesity (Figure 8E), followed by diets where 45% of kcal was derived from fat.

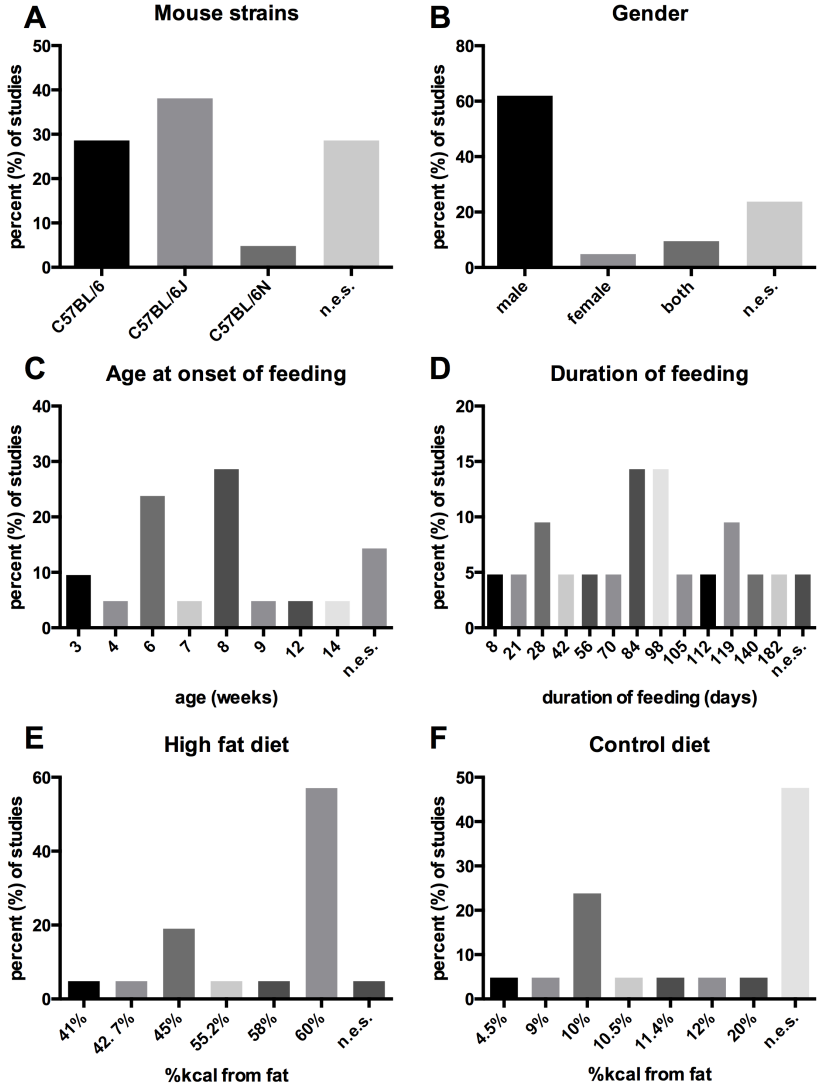

Figure 8 Results of the literature research.
(A) Mouse strains, (B) gender distribution among the mice studied, (C) age at the onset of feeding, (D) duration of feeding, (E) high fat diets and (F) control diets used, in selected DIO studies (n=19-21).

Importantly, most of implicated studies failed to indicate or did not use proper control diets (Figure 8F). Indicating a general substantial variety in DIO protocols, that lead to results, which might not be comparable or reproducible.

3.1.2 C57BL/6N and not C57BL/6J mice are more susceptible to weight gain

At 7 weeks of age and prior to any experimental feedings with HFD or control diets, body weights and body composition of male C57BL/6NCrl and C57BL/6JCrl were determined. Thereby, C57BL/6NCrl mice exhibited lower lean- and body mass than age-matched C57BL/6JCrl mice (Figure 9).

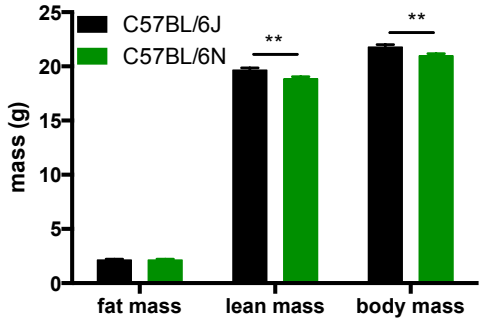

Figure 9 Male C57BL/6N mice exhibit lower body mass than male C57BL/6J mice at 7 weeks of age.
Body composition including fat-, lean- and total body mass of 7 weeks old, male C57BL/6N and C57BL/6J mice (n=18). Significance was tested via Two-Way ANOVA followed by Sidak's Multiple comparison test.

Feeding the Ssniff 60% HFD rapidly increased body weight of both male C57BL/6J and C57BL/6N mice, compared to mice, fed the Ssniff Ctrl LFD (Figure 10A). Thereby, the onset of weight gain was detected in C57BL/6N mice, already starting from week three (C57BL/6N Ctrl vs. C57BL/6N 60%: 23.53±0.34 vs. 27.40±0.55, $p<0.05$), whereas the onset of weight gain in C57BL/6J mice was first noticed after 5 weeks of feeding (C57BL/6J Ctrl vs. C57BL/6J 60% 27.84±0.50g vs. 31.83±0.90g). After 12 weeks of feeding, C57BL/6N mice on the 60% HFD displayed significantly more body mass than the C57BL/6J mice (44.04±1.05g vs. 40.13±2.08g, $p<0.05$). This difference in body weight between the C57BL/6 substrains was still present after 16 weeks of feeding and based on increased fat- and not lean mass of C57BL/6N mice (Figure 10A and B). Interestingly, at 23 weeks of age and 16 weeks of experimental feeding, also control fed C57BL/6N mice showed an increased fat mass, compared to C57BL/6J mice. Prolonged HFD-feeding is known to deregulate glucose homeostasis, which can be assessed by fasting circulating glucose levels and glucose tolerance tests. Here, 16 weeks of Ssniff 60% HFD feeding induced fasting hyperglycemia in C57BL/6J but not C57BL/6N mice (Figure 10C), supporting the previously described notion that C57BL/6J mice are more susceptible to DIO [109]. Consistently, 16 weeks of 60% HFD feeding caused an impaired glucose tolerance in both C57BL/6 substrains (Figure 10D). Regarding the C57BL/6J mice, this decreased glucose tolerance was however revoked when basal glucose values were subtracted (Figure 10E). Interestingly, C57BL/6J mice on the control diet also showed impaired glucose tolerance compared to C57BL/6N mice on the control diet ($p<0.05$) (Figure 10C). Indicating that in our experimental set up, C57BL/6N mice showed slightly more weight gain than C57BL/6J mice and decreased glucose tolerance, but the latter exhibited more impaired hyperglycemia in basal conditions.

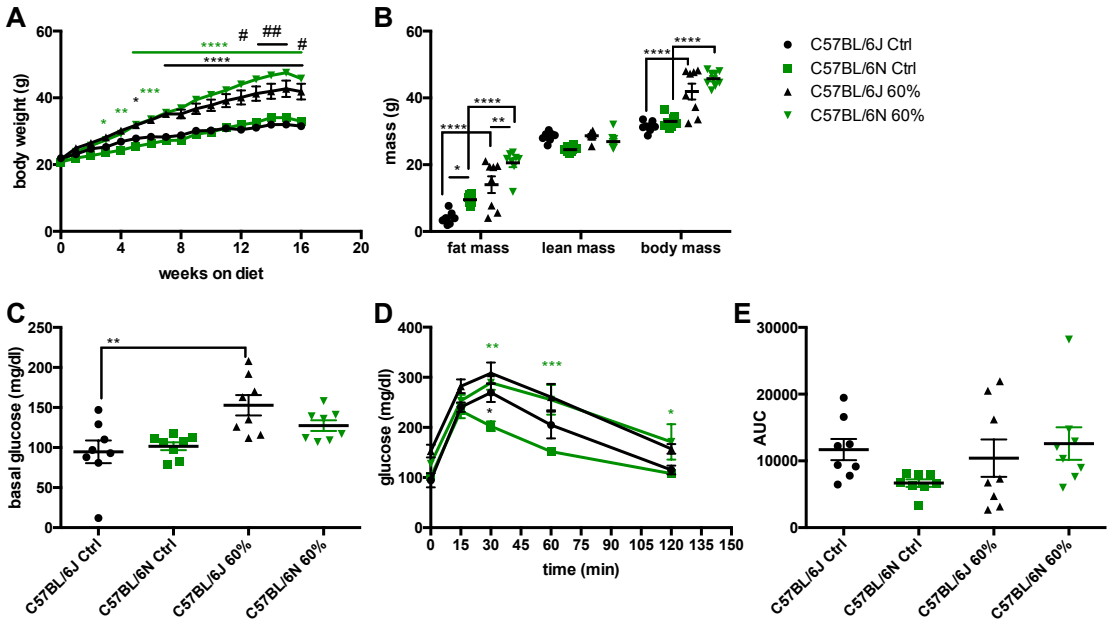

Figure 10 DIO phenotype after 16 weeks of 60% HFD feeding is more pronounced in C57BL/6N than C57BL/6J mice.
(A) Weight course of male C57BL/6N and C57BL/6J mice during 16 weeks of feeding either a 60% HFD (60% E15742-34 Ssniff, Germany) or the matched control LFD (Ctrl E15745-04, Ssniff Germany) n=(8). (B) Body composition of male C57BL/6N and C57BL/6J after 16 weeks of feeding the experimental diets (n=8). (C) Basal glucose levels of 6h fasted male C57BL/6N and C57BL/6J after 16 weeks of feeding the experimental diets (n=8). (D) I.p. Glucose tolerance test (2mg glucose/g body weight), of male C57BL/6N and C57BL/6J after 16 weeks of feeding the experimental diets (n=8). (E) Basal glucose subtracted area under the curve (AUC) calculated from i.p. GTT in (C) (n=8). Statistical significance was determined via One-Way ANOVA (C) and (E) or Two-Way ANOVA (A), (B) and (D) followed by Tukey's multiple comparisons test. Significance was indicated with black asteriks (*) regarding the comparison 'C57BL/6J Ctrl' vs. 'C57BL/6J 60%', in green asteriks (*) regarding the comparison 'C57BL/6N Ctrl' vs. 'C57BL/6N 60%' and in pounds (#) regarding the comparison 'C57BL/6J 60%' vs. 'C57BL/6N 60%'.

3.1.3 No difference in the weight-inducing potential of the 60% HFD from Ssniff and Research Diets

In parallel to investigating, which C57BL/6 substrain was more susceptible to DIO, it was further assessed whether the manufactural source of diets influenced the onset of DIO. Therefore, a different cohort of male, 7 weeks old C57BL/6N mice was fed a 60% HFD from Research Diets (Research diets, New Brunswick (NJ), USA) for 16 weeks (Table 4 and Figure 5).

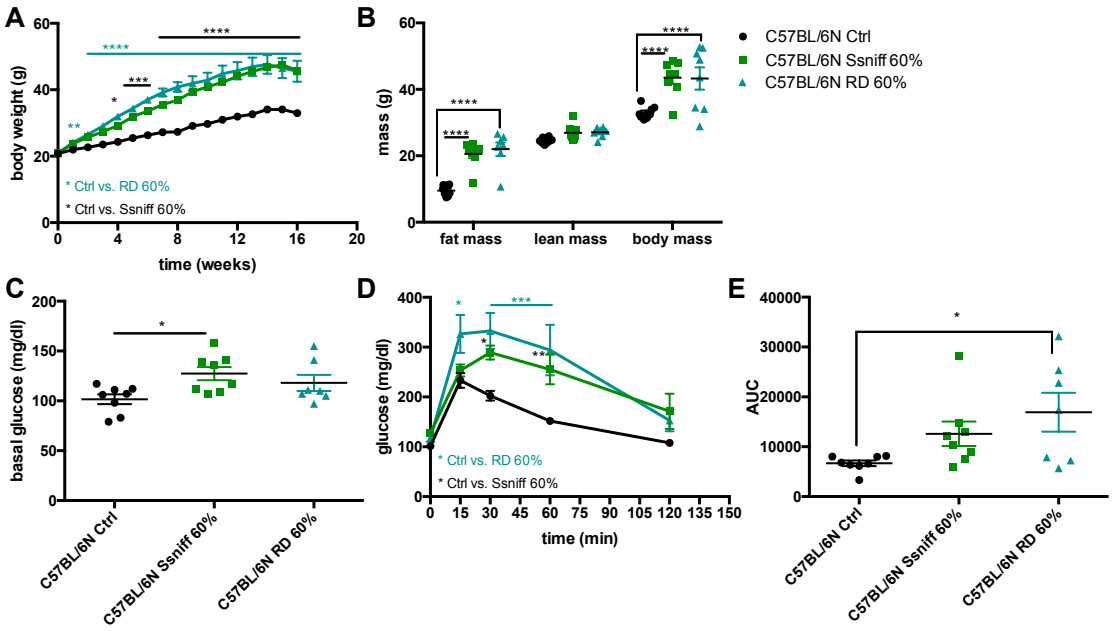

Figure 11 DIO phenotype of male C57BL/6N mice after 16 weeks of feeding a 60% HFD is not impacted by the source of HFD manufacturers.
(A) Body weight course of male C57BL/6N mice given a 60% HFD, either derived from Ssniff Germany (Ssniff 60%, E15742-34 Ssniff, Soest, Germany) or Research diets (RD 60%, RD 12492 Research Diets, New Brunswick (NJ) USA) or a matched control diet (Ctrl, E15745-04, Ssniff, Soest, Germany) (n=8). (B) Body composition of male C57BL/6N after 16 weeks of feeding the experimental diets (n=8). (C) Basal glucose levels of 6h fasted male C57BL/6N mice after 16 weeks of feeding the experimental diets (n=7-8). (D) I.p. GTT (2mg glucose/g body weight) of male C57BL/6N mice after 16 weeks of feeding the experimental diets (n=7-8). (E) Basal glucose-subtracted area under the curve (AUC), calculated from i.p. GTT in (D). Statistical significance was determined via One-Way ANOVA (C) and (E) or Two-Way ANOVA (A), (B) and (D) followed by Tukey's multiple comparisons test. * in turquoise are indicating statistical significance between the 'Ctrl' and 'RD 60%' group, * in black are indicating statistical significance between the 'Ctrl' and 'Ssniff 60%' group.

In line with what has been shown before (Figure 10), 16 weeks of feeding the 60% HFD from Research diets (RD 60%) increased the body mass of male C57BL/6N mice to the same extent as the 60% HFD from Ssniff (Ssniff 60%) (Figure 11A), despite an earlier onset of weight gain, already after 3 weeks of HFD feeding, when compared to control diet fed mice (C57BL/6N RD 60%: 23.53±0.34g vs. C57BL/6N Ctrl: 29.06±0.63g, $p<0.05$). Apart from this, fat mass was increased by either of the HFD feedings, with no difference due to the manufactural source (Figure 11B). Moreover, basal glucose levels were only significantly increased in C57BL/6N mice which were given the 60% HFD from Ssniff and not the 60% HFD from Research Diets, despite a trend in the latter (Figure 11C). Feeding both HFDs for 16 weeks decreased glucose tolerance, whereby no difference in glucose tolerance was found between either of the 60% HFDs Figure 11D. The calculated basal glucose subtracted area under the curve was significantly augmented due to feeding the 60% HFD from Research diets (Figure 11D and E). As there were no significant differences in the weight inducing potential between the two HFDs, it was decided to perform the following DIO experiments of chapter 3.1.4 in C57BL/6N given different types of Ssniff HFDs, which were varying in their fat contents.

3.1.4 Differences in the DIO phenotype, due to gender, HFD composition and feeding durations

Next, the development of DIO in mice, which were housed in the same facility, but were exposed to different, most frequently used high-fat diets (HFDs), for various experimental durations, was characterized. In detail, male and female C57BL/6N mice, at the age of 7 weeks, were given either a Ssniff 60%- or Ssniff 45% kcal of fat containing HFD or a matched control LFD (10% kcal from fat) *ad libitum* for five different periods, ranging from 3 days to 140 days (n=6 per sex, diet and time point) (Figure 6 and Table 4).

The individual body weight curves of cohorts of mice of the same sex and on the same diets diverge from each other, indicating a high inter-study variability, especially present in female mice (Figure 12A and B). The individual body weight curves of the cohorts of mice of the same sex and on the same diet were grouped for and thereby, a time-dependent increase in body mass was observed in male and female mice, given either of the HFDs (Figure 12C and D).

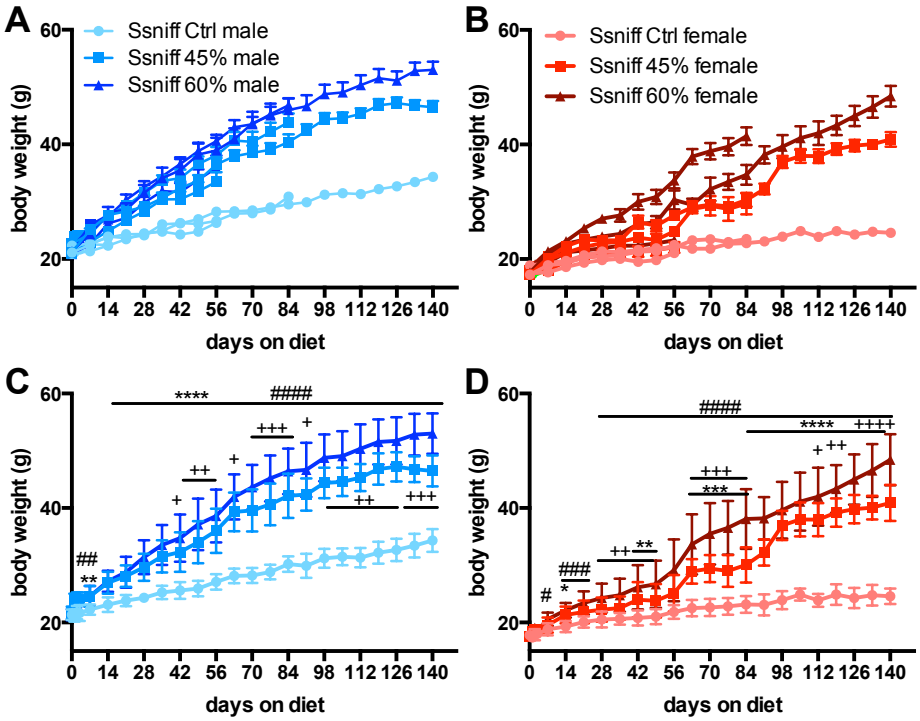

Figure 12 Diet-induced weight gain in male and female C57BL/6N mice is influenced by various feeding conditions.
Individual weight curves of male (A) and female (B) C57BL/6N mice, which were given either a 60% HFD (60% kcal from fat (lard), E15742-34 Ssniff GmbH, Soest, Germany), 45% HFD (45% kcal from fat (lard), E15744-34, Ssniff GmbH, Soest, Germany) or a low-fat containing control diet (E15745-04, Ssniff GmbH, Soest, Germany) for 3, 14, 56, 84 or 120 days (n=6 per diet and time point). Overlay of the individual curves (shown in (A) and (B)), of male (C) and female (D) C57BL/6N mice. Data are presented as mean ± SEM ((A) and (B)) or mean ± SD in ((C) and (D)). Statistical significance was calculated via Two-Way ANOVA followed by Tukey's multiple comparisons test. Black asteriks (*) are indicating statistical significance in Ssniff Ctrl vs. Ssniff 45% HFD-fed mice, pounds (#) are indicating statistical difference between Ssniff Ctrl and Ssniff 60% HFD, and crosses (+) are indicating statistical significance between Ssniff 45% and Ssniff 60% HFD groups.

The onset of obesity was not as pronounced in female mice as in male C57BL/6N mice, indicating that throughout the cohorts male mice were more susceptible to DIO than female mice (Figure 12A and B), which was already known [111, 112]. Interestingly, the higher fat content of the 60% HFD did not immediately impact the level of weight gain. Instead, the higher fat content only fueled accelerated body mass increase in comparison to the 45% HFD from 28 days on in female (Ssniff 60%: 24.30 ± 0.60g vs. Sniff 45%: 22.25 ± 0.51 g), and 56 days on in male (Ssniff 60%: 38.61 ± 1.12g vs. Ssniff 45%: 36.02 ± 0.91g) C57BL/6N mice (Figure 12C and D). This is suggesting that the fat content of the HFD impacts the severity of body mass gain only during long-term feeding conditions. Moreover, male mice on the control diet gained a substantial amount of body weight in comparison to female mice (male Ctrl Δ140days: 13.20 ±1.92g vs. female Ctrl Δ140days: 7.33g ± 0.72g, $p<0.0001$) (Figure 13A and B).

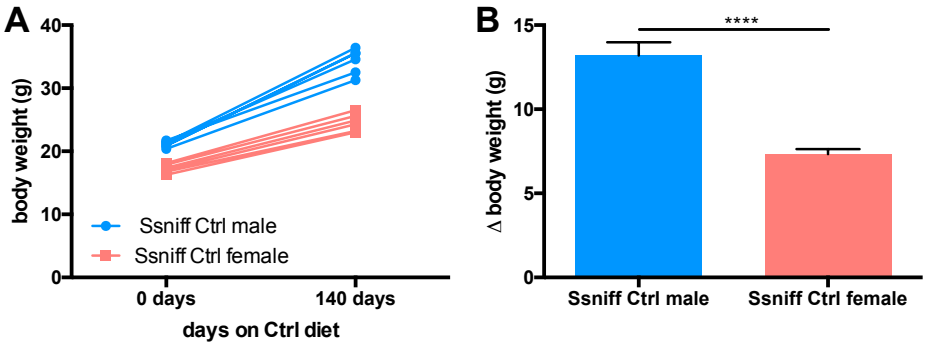

Figure 13 Control diet increases body weight of male and female C67BL/6N mice within 140 days of feeding.
(A) Body weights of male and female C57BL/6N before (0 days) and after (140 days) 140 days of Ssniff Ctrl feeding (n=6). (B) Body weight gain of male and female C57BL/6N within 140 days of Ssniff Ctrl feeding (n=6). Statistical significance was calculated via Student's t-test and indicated via asteriks (*).

Body composition analyses prior to sacrificing the mice at the respective study end points displayed that the time-dependent gain in body weight was paralleled by an increase in body fat mass, which was already present in the 3days cohort in male (Figure 14C) but became only significant in the 84days cohort in female mice and (Figure 14 D).

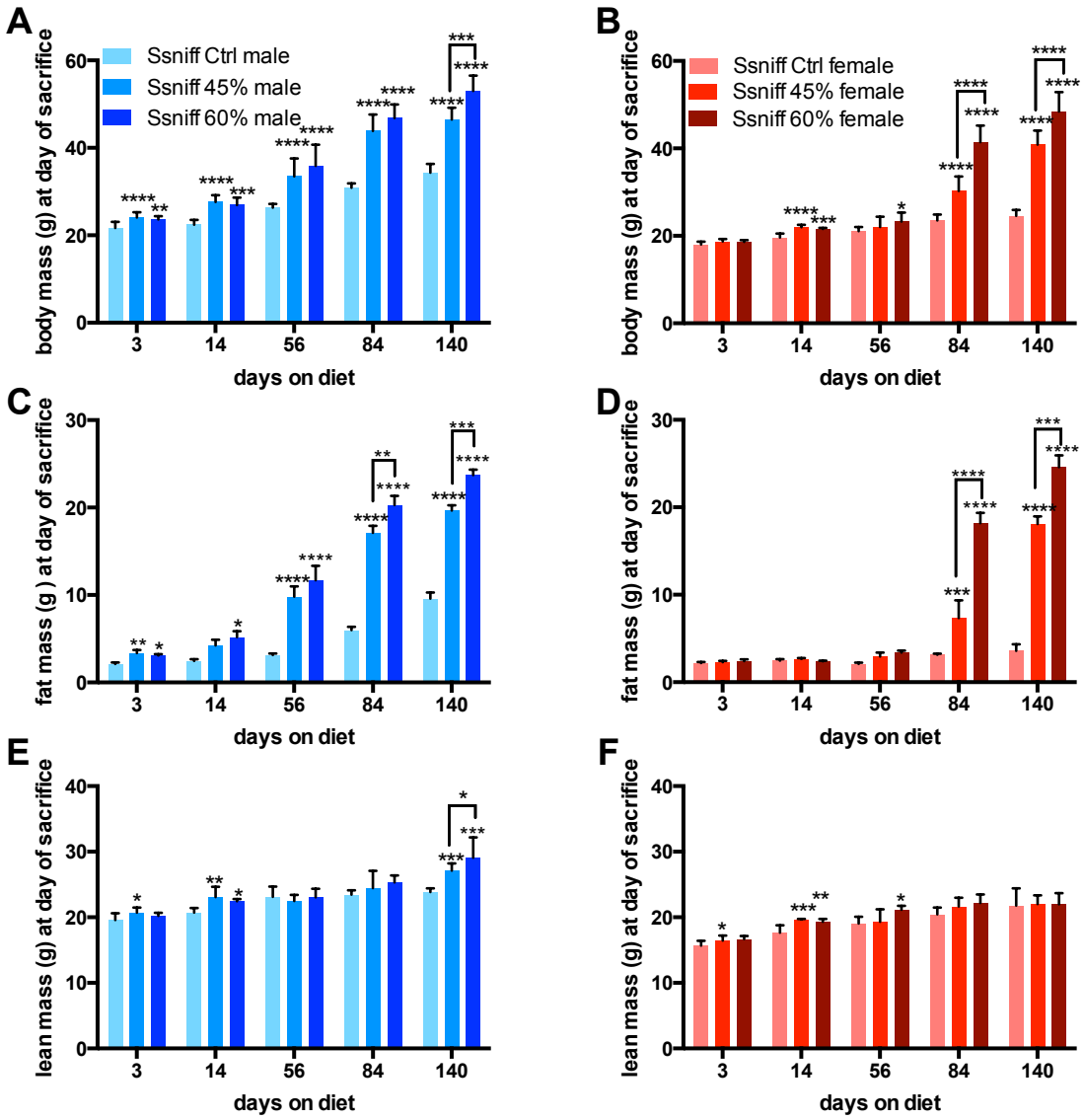

Figure 14 The gain of fat mass is more impacted by the HFD composition in female than in male C57BL/6N mice. Body mass, fat mass and lean mass of male ((A), (C) and (E)) and female ((B), (D) and (F)) C57BL/6N mice of the respective feeding groups at the days of sacrifice (n=6). Statistical significance was calculated by Two-Way ANOVA followed by Tukey's multiple comparisons test. Statistical significance is indicated with asterisks (*) and refers to the comparison of HFD vs. Ctrl, unless supported by a line.

In line with the body weight data, the 60% HFD was more potent in elevating fat mass than the 45% HFD, regarding both genders (Figure 14C and D). Yet, HFD-specific differences manifested only in the 84 days cohort and were absent at earlier study end points (Figure 14C and D).

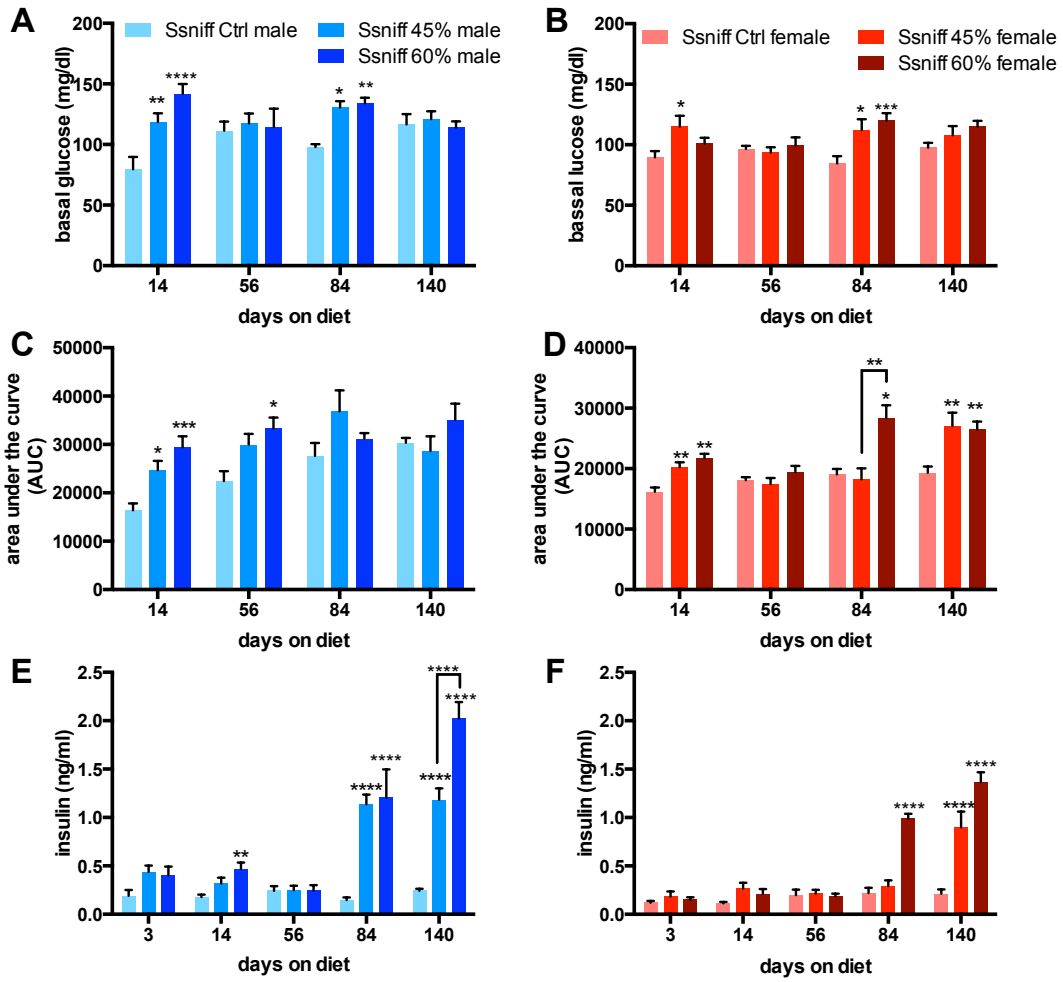

Figure 15 Hyperinsulinemia manifests with longer feeding durations.
Basal glucose levels, AUC of performed i.p. GTT and insulin levels of male ((A), (C) and (E)) and female ((B), (D) and (F)) C57BL/6N mice of the respective feeding groups at the end of the indicated feeding durations. Statistical significance was calculated by Two-Way ANOVA followed by Tukey's multiple comparisons test. Statistical significance is indicated with asterisks (*) and refers to the comparison of HFD vs. Ctrl, unless supported by a line.

Monitoring the blood glucose at selected study end points, a biphasic increase in fasting glucose levels after 14 days and 84 days of 45% and 60% HFD-feeding was detected, regarding both genders (Figure 15A and B). Suggesting that hyperglycemia can already be detected after short-term HFD. Analyzing the area under the curve (AUC) of glucose tolerance tests, an increase in glucose intolerance in male and female mice was detected, which was influenced by the duration of HFD-feeding, but not by the kind of HFD the mice were receiving (Figure 15C and D). Additionally, a time-dependent increase of glucose intolerance in male mice on the control diet was found, which was not seen in female mice on the same diet (AUC male Ssniff Ctrl 14days: 16398.75 ± 1432.61 vs. AUC male Ssniff Ctrl 140days 22430.00 ± 2068.81, $p<0.0001$). In these DIO studies, an earlier onset of hyperinsulinemia in male mice than in female mice was observed (Figure 15E and F), whereby the different fat contents of the HFDs only impacted the onset of hyperinsulinemia from 84 days on (Figure 15E and F).

Taken together, male C57BL/6N mice showed an earlier onset of obesity and overall more pronounced effects of body and fat mass gain, as well as obesity-induced hyperinsulinemia, than age-matched female mice. Moreover, some diet-specific differences to the induction of obesity were observed as the 60% HFD increased body weight, glucose intolerance and hyperinsulinemia more, than the 45% HFD, specifically in the long long-term HFD cohorts (≥56 days of HFD feeding).

*3.2 A switch from a HFD to a LFD (*ad libitum*) leaves an inflammatory fingerprint in liver and perigonadal adipose tissue of formerly obese mice*

In order to investigate molecular alterations caused by a history of DIO, age-matched HFD-fed mice as well as mice, which underwent a diet switch from a HFD to a control LFD after 20 weeks of feeding, and control diet fed mice, afterwards referred to as 'obese', 'formerly obese' and 'lean' mice, were characterized in terms of weight gain and weight loss-induced alterations of relevant metabolic parameters as well as molecular underpinnings in peripheral tissues. The following subsections of this chapter are containing results and figures, which were published by the author of this dissertation in the article "A history of obesity leaves an inflammatory fingerprint in liver and adipose tissue.", I.P. Fischer et al., International Journal of Obesity (London), 2018 [18].

*3.2.1 A switch from HFD to LFD (*ad libitum*) reverses the DIO phenotype*

To provide comparability with prior caloric restriction experiments performed by our group [127], here, for the induction of obesity, 8 week old, male C57BL/6JCrl mice were fed a 58% HFD (Research Diets RD 12331, Table 4) for 20 weeks. After 20 weeks of feeding, massive weight gain was observed in the HFD-fed, obese group when compared to the LFD, lean mice (32.75 g ± 0.74 g vs. 47.84 g ± 1.57 g, $p<0.0001$). The *ad libitum* switch from the HFD to the LFD induced a significantly reduced body weight, already within one week after the switch (47.62g ± 1.12g vs. 43.33g ± 1.19g, $p<0.05$). Weight loss was promoted in the formerly obese mice during the following six weeks, while mice receiving the HFD continuously gained weight. After 27 weeks of feeding, formerly obese mice weighed in average 35.24g and were not statistically different from the lean, control diet fed mice (32.00g ± 0.95g) (Figure 16A). In line with the normalization of body mass, total lean and fat mass were reduced in the diet switched mice and were not different to those of lean mice (Figure 16B). As previously mentioned, disturbed glucose tolerance is an important obesity-associated co-morbidity, which contributes to the onset of T2DM. After 27 weeks of feeding, HFD-fed, obese mice showed an impairment in glucose tolerance when compared to the lean mice, whereas diet-switched, formerly obese mice exhibited a normal response to the glucose challenge (Figure 16C and D). Moreover, no differences in basal glucose levels were identified in neither of the experimental groups (Figure 16E). In this diet-switch model, obesity induced hyperinsulinemia was however reversed in the formerly obese C57BL/6J mice (Figure 16F) [18].

In order to further characterize the metabolic status of the diet-switched mice, standard plasma metabolites were measured (Figure 17). *Ad libitum* switch to the LFD induced a significant reduction of circulating levels of triglycerides, cholesterol and NEFA, when compared to the obese HFD mice.

More importantly, plasma metabolites of formerly obese mice were not statistically different from those of lean mice (Figure 17) [18].

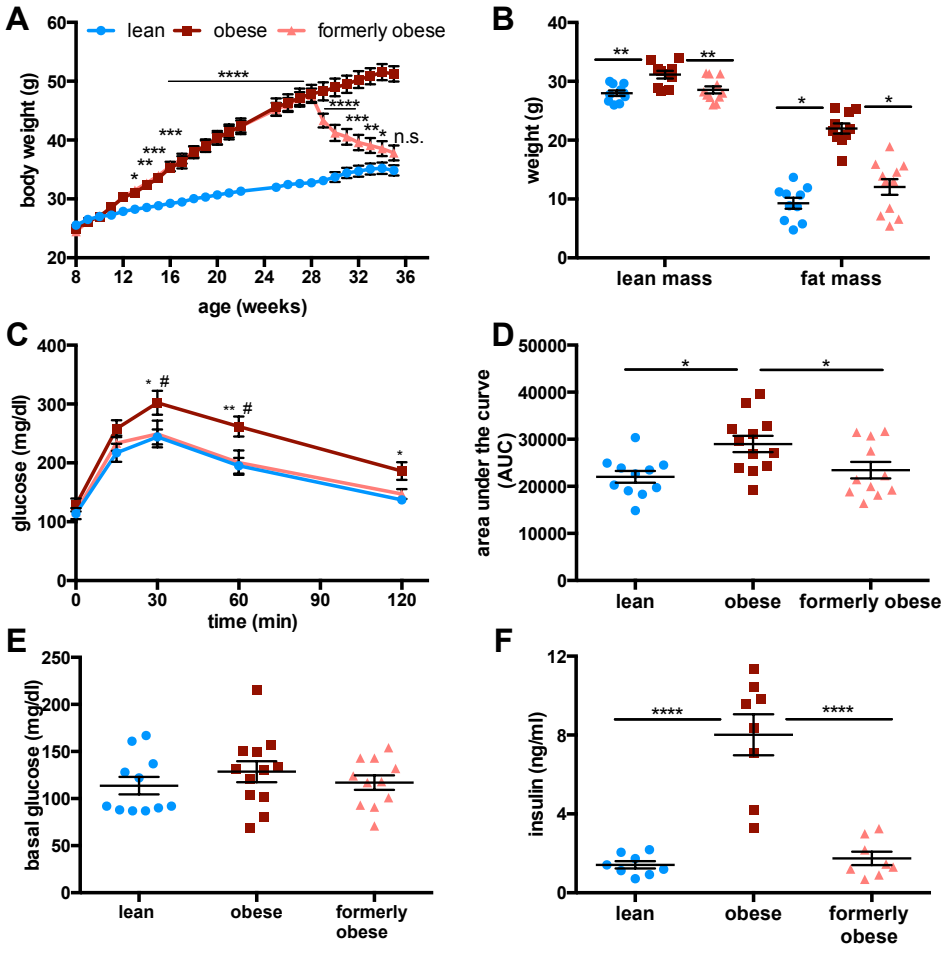

Figure 16 Switch from a HFD to a LFD (*ad libitum*) reverses DIO phenotype of male C57BL/6J mice.
(A) Body weight curve of lean (n=23), obese (n=24) and formerly obese mice (n=23) Statistical difference was determined via two-way ANOVA and reached significance with $p < 0.05$. (*) Significance is indicated for formerly obese against lean mice. (B) Lean mass and fat mass were determined in a subgroup of lean, obese and formerly obese mice (n=10-11), after 27 weeks of experimental feeding and 35 weeks of age. (C) I.p. GTT (glucose 2g/kg body weight) in a subgroup of formerly obese, lean and obese mice (n=11-12) at 35 weeks of age. (D) Area under the curve (AUC) of performed i.p.GTT (n=12). (E) Fasting basal glucose (mg/dl) of a subgroup of formerly obese, lean and obese mice (n=11-12) at 35 weeks of age. (F) Plasma insulin of a subgroup of formerly obese, lean and obese mice (n=8), measured after sacrifice at 35 weeks of age. Statistical significance was calculated via One-Way ANOVA ((D), (E), (F)) or Two-Way ANOVA ((A), (B) and (C)) followed by Tukey's multiple comparisons test.

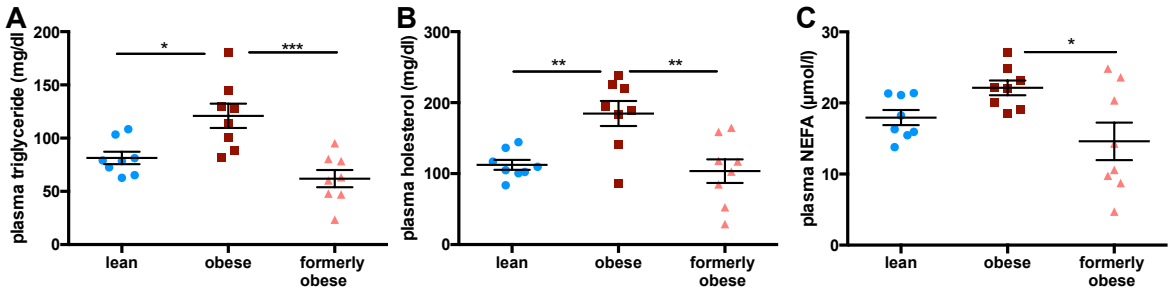

Figure 17 Plasma metabolites are normalized in diet-switched C57BL/6J mice.
Plasma triglycerides (A), cholesterol (B) and NEFA (C) in lean, obese and formerly obese mice (n=8), determined after sacrifice at 35 weeks of age. Statistical significance was calculated via One-Way ANOVA followed by Tukey's multiple comparisons test.

*3.2.2 A switch from HFD to LFD (*ad libitum*) does not fuel diet-induced thermogenesis*

Conflicting studies have reported that caloric restriction-induced-weight loss is associated with browning in WAT and activation of BAT, thereby contributing to an overall increase of energy expenditure [175]. To analyze whether the assessed weight loss in this model was caused by an increase of energy expenditure or a decrease of energy intake, the caloric intake was measured of lean, obese and formerly obese mice after 27 weeks of feeding the experimental diets. Thereby, a significant reduction of caloric intake was found in formerly obese mice, when compared to obese mice, with no difference to lean mice (Figure 18A). RT-qPCR analysis moreover revealed a down-regulation of the expression of thermogenic genes *Ucp1*, *Pgc1α*, *Cidea* and PR domain 16 (*Prdm16*) in scWAT of obese mice (Figure 18B). Transcription levels of these thermogenic genes were however not different in scWAT of formerly obese mice, compared to neither obese nor lean mice (Figure 18B), indicating that no browning occurred 7 weeks after the diet switch. In line with this, expression of *Ucp1* and *Pgc1α* was not different in BAT from either of the experimental groups (Figure 18C). Cytochrome C-oxidase (COX)- activity can be used as a surrogate for mitochondrial respiratory capacity. In this experiment, COX-activity was significantly reduced in BAT from obese mice, when compared to lean mice (Figure 18D). Importantly, oxygen consumption was not different in formerly obese mice and lean mice (Figure 18D). Concluding that the assessed weight loss was not related to an increase of thermogenic activity in scWAT or BAT, but related to a decrease in energy intake [18].

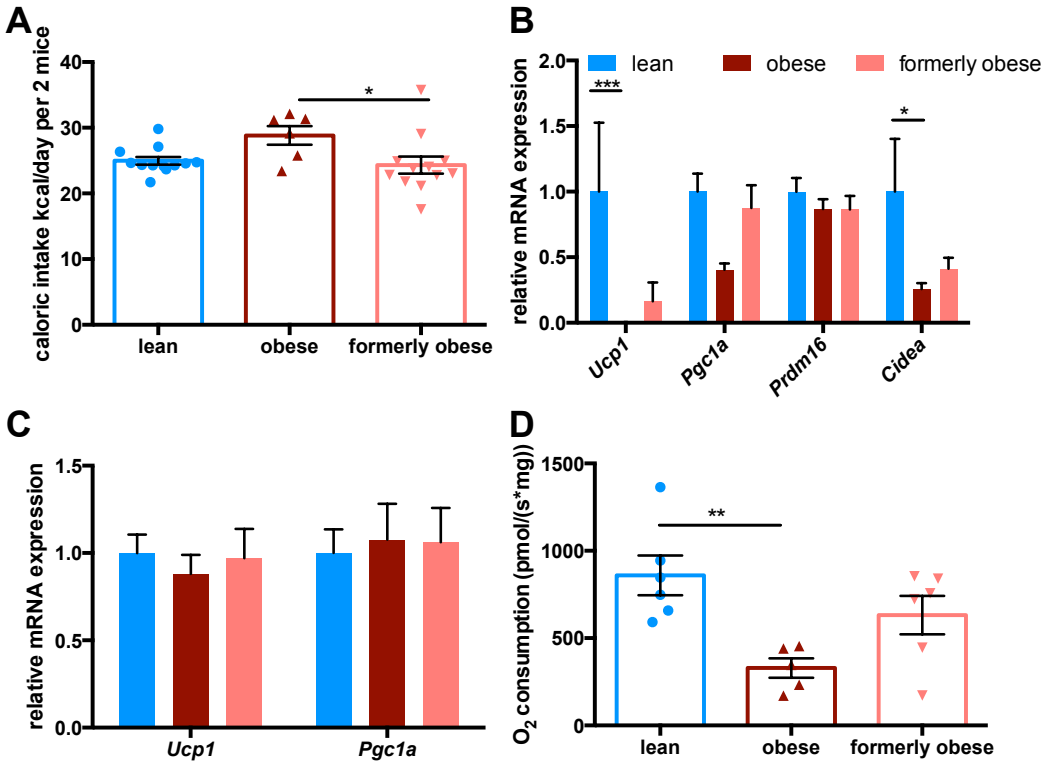

Figure 18 Switch from a HFD to a LFD (*ad libitum*) does not fuel diet-induced thermogenesis.
(A) Caloric intake measured in kcal/per two mice (per cage) at 35 weeks of age from lean, obese and formerly obese mice (n=6-12). (B) Relative mRNA expression of thermogenic genes in scWAT of lean, obese and formerly obese mice (n=12). (C) Relative mRNA expression of thermogenic genes in BAT from lean, obese and formerly obese mice (n=8). (D) COX-activity given as oxygen consumption (pmol/(s*mg tissue)) of BAT from lean, obese and formerly obese mice (n=6-8). Statistical significance was calculated via One-Way ANOVA followed by Tukey's multiple comparisons test [18].

3.2.3 Weight loss, induced by ad libitum *switch to a LFD does not facilitate hyperphagia within 48h of re-feeding*

Previous studies have shown that caloric restriction was followed by an up-regulation of hyperphagic pathways [127, 176]. To study whether body weight rebound and hyperphagia was facilitated in the diet-switched, formerly obese mice, lean and formerly obese mice (n=12) were further (re)- introduced to hypercaloric feeding for 48h at 35 weeks of age. Body weight and food intake were monitored every 24h. Interestingly, no significant difference in cumulative weight gain or energy intake between formerly obese and lean mice was found during the 48h of refeeding (Figure 19A and B). Moreover, HFD (re)-feeding did not induce any significant alteration in circulating levels of insulin, leptin, triglycerides, free fatty acids or cholesterol between formerly obese and lean mice (Figure 19C). Still, regarding the latter, a significant increase in cholesterol levels was found in lean-48h HFD mice when compared to lean mice (Figure 19C). The drive to overeat is regulated centrally [177]. Therefore, mRNA expression of hypothalamic neuronal marker Agouti-related peptide (*Agrp)* and Proopiomelanocortin (*Pomc)* was measured but no significant alterations were identified upon 48h

HFD (re-) feeding between mice that underwent the diet-switch and lean mice (Figure 19D).

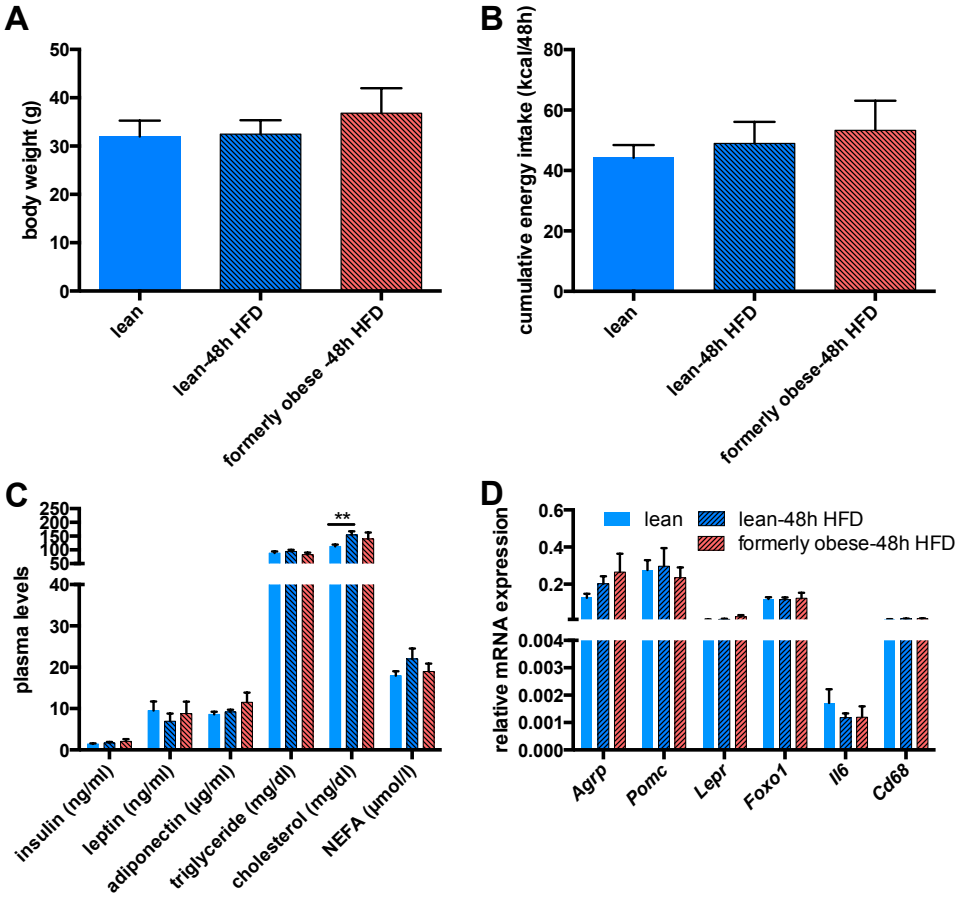

Figure 19 A history of DIO does not facilitate hyperphagia within 48h of re-feeding.
(A) Body weight of lean and formerly obese mice, (re-) fed with HFD for 48h (n=12). (B) Cumulative energy intake from lean and formerly obese mice, (re-) fed with HFD for 48h (n=6) calculated as kcal/48h/2 mice. (C) Plasma metabolites of lean and formerly obese mice (re-) fed with HFD for 48h (n=8). (D) mRNA expression of hypothalamic orexigenic and inflammatory genes lean and formerly obese mice (re-) fed with HFD for 48h and obese mice (n=6). Statistical significance was calculated via One-Way ANOVA ((D), (E), (F)) or Two-Way ANOVA ((A), (B) and (C)) followed by Tukey's multiple comparisons test [18].

Additionally, it has been repeatedly shown that leptin is a key regulator for food intake and body weight control [122]. In this study, a history of DIO did not impact the hypothalamic transcription of leptin receptor (*Lepr)* and forkhead box protein O1 (*Foxo1)* (Figure 19D). Previously it was shown by us that hypothalamic inflammation was caused by short-term high-fat diet feeding [178]. To see whether inflammation was aggravated by former obesity, mRNA levels of *Il6* and *Cd68* were determined, but both were not significantly altered between the experimental groups (Figure 18D). Concluding, a history of DIO did not facilitate body weight rebound and hyperphagia, nor impact hypothalamic response upon 48h of hypercaloric (re-) feeding in this experimental setup of diet-switched weight loss [18].

3.2.4 Weight loss, induced by ad libitum *switch to a LFD partly reverses obesity-associated hepatic steatosis*

NAFLD is often caused by extensive weight gain and contributes to the known co-morbidities of obesity [20]. To assess the grade of hepatic steatosis, liver weights and hepatic triglyceride contents of lean, obese and formerly obese mice were determined, 7 weeks after the diet switch (Figure 20A and B).

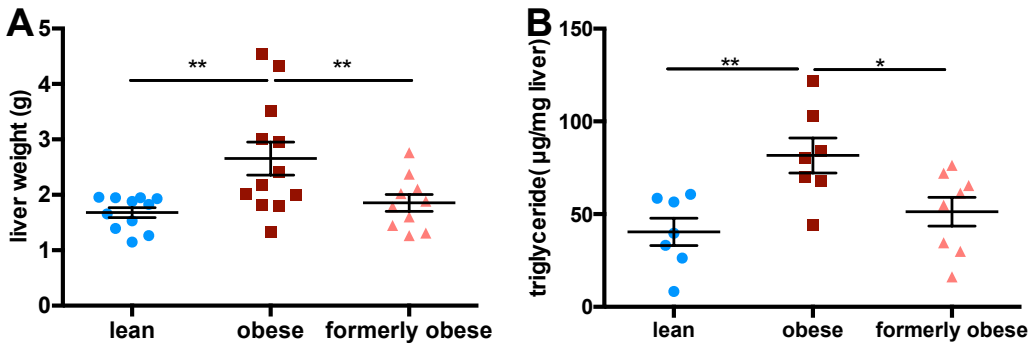

Figure 20 *Ad libitum* switch to a LFD reverses liver weight and triglyceride content.
(A) Liver weights of lean, obese and formerly obese mice, at 35 weeks of age and after 27 weeks of feeding the experimental diets (n=12). (B) Triglyceride contents (µg per mg of liver tissue) from livers of lean, obese and formerly obese mice (n=7-8). Statistical significance was calculated via One-Way ANOVA followed by Tukey's multiple comparisons test.

The 58% HFD feeding induced a significant increase of tissue weight and triglycerides in the liver, when compared to lean mice. Yet, liver weight and triglyceride contents were reversed in former obese mice, when compared to obese mice and were not different to those of lean mice (Figure 20A and B) [18]. Hepatic steatosis is marked by the excessive retention of lipids in the liver and can result in inflammation and fibrosis [20]. Therefore, the level of fatty liver disease was assessed histologically by H&E and masson's trichrome stainings. A persistent increase of fat accumulation in the livers of formerly obese mice was observed when compared to lean mice (Figure 21). The Masson's trichrome dye stains fibrotic tissue in blue, indicated in Figure 21 by black arrows [18].

Figure 21 *Ad libitum* switch to a LFD is associated with fibrosis.
Representative H&E stained liver sections of a lean, obese and formerly obese mouse (x200 magnification, scale 100µm). Arrows are indicating fibrotic lesions around the portal area and portal – to – portal bridging.

Determining the grade of fibrosis according to standard guidelines [170, 179], a slightly augmented level of portal to portal- and pericellular fibrosis in liver sections from formerly obese mice was observed, which was more comparable to those of obese, than lean mice (Figure 21) [18].

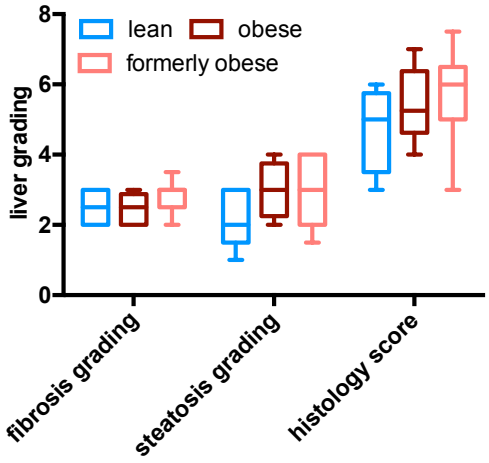

Figure 22 Histological scoring of H&E and Masson's Trichrome stained liver sections.
Data are given as boxplots indicating mean, minimum and maximum(n=5-8).

Quantitative real-time PCR further identified gene expression of pro-inflammatory cytokines *Tnfα* and *Il1ß to* be significantly up-regulated in the livers of formerly obese vs. lean mice ($p<0.05$). Sterol-regulating element binding factor (SREBP) 1 and 2 are key regulatory genes, controlling the transcription of genes, which are involved in the fatty acid uptake and *de novo* lipogenesis- (SREBP1) as well as the cholesterol- synthesis (SREBP2) pathway. RT-qPCR analysis revealed a transcriptional down-regulation of *Srebp1*, fatty acid synthase (*Fasn)*, steaoryl-CoA desaturase *(Scd1), Srebp2* and low-density lipoprotein receptor (*Ldlr)*, in livers of obese vs. lean mice (Figure 23A). While the hepatic expression of genes of the fatty acid synthesis pathway were normalized, mRNA levels of *Srebp2* and *Ldlr* were persistently down-regulated in livers of formerly obese mice compared to lean mice (Figure 23A) [18].

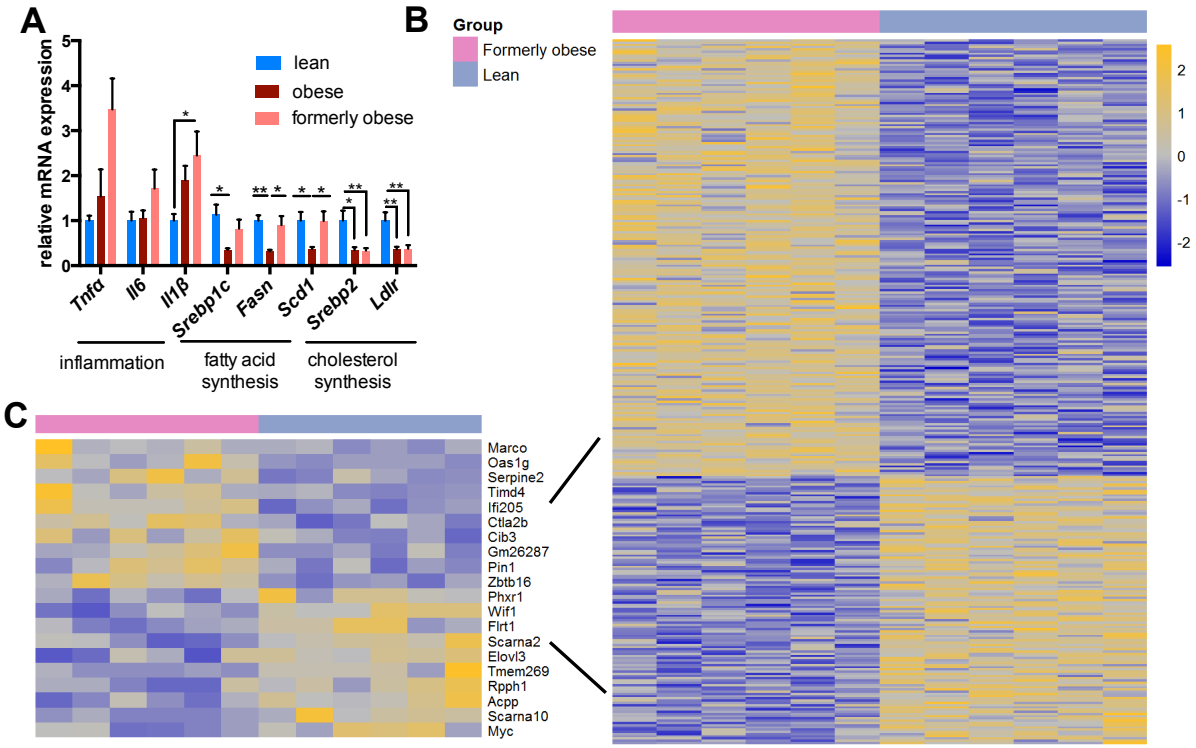

Figure 23 A history of DIO covers a pro-inflammatory hepatic transcription profile.
(A) RT-qPcr analysis of hepatic genes. Expression levels are normalized to housekeeping gene HPRT and given as FC to the lean group (=1). (B) Heat map of 322 significantly ($p<0.01$) regulated hepatic genes in the comparison of formerly obese and lean mice (n=6). (C) Top up- and down-regulated genes are presented separately. Detailed lists of significantly regulated genes can be found in Supplemental Table 6 of [18]. Raw data can be accessd via GEO database at NCBI (GSE97272). Statistical analysis was performed via One-Way ANOVA followed by Tukey's multiple comparisons test (A) and limma *t*-test ($p<0.01$) and further filtered for fold-change (FC>1.2).

Additionally, microarray analysis was performed by Dr. Martin Irmler, from the Institute of Experimental Genetics at the Helmholtz Zentrum München, in livers of lean, obese and formerly obese mice, to further identify hepatic genes, which were differentially regulated in the direct comparison between formerly obese and lean mice. In total, 322 differentially regulated genes were identified, of which 199 genes were up- and 123 significantly down-regulated (FC >1.2, p< 0.01, Av>8) (Figure 23B) [18].

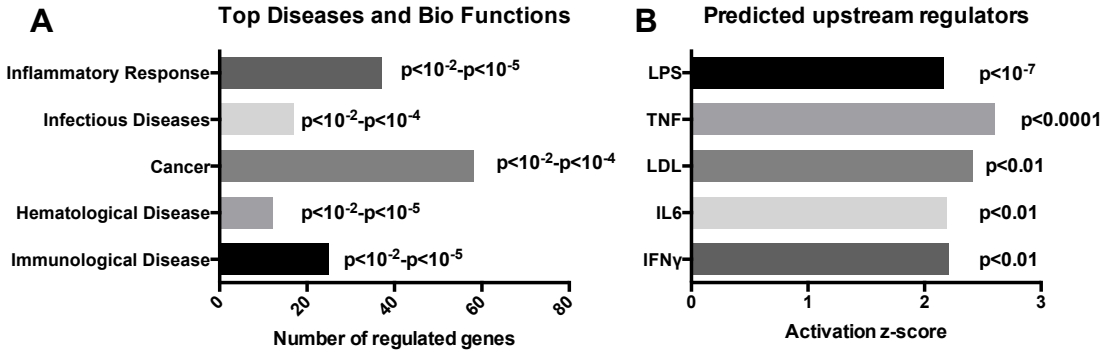

Figure 24 Associated pathways and predicted upstream regulators of transcriptionally regulated hepatic genes of formerly obese mice.
(A) Top 5 statistically significant (by p-value; p<0.01) activated 'Diseases and Bio Functions' associated with the 322 regulated genes. (B) Significantly activated predicted upstream regulators of the 322 regulated hepatic genes in the livers of formerly obese mice. Detailed lists of enriched pathways and upstream regulators can be found in Supplementary Tables 7-8 of [18].

Furthermore, Ingenuity Pathway Analysis identified 'inflammatory response' to be the top-associated 'disease and bio-function' pathway ($p<0.01$- $p<10^{-5}$) (Figure 24A) and additionally identified LPS, TNF, LDL, IL6 and IFNγ as predicted 'activated upstream regulators' of the 322 differentially regulated hepatic genes (Figure 24B) [18]. Further, 45 genes were identified, which were regulated in both the livers of formerly obese and obese mice, when compared with lean mice (Figure 25). These included pro-inflammatory cytokine *Ccl5* and *Il2r*.

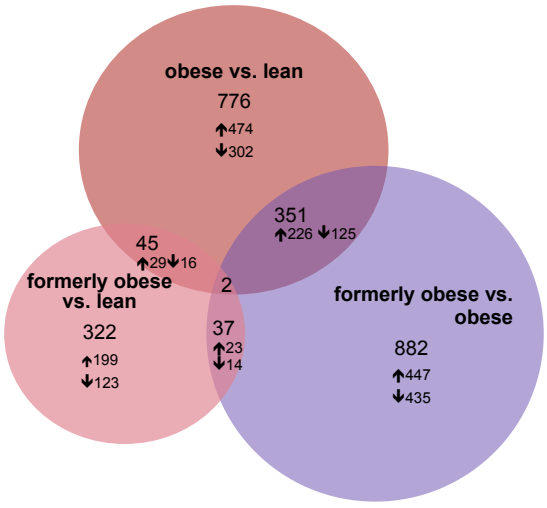

Figure 25 Venn-diagramm of overlapping hepatic genes in pairwise comparisons.
Venn-diagram of (overlapping) differentially expressed genes (FC>1.2 p<0.01) in three pairwise comparisons 'formerly obese vs. lean' (left panel), 'obese vs. lean' (upper panel) and 'formerly obese vs. obese' (right panel). A detailed list of the differentially expressed genes regarding each comparison can be found in the Supplementary Tables 9-13 of [18].

Taken together, the diet-switch-induced weight loss normalized some of the obesity-associated fatty liver phenotypes, such as tissue weight and triglyceride content. However, histological scoring and RT-qPCR analysis revealed slightly increased levels of inflammation and fibrosis and a down-regulation of genes involved in the cholesterol synthesis pathway, caused by a history of DIO. Moreover, deep transcriptional profiling revealed 322 hepatic genes to be differentially regulated by a history of obesity, which were mostly associated with inflammation [18].

3.2.5 Depot-specific adipocyte plasticity after diet-induced weight loss

After sacrifice, the weight of adipose tissue depots was measured. 58% HFD-feeding significantly increased fat mass of scWAT and gWAT adipose tissue compared to LFD-fed, lean mice. Consistent with total fat mass, the diet switch normalized scWAT and gWAT mass of the formerly obese mice, which were not different to fat depot masses of lean mice (Figure 26A and B) [18].

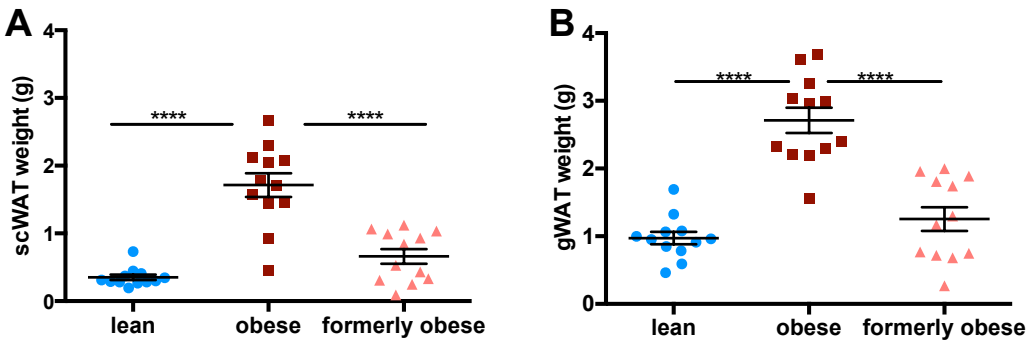

Figure 26 Switch from a HFD to a LFD (*ad libitum*) normalizes adipose tissue weights.
(A) Subcutaneous (scWAT) and (B) perigonadal (gWAT) tissue wet weight (g) of lean, obese and formerly obese mice at 35 weeks of age and after 27 weeks of experimental diet (n=12). Statistical analysis was performed via One-way ANOVA followed by Tukey's multiple comparisons test.

Leptin and adiponectin are two of the most prominent secreted adipokines from WAT [180] and circulating levels of these hormones were determined in plasma post mortem. 58% of HFD-feeding induced a hyperleptinemia, which was reversed in the diet-switched, formerly obese mice (Figure 27A). It is known that obesity is associated with decreased adiponectin levels [181]. In this experiment, diet-switched formerly obese mice displayed significantly increased adiponectin levels in comparison to obese mice (Figure 27B).

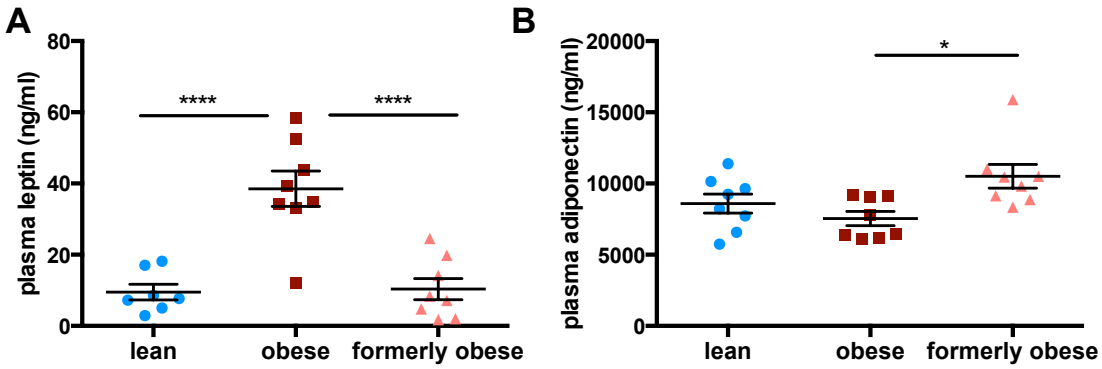

Figure 27 Switch from a HFD to a LFD (*ad libitum*) reverses circulating adipokine levels.
Plasma leptin (A) and adiponectin (B) levels of lean, obese and formerly obese (n=7-8). Statistical analysis was performed via One-way ANOVA followed by Tukey's multiple comparisons test.

It is known that weight gain is paralleled by an expansion of adipocyte size [55]. Accordingly, in this experiment, adipocyte cell sizes of scWAT and gWAT were increased in obese mice compared to lean mice (Figure 28) [18].

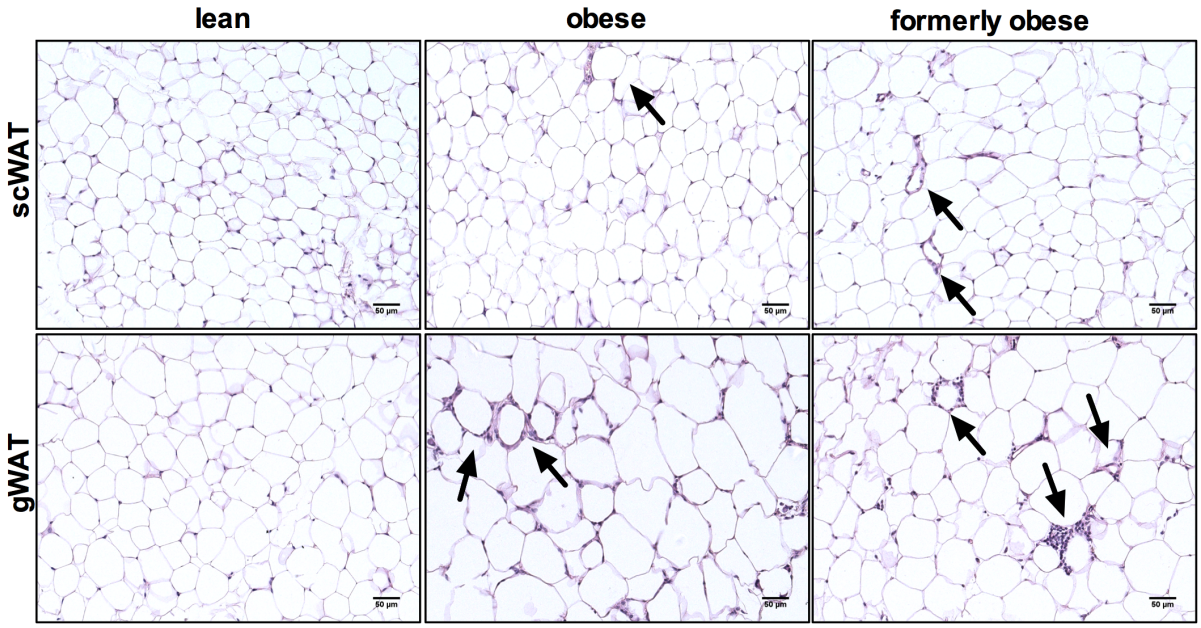

Figure 28 A history of obesity is associated with depot-specific hypertrophy and CLS formation.
Representative sections from H&E stained scWAT (upper panel) and gWAT (lower panel) of lean, obese and formerly obese mice (200x magnification, scale bar= 50µm). Arrows are indicating CLS.

Strikingly, weight loss only reduced adipocyte cell size expansion in the scWAT but not the gWAT of formerly obese mice, when compared to lean mice ($p<0.001$) (Figure 29A and B) [18].

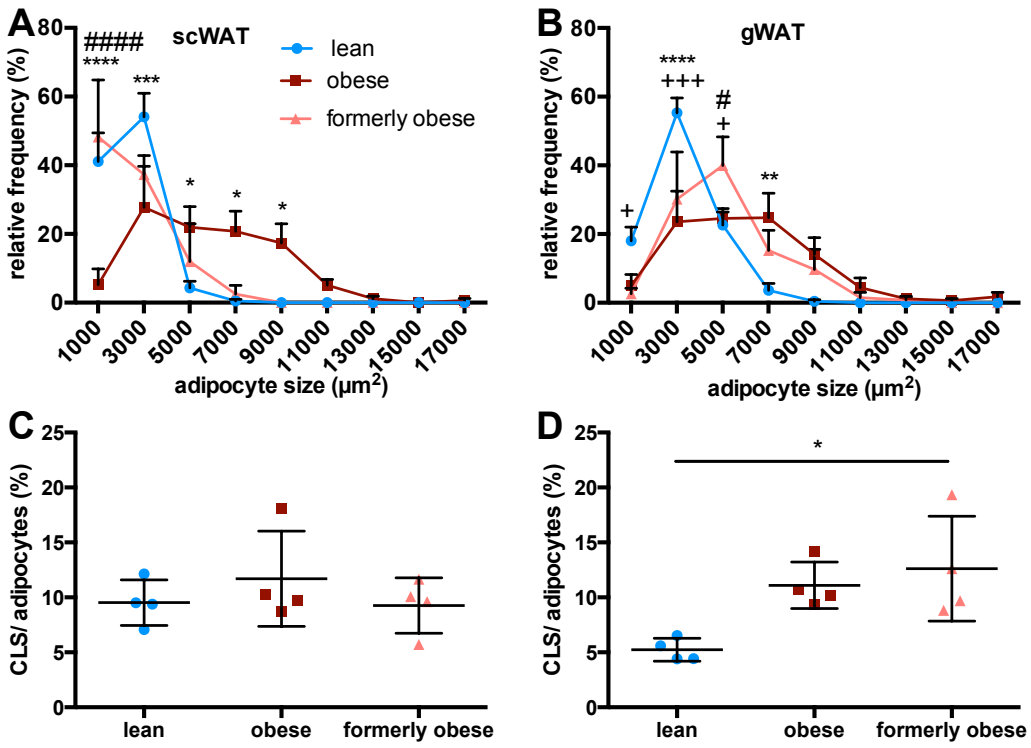

Figure 29 Quantification of depot-specific hypertrophy and CLS formation.
Frequency distribution of adipocyte cell sizes (µm^2) from scWAT and gWAT of lean, obese and formerly obese mice (n=4-5). Statistical significance was tested via One-Way ANOVA (C and D) or Two-Way ANOVA (A and B) followed by Tukey's multiple comparisons test. Significant differences are indicated with + (formerly obese vs. lean mice), # (obese vs. formerly obese) and *=$p<0.05$ (obese vs. Lean). % of counted Crown like structures (CLS) per number of counted adipocytes of scWAT (C) and gWAT (D) (n=4-5).

Obesity is often associated with a state of low-grade inflammation [44]. To assess the extent of white adipose tissue inflammation, mRNA levels of the pro-inflammatory cytokines IL6 and Tumor necrosis factor TNF, as well as the adipokines leptin and adiponectin were measured via quantitative real-time PCR in both adipose depots. There, HFD-feeding induced an increase in gene expression of *Il6* and *Tnfα* (Figure 30A and B). This increase in pro-inflammatory gene expression was reversible, as mRNA levels of formerly obese mice were not statistically different to those of lean mice, regarding both depots. Leptin mRNA levels were augmented in scWAT, but not in gWAT of obese mice. Consequently, the diet-switch caused a reduction of leptin mRNA levels in the scWAT, while leptin mRNA levels remained unchanged in the perigonadal adipose depots among all treatments. Interestingly, adiponectin mRNA levels were only altered by obesity in the gWAT, but not scWAT. Intriguingly, *Adiponectin* expression was not completely reversed by the diet-switch, when comparing formerly obese vs. lean mice (Figure 30A and B). Moreover, RT-qPCR analysis of different macrophage- and inflammation markers showed an increase in *F4/80*, *Cd11b*, *Cd11c*, *Cd68* in both

adipose tissue depots of obese mice, which was reversed in formerly obese mice, albeit a trend to elevated levels compared to lean controls remained. The only statistically significant difference between formerly obese and lean mice was identified regarding the expression of M2 type macrophage marker *CD301*in scWAT (Figure 30) [18].

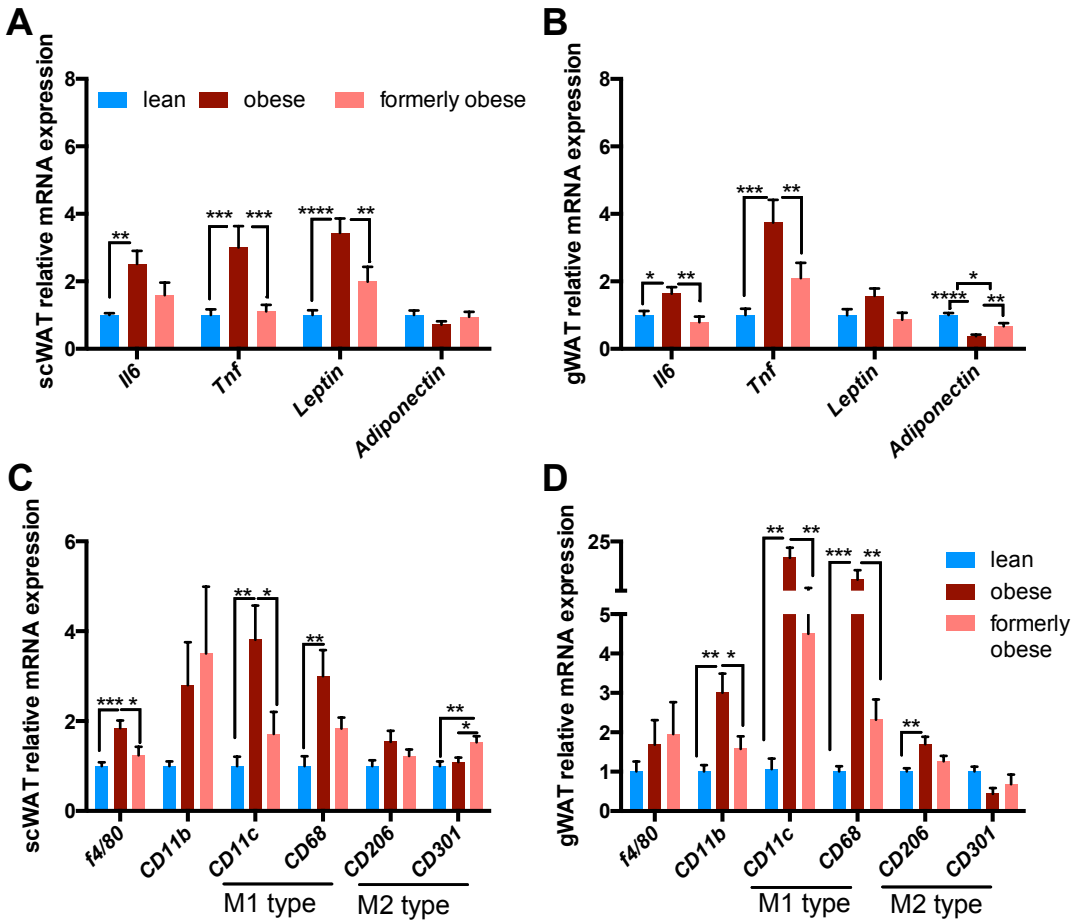

Figure 30 A history of DIO is associated with a depot-specific pro-inflammatory transcriptional profile in WAT. RT-qPCR analysis of adipose tissue related cytokines, adipokines and macrophage markers in scWAT (A and C) and gWAT (B and D). (n=7-11). Expression levels are normalized to housekeeping gene HPRT and given as FC to the lean group (=1). Statistical analysis was performed via Two-way ANOVA followed by Kruskall-Wallis test.

In order to further clarify molecular alterations in the gWAT, transcriptional profiling was performed by Dr. Martin Irmler, from the Institute of Experimental Genetics at the Helmholtz Zentrum München, on the gWAT of formerly obese, obese and lean mice. In the direct comparison between formerly obese and lean mice, we identified 309 differentially expressed genes (FC < 1.3, p<0.01, Av> 16), of which 234 were up-and 75 were down- regulated in the gWAT of formerly obese mice (Figure 31A) [18].

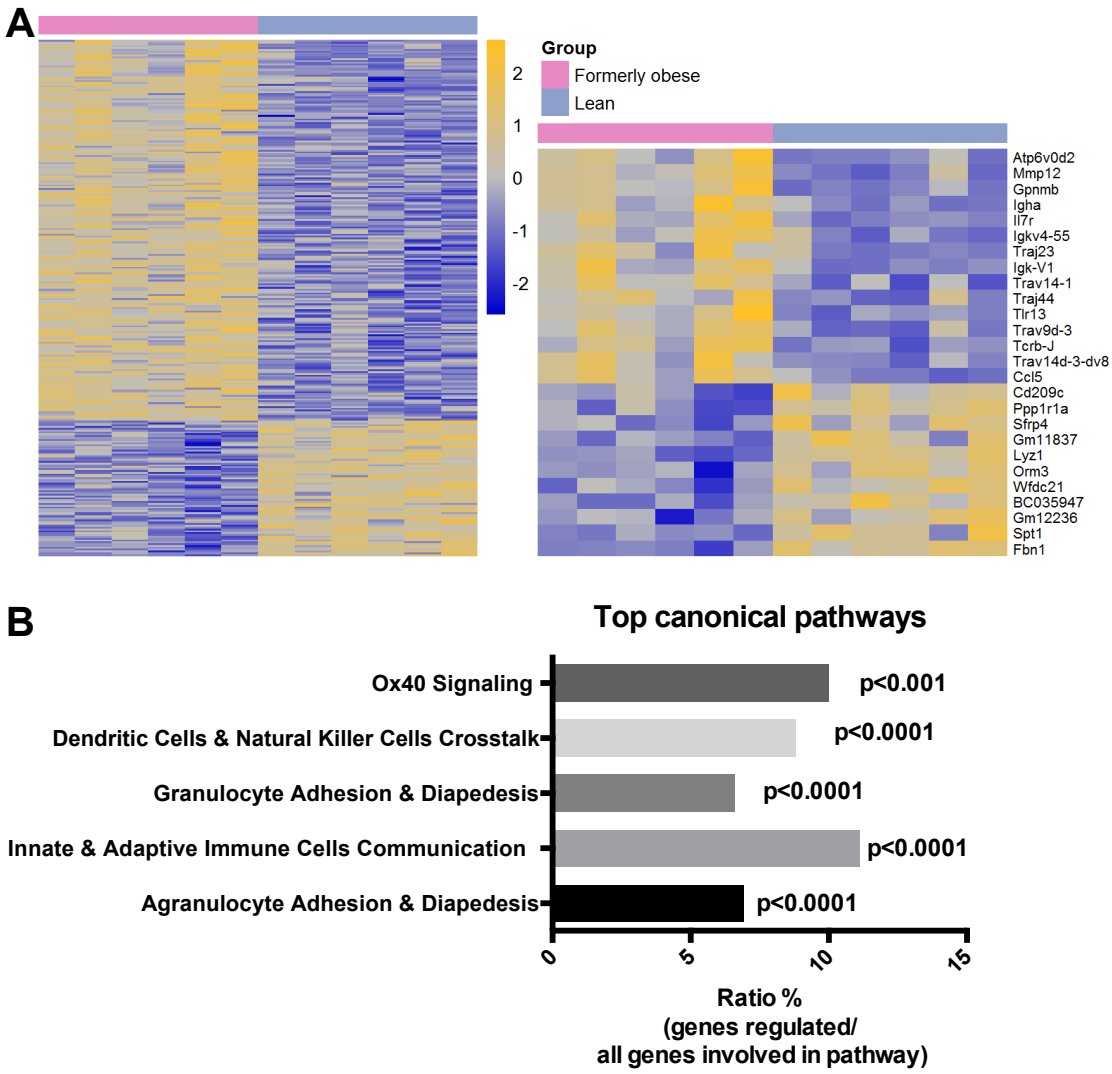

Figure 31 A history of DIO covers a proinflammatory adipogenic transcription profile.
Heat map of 309 significantly (p<0.01) regulated genes in gWAT of formerly obese versus lean mice (n=6). Top up- and down-regulated genes are presented separately. A detailed list of the 309 differentially expressed genes can be found in Supplemental Tables 2-3 of [18] and accessed via GEO database at NCBI (GSE97272). (B) Top 5 statistically significant (p<0.001) enriched canonical pathways associated with the 309 differentially expressed genes of formerly obese vs. lean mice. Genewise testing for differential expression was done employing the limma *t*-test and Benjamini-Hochberg (BH) multiple testing correction (FDR<10%) and further filtered for FC >1.3.

Among the top-regulated canonical pathways, we identified immunity- and inflammation-associated pathways as 'innate & adaptive immune cells communication' pathways to be up-regulated ($p<0.00001$) (Figure 31B).

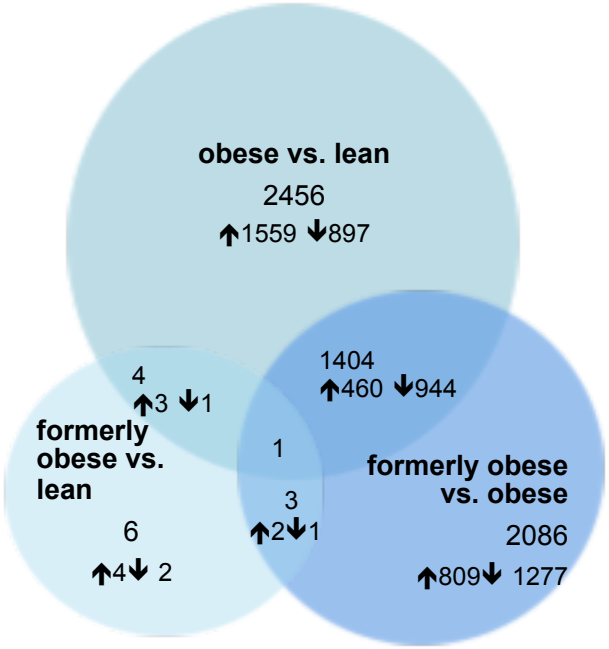

Figure 32 Venn-diagram of significantly regulated genes from gWAT.
Venn diagram of (overlapping) significantly differentially expressed genes (FC>1.3, FDR<10%) in three pairwise comparisons 'formerly obese vs. lean' (left panel), 'obese vs. lean' (upper panel) and 'formerly obese vs. obese' (right panel). A detailed list of the differentially expressed genes regarding each comparison can be found in Supplemental Tables 4-5 of [18].

Comparing the differentially regulated genes in the formerly obese vs. lean state in a more restrictive way (FC> 1.3x, FDR<10%, Av>16), the list was narrowed down to six genes, which were associated to with immune function (*Vcam1, Lyz1, H2-q5*), cellularity (*Fbn1*) and body weight regulation (*Nmb*) or have not been described before (G*gm26523*) (Figure 32). Interestingly, four of these identified candidate genes are also significantly regulated in the same direction when compared in obese vs. lean mice (*Gm2635*, *H2-q5*, *Vcam1* and *Lyz1*) (Figure 32) [18].

Taken together, the observed weight loss and associated normalization of total fat mass was only partly, and depot-specifically accompanied by the restoring of adipocyte hypertrophy and obesity-associated inflammation. The persisting gWAT hypertrophy was further paralleled by a differential regulation of genes, which were associated with immune function, cellularity and body weight regulation. To elucidate the function of identified candidate genes in the context of adipose tissue metabolism and weight loss, future studies will focus on respective genes.

One of the top regulated genes in gWAT of both obese and formerly obese mice was Activating transcription factor 3 (*Atf3*) with an FC of 4.5 ($p<0.001$) in the comparison obese vs. lean and a FC of 1.71 ($p<0.01$) in the comparison of formerly obese vs. lean mice (Figure 33 A and B).

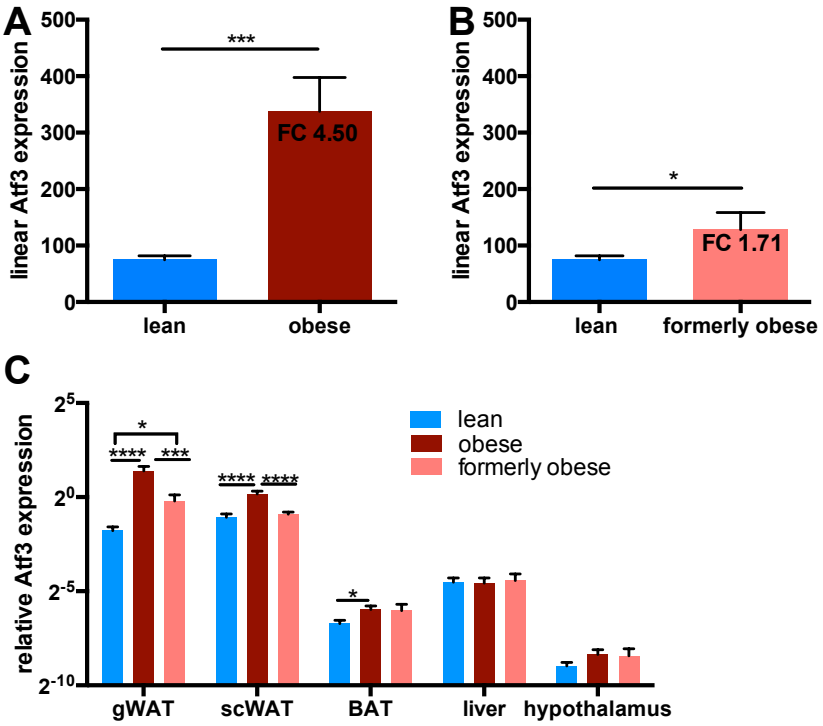

Figure 33 Activating Transcription Factor 3 is regulated in obese and formerly obese conditions in adipose tissue. (A) Linear expression of Atf3 in the microarray analysis of gWAT from obese vs. lean (A) and formerly obese vs. lean (B) mice (n=6). (C) RT-qPCR analysis of ATF3 expression in different tissues of lean, obese and formerly obese mice (n=8-12).

The up-regulation of *Atf3* in gWAT of obese and formerly obese mice was further validated via RT-qPCR of (Figure 33C). Moreover, an up-regulation of *Atf3* was further identified in scWAT and BAT of obese mice, whereby the latter has not been described before. In the following section 3.3 the function of ATF3 in BAT was addressed.

3.3 UCP1-specific ATF3 knockout does not impact HFD-induced weight gain and glucose intolerance

3.3.1 The UCP1-specifc ATF3 ablation is barely detectable at basal states but becomes evident upon isoproterenol stimulation

ATF3 has been shown to have detrimental, as well as beneficial functions in various (white adipose) tissues. Yet the function of ATF3 in murine and human brown adipocytes has not been described. To specifically elucidate the function of ATF3 in murine brown adipocytes, a UCP1-cell specific knockout line was created, by crossing mice carrying Atf3-floxed alleles with Ucp1^{cre+} mice [167]. It is known that the whole body knockout of ATF3 in mice does not display any phenotypic changes in basal state [148]. However, pancreatic and duodenal homebox1 (Pdx1)-specific ATF3 knockout mice were shown to have reduced body mass [155]. In this experimental set up, female and male Atf3$^{fl/fl}$;Ucp1^{cre+} mice did not show a decrease in body weight (Figure 34A), nor lean mass and fat mass (Figure 34B), when compared to their floxed littermates with an age of 12 weeks.

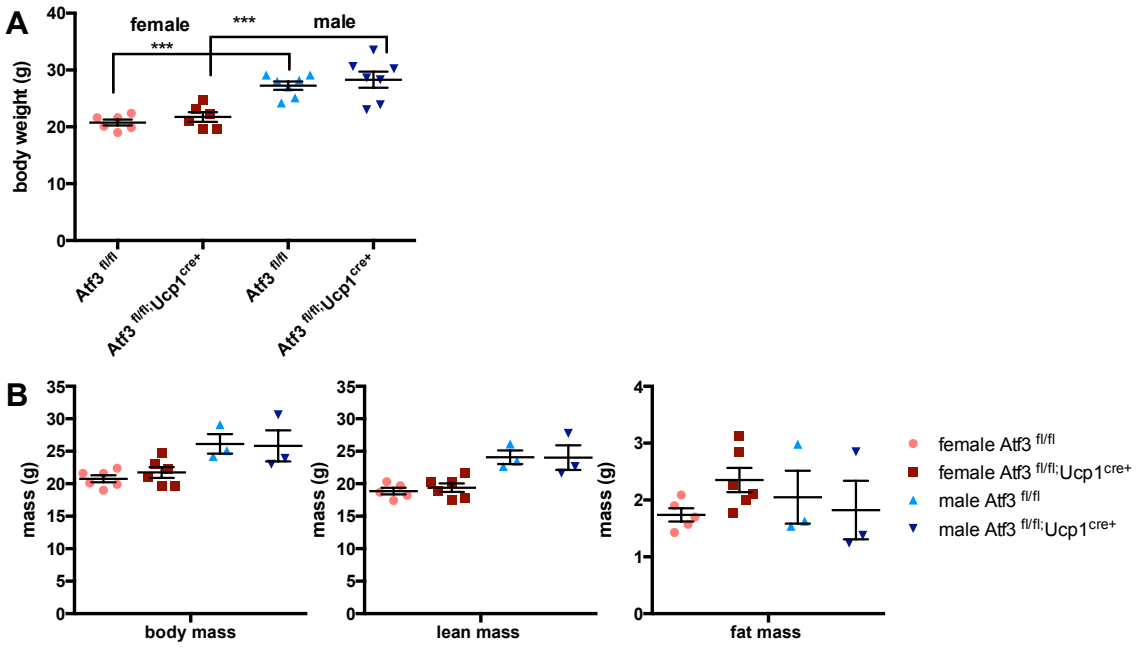

Figure 34 UCP1-specific ablation of ATF3 has no impact on body weight development in C57BL/6N male and female mice.
(A) Body weight of 12 week old male (n=7) and female (n=6) Atf3$^{fl/fl}$ and Atf3$^{fl/fl}$;Ucp1^{cre+} mice. (B) Body composition of male (n=3) and female (n=6) Atf3$^{fl/fl}$ and Atf3$^{fl/fl}$;Ucp1^{cre+} mice. Statistical analysis was determined via One-way ANOVA followed by Tukey's multiple comparisons test.

Moreover, no differences in random fed glucose levels could be detected in male and female Atf3$^{fl/fl}$;UCP1^{cre+} mice when compared to their floxed littermates (Figure 35).

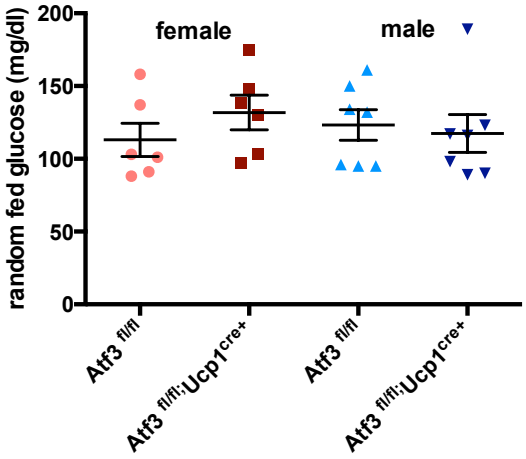

Figure 35 UCP1-specific ablation of ATF3 has no impact on random fed glucose levels in C57BL/6N male and female mice.
Random fed glucose levels of 12 week old male (n=7) and female (n=6) Atf3$^{fl/fl}$ and Atf3$^{fl/fl}$;Ucp1^{cre+} mice. Statistical significance was tested via One-Way ANOVA followed by Tukey's multiple comparisons test.

As ATF3 is known to regulate the expression of a variety of genes involved in adipose tissue metabolism, and contributing to overall systemic energy homeostasis, one aim was to identify the target genes of ATF3 in brown adipose tissue, which would be affected by the loss of function in this transgenic model. Therefore, RNA-sequencing from BAT of female Atf3$^{fl/fl}$ and Atf3$^{fl/fl}$;Ucp1^{cre+} mice at the age of 8 weeks were performed with the help of Dr. Elisabeth Graf and Thomas Schwarzmayr from the Institute of Human Genetics and Dr. Dominik Lutter from the Institute of Diabetes and Obesity at the Helmholtz Zentrum München. Surprisingly, only 11 significantly regulated genes ($p<0.01$) were identified when comparing BAT RNA from Atf3$^{fl/fl}$;Ucp1^{cre+} vs. Atf3$^{fl/fl}$ mice (Figure 36A). Among those, neither *Atf3*, nor brown adipocyte specific *Ucp1* were differentially expressed between the genotypes. These findings were validated by measuring the relative mRNA expression of ATF3, UCP1 and other known ATF3 targets by qRT-PCR, whereby no significant differences between Atf3$^{fl/fl}$ and Atf3$^{fl/fl}$;Ucp1^{cre+}were found (Figure 36B), indicating that the expression of ATF3 is hardly detectable at basal, unstressed states. Yet, among the regulated genes Protein phosphatase 1 (Ppp1r10), B-cell lymphoma 6b (Bcl6b) and Actin philament associated protein 1 (Afap1) were significantly up-regulated in BAT of Atf3$^{fl/fl}$;Ucp1^{cre+} mice. Of note, these genes have already been described to be significantly up-regulated in cardiac fibroblasts of whole body ATF3ko mice, which were stimulated with angiotensin II [164].

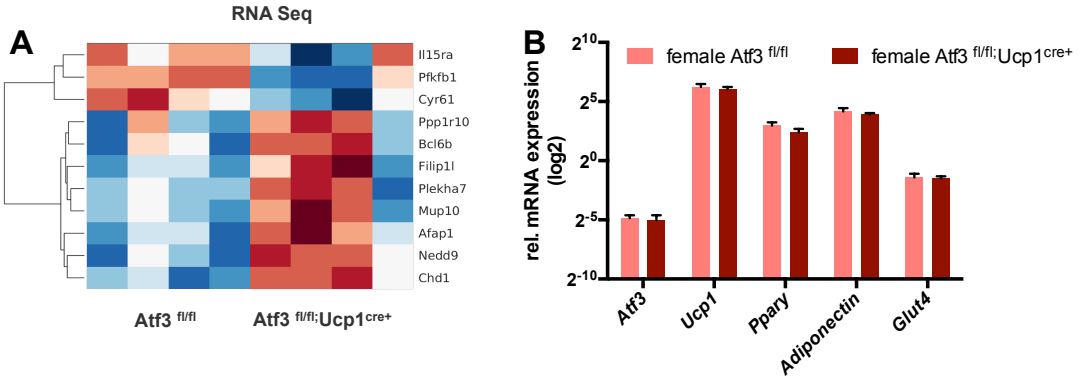

Figure 36 ATF3 mRNA expression is hardly detectable in BAT from Atf3$^{fl/fl}$;Ucp1^{cre+} vs. Atf3$^{fl/fl}$ mice in basal states.
(A) Heat map of significantly differently regulated genes in BAT from 8 week old female Atf3$^{fl/fl}$ and Atf3$^{fl/fl}$;Ucp1^{cre+} mice (n=4) during RNA-Sequencing ($p<0.01$). (B) mRNA expression of ATF3 and Ucp1 as well as known Atf3 target genes in BAT from 8 week old female Atf3$^{fl/fl}$ and Atf3$^{fl/fl}$;Ucp1^{cre+} mice (n=4). Y-axes underwent a log2 scaling to better visualize the data scatter.

To further elucidate whether *Atf3* expression was down-regulated in the created transgenic model, primary mature brown adipocytes were isolated and ATF3 and UCP1 mRNA expression was measured. Also thereby, no differences could be detected (Figure 37).

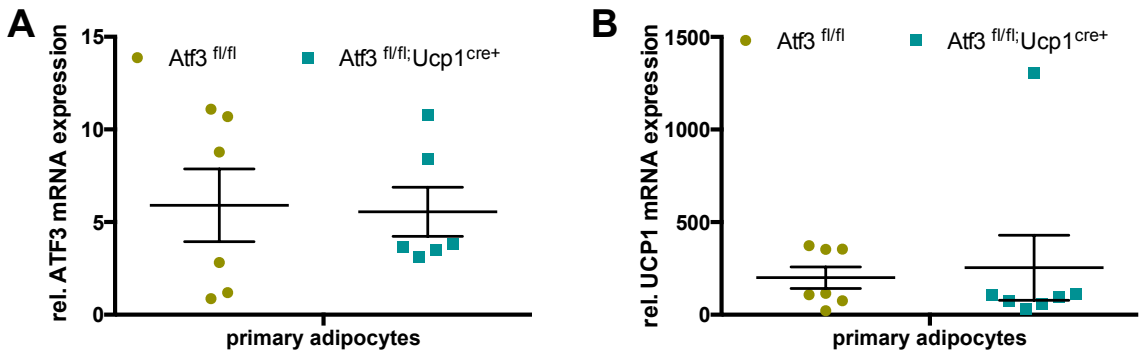

Figure 37 ATF3 mRNA expression is not different in isolated primary brown adipocytes from Atf3$^{fl/fl}$;Ucp1^{cre+} vs. Atf3$^{fl/fl}$ mice.
(A) mRNA expression of ATF3 in isolated mature adipocytes from male and female Atf3$^{fl/fl}$ (n=6) and Atf3$^{fl/fl}$;Ucp1^{cre+} (n=6) mice. Data are not separated by gender. (B) mRNA expression of UCP1 in isolated mature adipocytes from male and female Atf3$^{fl/fl}$ (n=6) and Atf3$^{fl/fl}$;Ucp1^{cre+} (n=6) mice.

In another validation approach, primary subcutaneous pre-adipocytes from Atf3$^{fl/fl}$ and Atf3$^{fl/fl}$;Ucp1^{cre+} mice were isolated and differentiated *in vitro* to mature brown adipocytes with or without the presence of 1µM rosiglitazone in the induction medium.

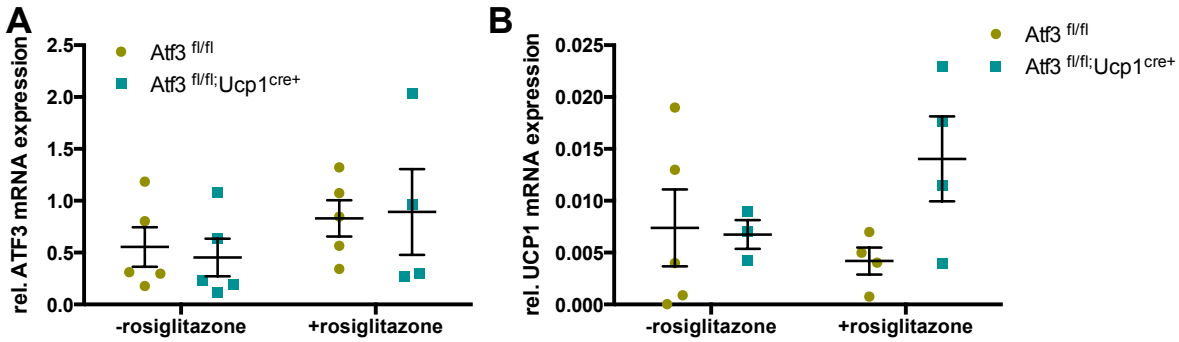

Figure 38 ATF3 mRNA expression is not altered in rosiglitazone differentiated subcutaneous adipocytes from Atf3$^{fl/fl}$;Ucp1^{cre+} mice.
(A) ATF3 mRNA expression from with or without 1µM rosiglitazone differentiated primary preadipocytes from scWAT from male and female Atf3$^{fl/fl}$ (n=5) and Atf3$^{fl/fl}$;Ucp1^{cre+} (n=4-5) mice. Data are not separated by gender. (B) Ucp1 mRNA expression from with or without 1µM rosiglitazone differentiated primary preadipocytes from scWAT of from male and female Atf3$^{fl/fl}$ (n=5) and Atf3$^{fl/fl}$;Ucp1^{cre+} (n=4-5) mice. Data are not separated by gender.

Thereby rosiglitazone-differentiated adipocytes showed no difference in ATF3 mRNA expression to cells differentiated without rosiglitazone (Figure 38A). Further no significant difference in *Ucp1* expression was identified between the genotypes, despite a trend to oppositely regulated UCP1 mRNA expression in – and + rosiglitazone treated cells (Figure 38B). From human and rodent studies, we know that in obese states, adaptive thermogenesis and BAT activity are diminished [85, 86, 182]. The main function of brown adipocytes is to provide energy in form of heat through uncoupling of the mitochondrial respiratory chain via UCP1. This adaptive thermogenesis can be activated by noradrenergic stimulation and other external stimuli via the sympathetic nervous system. One known activator of adaptive thermogenesis is isoproterenol, which acts on β-adrenoreceptors. In order to answer the question whether ATF3 is involved in the brown fat function, brown pre-adipocytes from Atf3$^{fl/fl}$ and Atf3$^{fl/fl}$;Ucp1^{cre+} mice were isolated, and upon full differentiation, stimulated with 0.5µM isoproterenol for 2h.

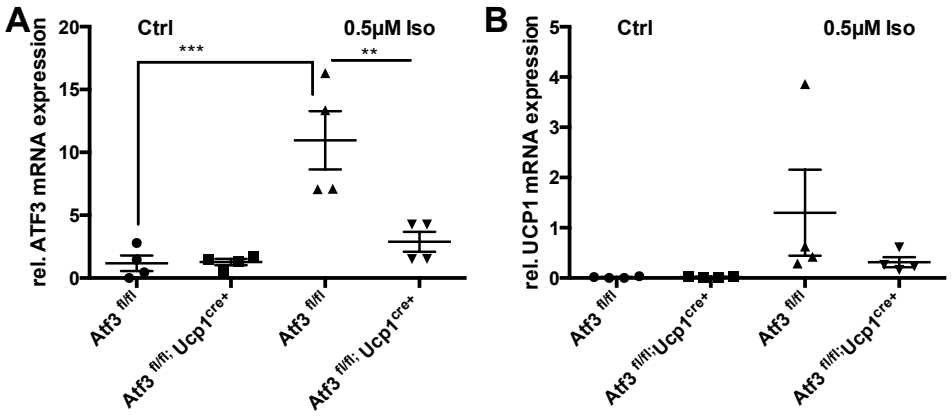

Figure 39 UCP1-specifc ATF3 ablation in primary brown adipocytes emerges upon isoproterenol stimulation. (A) Atf3 and (B) Ucp1 mRNA expression from primary differentiated brown adipocytes, treated with 0.5µM isoproterenol for 2h, isolated from female Atf3$^{fl/fl}$;Ucp1^{cre+} mice (n=4). Statistical analysis was tested via One-Way ANOVA, followerd by Tukey's multiple comparisons test.

Thereby, a significant up-regulation of *Atf3* expression upon isoproterenol stimulation was observed in Atf3$^{fl/fl}$ mice, which was diminished in Atf3$^{fl/fl}$;Ucp1^{cre+} mice.

In this chapter, it was shown that a deletion of ATF3 in brown adipocytes was barely detectable at baseline, but became visible when brown adipocytes were challenged with isoproterenol. Thus, ATF3 ablation in BAT did not make an impact on the phenotype of the transgenic male and female Atf3$^{fl/fl}$;Ucp1^{cre+} mice in basal conditions.

3.3.2 The UCP1-specific ablation of ATF3 does not impact the DIO phenotype

We and others have shown that ATF3 expression is up-regulated in white adipose tissue of rodent DIO models as well as genetic obesity models [18, 156, 157]. To elucidate the role of ATF3 in BAT, Atf3$^{fl/fl}$ and Atf3$^{fl/fl}$;Ucp1^{cre+} mice were challenged with RD 58% HFD (Table 4) for 13 weeks. Consistent with what has been shown before in wildtype mice (3.1.3), the RD 58% HFD increased the body weights of male and female Atf3$^{fl/fl}$ and Atf3$^{fl/fl}$;Ucp1^{cre+} mice over the time course of 13 weeks (Figure 40A and B). In this course, no significant genotypic difference in body weight gain was noticed in male and female mice, despite a slight trend to increased weight gain in female Atf3$^{fl/fl}$;Ucp1^{cre+} mice (Figure 40 A and B).

Only a gender-specific effect was seen, as male mice gained more body weight than female mice regarding both genotypes (Figure 40 A and B).

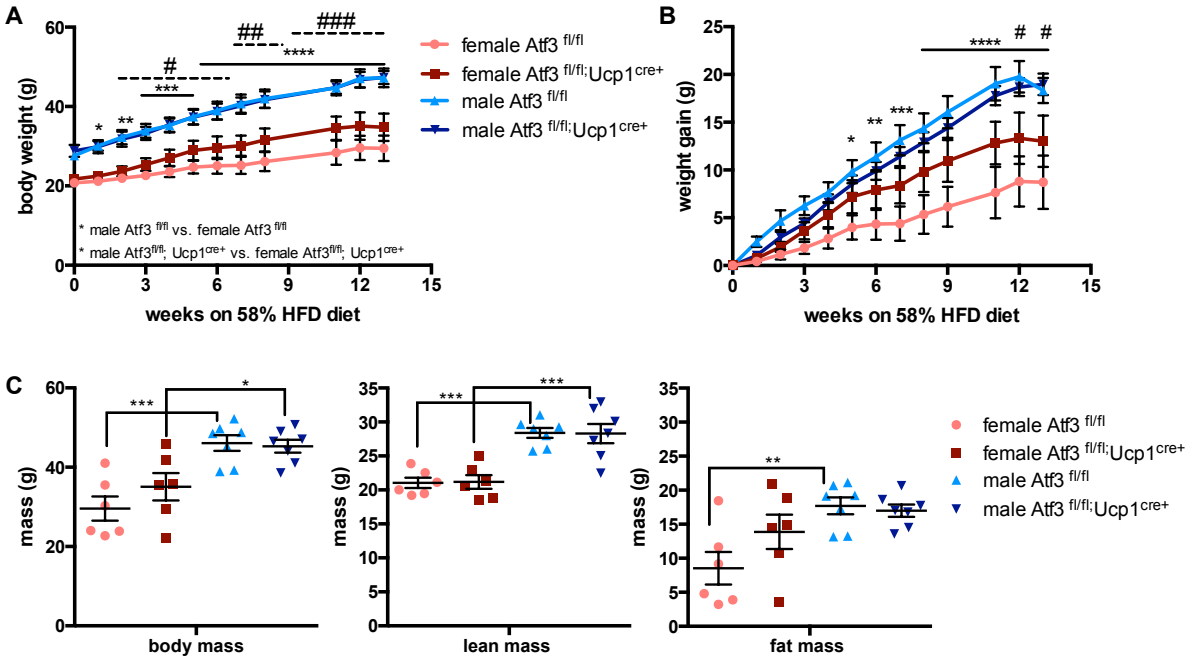

Figure 40 UCP1-specific ablation of ATF3 does not impact HFD-induced weight gain.
(A) Body weight course and (B) weight gain of male (n=7) and female (n=6) Atf3$^{fl/fl}$ and Atf3$^{fl/fl}$;Ucp1^{cre+} mice during 13 weeks of 58% kcal from fat HFD feeding. Significance was indicated with asteriks (*) regarding the comparison between male and female Atf3$^{fl/fl}$ mice and with pounds (#) regarding male and female Atf3$^{fl/fl}$;Ucp1^{cre+} mice. (C) Body-, lean-, and fat mass of male (n=7) and female (n=6) Atf3$^{fl/fl}$ and Atf3$^{fl/fl}$;Ucp1^{cre+} mice at 25 weeks of age, which were given a 58% kcal from fat HFD for 13 weeks. Statistical significance was determined via One-Way- or Two-Way ANOVA followed by Tukey's multiple comparisons test.

Yet, the difference in body weight gain of male vs. female Atf3$^{fl/fl}$;Ucp1^{cre+} mice became only apparent after 12 weeks of feeding, as female Atf3$^{fl/fl}$;Ucp1^{cre+} gained a substantial amount of body weight (male vs. female Atf3$^{fl/fl}$;Ucp1^{cre+}: 18.69 ± 0.95g vs. 13.33 ± 2.69g, $p<0.05$). Consistently, no significant change in body composition was detected due to the ablation of ATF3, as no differences in body mass, lean mass nor fat mass were seen in male and female Atf3$^{fl/fl}$ vs. Atf3$^{fl/fl}$;Ucp1^{cre+} mice (Figure 40C). Again, only a small, but insignificant trend to increased fat mass in female Atf3$^{fl/fl}$;Ucp1^{cre+} mice was found (Figure 40C).

Regarding both genders, no significant difference in perigonadal adipose tissue weights, liver weights or ectopic liver triglyceride accumulation were identified between Atf3$^{fl/fl}$ and Atf3$^{fl/fl}$;Ucp1^{cre+} mice after 13 weeks of HFD feeding (Figure 41A, B, C). Moreover, no genotype-specific alterations in the expression of hepatic phosphoenylpyruvate carboxykinase 1 (*Pepck 1*), acetyl-coA-carboxylase (*Acaca*), *Srebp1c* or *Srebp2* were identified. Only a down-regulation of *Srebp2* in the livers of male Atf3$^{fl/fl}$ mice was found when compared to female Atf3$^{fl/fl}$ mice (Figure 41D).

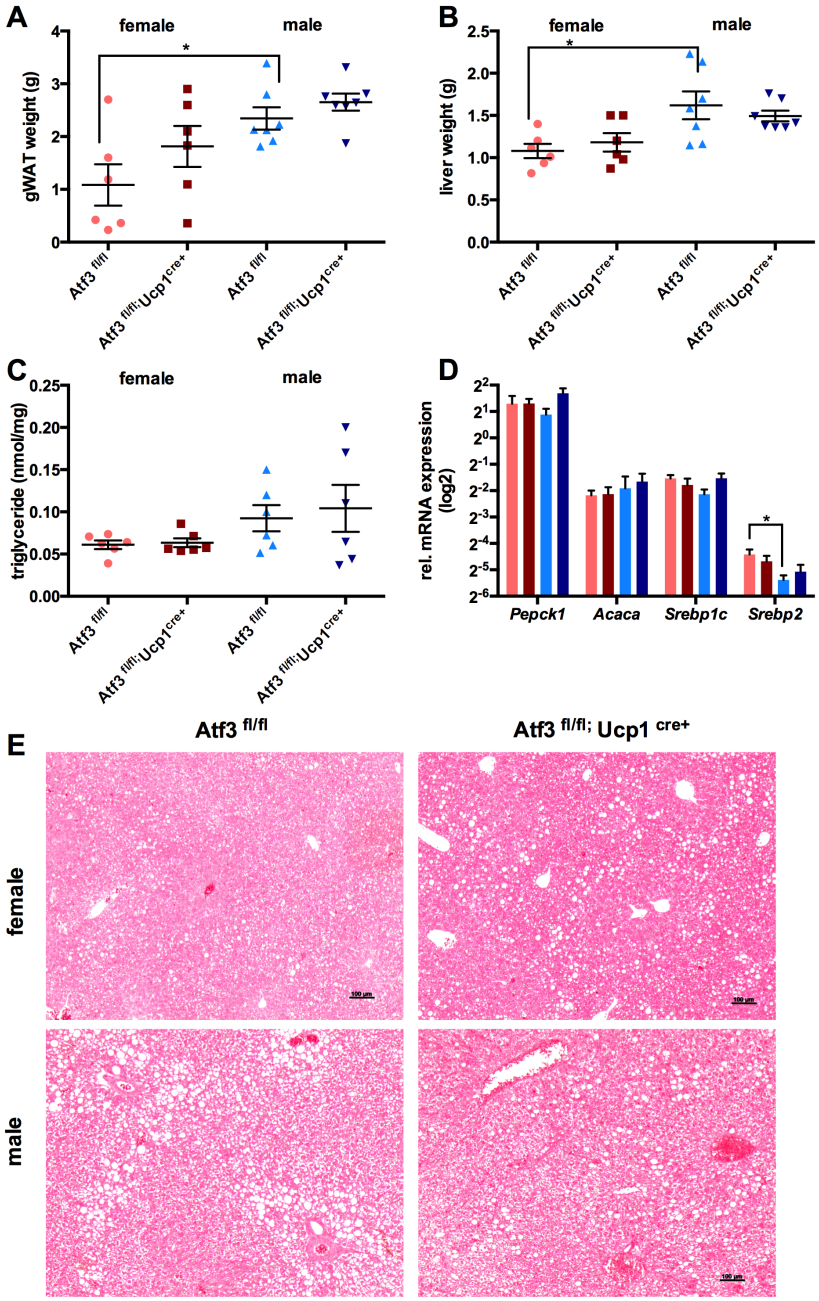

Figure 41 UCP1-specific ablation of ATF3 does not impact perigonadal adipose tissue and liver fat accumulation upon HFD feeding.
(A) gWAT and (B) liver weights and (C) liver triglycerides of male (n=7) and female (n=6) Atf3$^{fl/fl}$ and Atf3$^{fl/fl}$;Ucp1^{cre+} mice after 13 weeks of HFD. (D) mRNA expression of hepatic genes and representative pictures of livers from male (n=7) and female (n=6) Atf3$^{fl/fl}$ and Atf3$^{fl/fl}$;Ucp1^{cre+} mice. Statistical significance was determiend via One-way ANOVA followed by Tukey's multiple comparisons test.

This indicates, together with the elevated liver weights in male Atf3$^{fl/fl}$ mice (Figure 41C), that the cholesterol metabolism was more altered in male than female mice upon HFD, but was not altered by the ablation of ATF3 (Figure 41C, D).

13 weeks after the HFD-feeding, glucose tolerance was tested in male and female Atf3$^{fl/fl}$ and Atf3$^{fl/fl}$;Ucp1^{cre+} animals. As expected, male mice displayed a decreased glucose tolerance compared to

female mice (Figure 42A and B). However, no significant difference in the glucose tolerance was detected between HFD-fed Atf3$^{fl/fl}$ and Atf3$^{fl/fl}$;Ucp1^{cre+} mice of both genders, despite a trend to decreased glucose tolerance in the ATF3 ablated animals (Figure 42A and B).

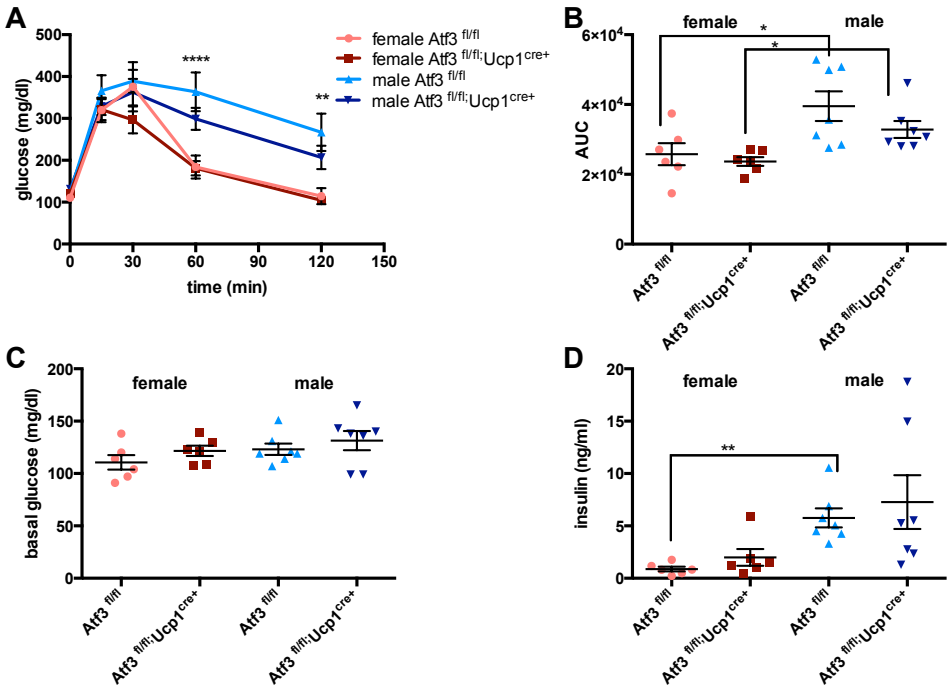

Figure 42 UCP1-specific ablation of ATF3 does not alter glucose homeostasis.
(A) Intraperitoneal glucose tolerance test (i.p. GTT with 2mg glucose/g body weight) of male (n=7) and female (n=6) Atf3$^{fl/fl}$ and Atf3$^{fl/fl}$;Ucp1^{cre+} mice at the end of the HFD feeding. * marks gender-specific statistical significance. (B) Calculated AUC during the i.p. GTT. (C) Basal glucose levels from male (n=7) and female (n=6) Atf3$^{fl/fl}$ and Atf3$^{fl/fl}$;Ucp1^{cre+} mice which were fasted for 6h. (D) Plasma levels of insulin after 13 weeks of HFD feeding. Statistical significance was determiend via One-way (B, C, D) - or two-way ANOVA (A) followed by Tukey's multiple comparisons test.

Consistent, no genotype-specific difference in basal glucose levels was found after 13 weeks of HFD feeding (Figure 42C). Circulating levels of insulin were generally significantly augmented in HFD-fed males when compared to females, but no differences were detected due to the depletion of ATF3 in BAT (Figure 42D). Concluding, HFD treatment did not induce any significant phenotypic differences between Atf3$^{fl/fl}$ and Atf3$^{fl/fl}$;Ucp1^{cre+} mice, neither in male, nor in female.

3.3.3 Atf3$^{fl/fl}$;Ucp1^{cre+} mice show increased BAT whitening after 13 weeks of HFD

Consistent with body mass, BAT weight was generally elevated in male mice, when compared to female mice. However, no genotype-specific differences in BAT weight were observed in male and female Atf3$^{fl/fl}$ and Atf3$^{fl/fl}$;Ucp1^{cre+} mice (Figure 43A). Regarding the mRNA expression of ATF3 in BAT from HFD fed mice, a trend to a down-regulation of *Atf3* was detected in Atf3$^{fl/fl}$;Ucp1^{cre+} compared to their Atf3$^{fl/fl}$ littermates. Yet, these differences were not statistically significant (Figure 43B).

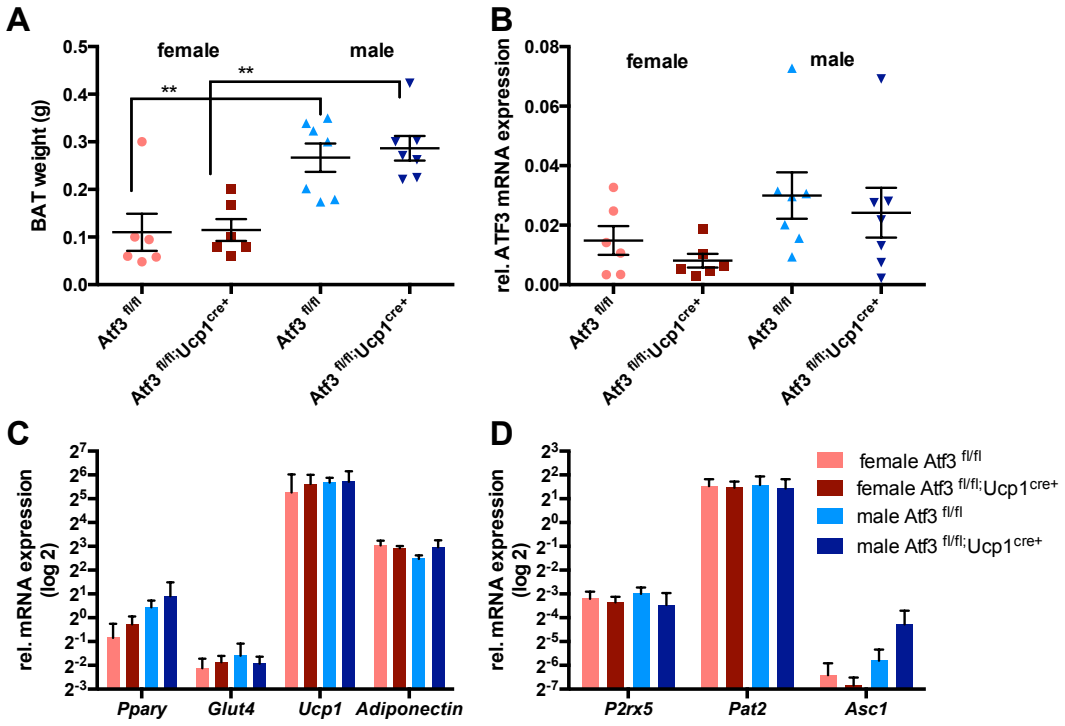

Figure 43 Expression of ATF3 and its downstream targets is not significantly altered in DIO Atf3$^{fl/fl}$;Ucp1^{cre+} male and female mice.

BAT weight of male (n=7) and female (n=6) Atf3$^{fl/fl}$ and Atf3$^{fl/fl}$;Ucp1^{cre+} mice after 13 weeks of HFD feeding. (B) ATF3 mRNA expression in BAT from of male (n=7) and female (n=6) Atf3$^{fl/fl}$ and Atf3$^{fl/fl}$;Ucp1^{cre+} mice after 13 weeks of HFD feeding. (C) mRNA expression of ATF3 target genes in BAT of male (n=7) and female (n=6) Atf3$^{fl/fl}$ and Atf3$^{fl/fl}$;Ucp1^{cre+} mice after 13 weeks of HFD feeding. (D) mRNA expression of brown and white adipocyte surface markers in BAT from of male (n=7) and female (n=6) Atf3$^{fl/fl}$ and Atf3$^{fl/fl}$;Ucp1^{cre+} after 13 weeks of HFD feeding. Statistical significance was determined via One-way or Two-way ANOVA followed by Tukey's multiple comparisons test.

In line with this, no changes in the expression of ATF3-downstream targets, such as *Ppary*, *Glut4* and *Adiponectin*, nor BAT-specific genes *Ucp1* and *P2rx5* and *Pat2* were observed in BAT from either male or female Atf3$^{fl/fl}$;Ucp1^{cre+} mice (Figure 43C and D).

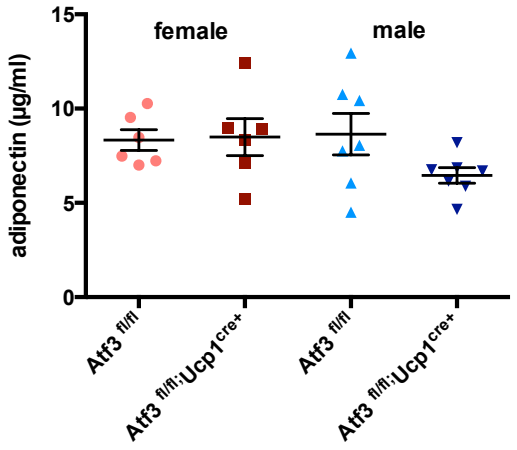

Figure 44 UCP1-specifc ablation of ATF3 does not change adiponectin levels after HFD feeding.
Plasma adiponectin (µg/ml) of male and female Atf3 $^{fl/fl}$ and Atf3$^{fl/fl}$;Ucp1^{cre+} mice (n=6-7).

Adiponectin is one of the known downstream target genes of ATF3, however the BAT specific deletion of ATF3 did not significantly impact circulating levels of this adipokine (Figure 44). Yet, a trend to an increased expression of white-adipocyte specific surface marker *Asc1* was found (Figure 43D) , especially in male Atf3$^{fl/fl}$;Ucp1^{cre+} mice, indicating the appearance of white adipocytes in BAT (Figure 45). Moreover, histological assessment of BAT revealed a trend to an increased whitening of the tissue in Atf3$^{fl/fl}$;Ucp1^{cre+} which was more pronounced in male than in female mice (Figure 45).

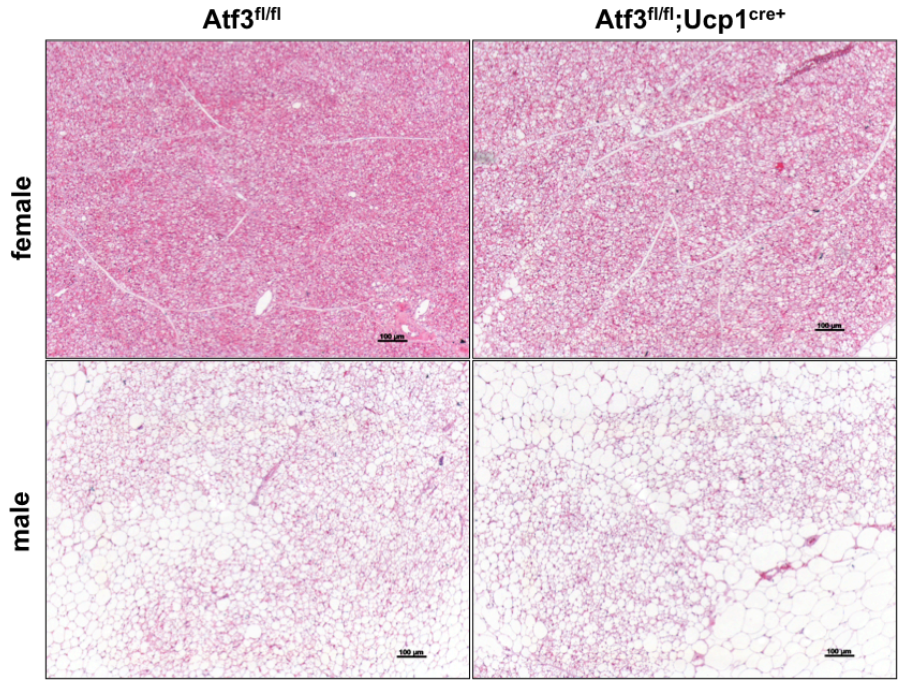

Figure 45 UCP1-specific ablation of ATF3 coincides with a whitening of BAT morphology.
Representative H&E stained sections of BAT from of male and female Atf3$^{fl/fl}$ and Atf3$^{fl/fl}$;Ucp1^{cre+} mice after 13 weeks of HFD feeding (100x magnification).

Therefore we can conclude that the specific deletion of ATF3 in brown adipocytes, is hardly detectable in BAT from HFD-fed mice. Yet, histologically, a trend to a "whitening" of the tissue has been observed in Atf3$^{fl/fl}$;Ucp1^{cre+} mice.

3.3.4 Female Atf3$^{fl/fl}$;Ucp1^{cre+} mice show decreased expression of beige cells in scWAT after 13 weeks of HFD

As UCP1-expressing cells can also be present in scWAT, as so-called brown-like or beige adipocytes, scWAT of male and female Atf3$^{fl/fl}$ and Atf3$^{fl/fl}$;Ucp1^{cre+}mice were analyzed. Consistent with the BAT tissue weights, no significant differences in scWAT tissue weights of male and female Atf3$^{fl/fl}$;Ucp1^{cre+}mice were observed, when compared to their Atf3$^{fl/fl}$ littermates (Figure 46A) despite a trend to higher scWAT weight in female Atf3$^{fl/fl}$;Ucp1^{cre+}mice. Moreover, ATF3 mRNA expression was not different between male and female Atf3$^{fl/fl}$ and Atf3$^{fl/fl}$;Ucp1^{cre+} mice (Figure 46B). A gender-specific down-regulation of *Ucp1*, *Adiponectin* and *Glut4* was found in male Atf3$^{fl/fl}$ mice ($p<0.05$ and $p<0.01$) (Figure 46C). However, UCP1 and GLUT4 mRNA expression was significantly down-regulated in female Atf3$^{fl/fl}$;Ucp1^{cre+} mice, compared to female Atf3$^{fl/fl}$ mice ($p<0.05$) (Figure 46C).

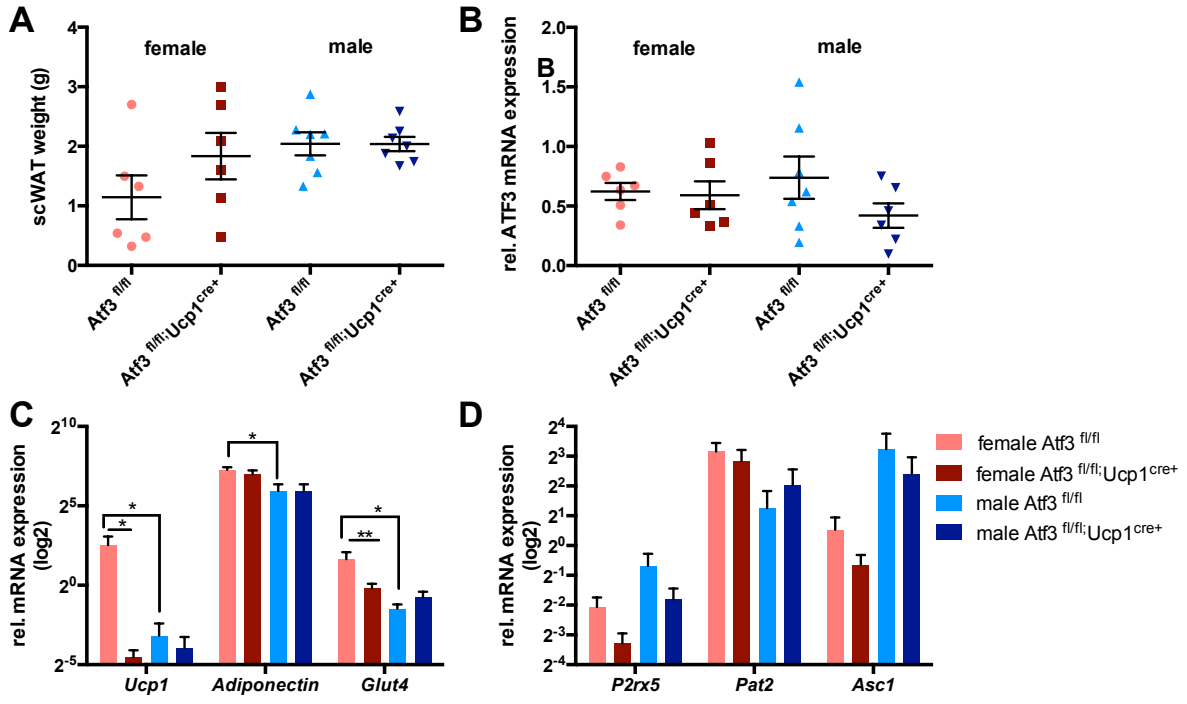

Figure 46 UCP1-specific ablation of ATF3 is associated with a gender-specific down-regulation of *Ucp1* and *Glut4* in female mice.
(A) scWAT weight of male (n=7) and female (n=6) Atf3$^{fl/fl}$ and Atf3$^{fl/fl}$;Ucp1^{cre+} mice after 13 weeks of HFD feeding. (B) ATF3 mRNA expression in scWAT from of male (n=7) and female (n=6) Atf3$^{fl/fl}$ and Atf3$^{fl/fl}$;Ucp1^{cre+} mice after 13 weeks of HFD feeding. (C) mRNA expression of ATF3 target genes in scWAT of male (n=7) and female (n=6) Atf3$^{fl/fl}$ and Atf3$^{fl/fl}$;Ucp1^{cre+} mice after 13 weeks of HFD feeding. (D) mRNA expression of brown and white cell surface markers in scWAT from of male (n=7) and female (n=6) Atf3$^{fl/fl}$ and Atf3$^{fl/fl}$;Ucp1^{cre+} mice after 13 weeks of HFD feeding. Statistical significance was determiend via One-way- or two-way ANOVA followed by Tukey's multiple comparisons test.

Moreover, mRNA levels of P2RX5, PAT2 and ASC1 were not differentially expressed in scWAT from male and female Atf3$^{fl/fl}$ and Atf3$^{fl/fl}$;Ucp1^{cre+}mice (Figure 46D), despite a trend to decreased *P2rx5* levels in Atf3$^{fl/fl}$;Ucp1^{cre+}mice.

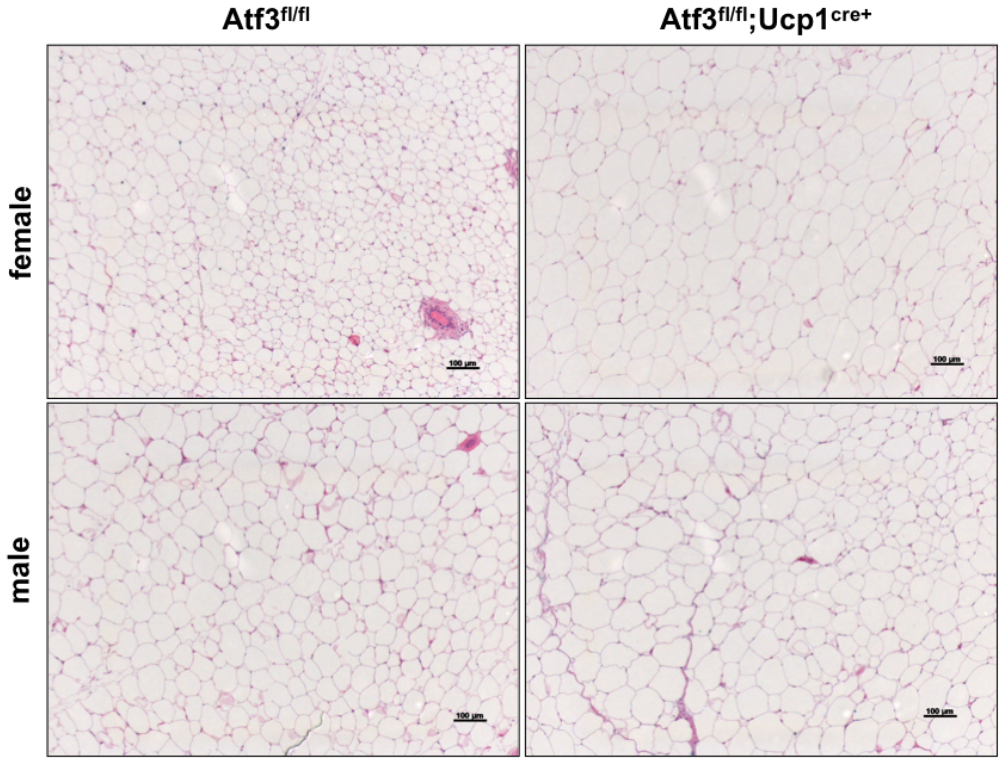

Figure 47 Female Atf3$^{fl/fl}$;Ucp1^{cre+} mice show increased hypertrophy in scWAT than Atf3$^{fl/fl}$ mice.
(A) Representative H&E stained sections of scWAT from of male and female Atf3$^{fl/fl}$ and Atf3$^{fl/fl}$;Ucp1^{cre+} mice after 13 weeks of HFD feeding (100x magnification).

However, histological assessment of scWAT revealed increased adipocyte sizes in female, as well as male Atf3$^{fl/fl}$;Ucp1^{cre+} mice, when compared to their floxed littermates (Figure 47). Concluding that despite no significant alteration of *Atf3* expression in scWAT, a lower expression of *Ucp1* and *Glut4* was found specifically in female Atf3$^{fl/fl}$;Ucp1^{cre+} mice, which was accompanied by increased adipocyte cell sizes.

4. Discussion

4.1 Standardization problems in DIO Studies

Obesity is a multifactorial disease, whose prevalence is dramatically growing and strongly associated with the development of other diseases, such as type 2 diabetes, NAFLD and cardiovascular diseases, contributing to the metabolic syndrome [183]. Therefore, finding ways to overcome obesity is one aim of current research worldwide. Especially pharmacological approaches to activate energy expenditure or to decrease energy intake are of interest [184, 185]. As previously mentioned (1.1), in humans, the development of obesity is impacted by various factors such as the (epi-) genetic predisposition, the composition of microbiota, a sedentary lifestyle and constant nutrient excess, individually contributing to the grade of overweight and obesity [1]. Therefore, precision medicine, an attempt to a more personalized medicinal approach to cure obesity, is the aim of the future [186, 187]. When studying novel therapeutics to cure obesity, diet-induced obese (DIO) animals are often the experimental model of choice, as they are considered more representative for the human situation, compared to genetic obesity models. Yet, the outcome of DIO experiments in mice is quite variable, depending on certain factors, such as the background of the animals used, the maintenance conditions of the animals, the detailed study design and most importantly the experimental diets used (Figure 48).

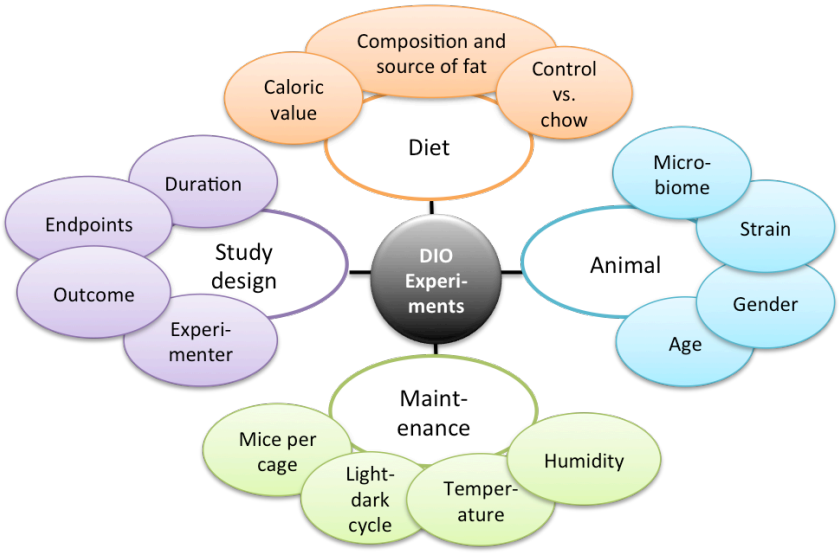

Figure 48 Factors impacting the development of DIO in mice.

Therefore, one aim of this thesis was to extend the knowledge on how the development of DIO can be influenced, by testing various experimental conditions. As previously mentioned before, C57BL/6 mice bred at the Jackson Laboratory (C57BL/6J) and the NIH (C57BL/6N) deviated already between 1940 and 1950 from the ancestral C57BL/6 line [188]. Known mutations affecting the susceptibility to DIO, such as the deletion of *Nnt* and 10 other SNPs occurred at the Jackson Laboratory after C57BL/6N mice were isolated [188]. According to the small literature research performed, most of the DIO publications from 2013 were performed in C57BL/6 mice, with little attribution to the used substrain. Thus, it was aimed to see what impact the substrain had on the development of DIO, in our housing conditions. At basal conditions, C57BL/6N mice displayed lower body mass, which was mainly due to lower lean, but not fat mass. Yet, a study by Nicholson et al. showed no difference in body mass between C57BL/6N and C57BL/6J mice, at 6 weeks of age and prior to any HFD feeding [109]. In the present study, male C57BL/6N mice showed an earlier onset of body weight gain and a higher final body weight after 16 weeks of feeding a lard-based 60% kcal HFD from Ssniff than C57BL/6J mice. This was in contrast to what was expected, as the opposite phenotype was previously described [108, 109, 189]. However, it was already reported in a study by Kahle et al that C57BL/6N mice displayed a higher fat- mass and body mass gain within 3 weeks feeding a plant-based 60% kcal from fat HFD [190], indicating that the contribution of the *Nnt* mutation to the susceptibility to DIO was possibly over-estimated. What should be also taken into consideration is the fact that C57BL/6J mice displayed a high variability in HFD-induced weight and fat mass gain, as the standard error of the mean was substantially higher than in C57BL/6N mice. This is suggesting that some C57BL/6J mice were not responding to the HFD feeding, a phenomenon, which was previously described [191], and could explain why C57BL/6N mice showed significantly increased weight gain in this experiment. Despite this, C57BL/6J mice displayed a higher fasting glycemia upon 60% HFD feeding, whereas C57BL/6N mice only presented slight, insignificant elevations of fasting glucose levels, confirming what has been previously shown and expected [104]. Still, glucose clearance during the i.p.GTT was comparable between HFD-fed C57BL/6N and C57BL/6J mice. Rather surprising was however the fact that C57BL/6J mice on the control diet developed a decreased glucose tolerance when compared to C57BL/6N mice, at 23 weeks of age.

Next, it was assessed, whether the type of HFD made an impact on the outcome of DIO experiments. The previously performed literature research identified Research Diets as the most popular company for experimental HFDs. However, many European research facilities obtain their experimental HFDs from different companies, which produce HFDs corresponding to the recipes from research diets. Therefore, the onset of obesity in male C57BL/6N mice was compared using two lard-based 60% kcal from fat HFDs, derived from Research Diets and Ssniff. Thereby, no difference in body weight development was found between the mice on either HFD. Only minor alterations were

found in glucose tolerance, as mice on the 'original' 60% HFD from Research Diets showed slightly worsened glucose tolerance than mice on the control diet did. Yet, this impact was respectively negligible.

Most publications use regular chow diets, instead of purified, compositionally defined, HFD-matched control or low-fat diets. This has some drawbacks, as it has been for instance shown that chow diets not only vary between vendors, but also show batch-to-batch differences in composition and source of nutrients (plant vs. animal based) [192]. On the other hand, energy-matched control diets may be enriched in sucrose, which can also impact the onset of glucose intolerance in 'control' mice and thus falsify the outcome of obesity studies. Chassaing et al nicely unraveled how feeding a 10% kcal from fat and 33% kcal from sucrose control diet increased body mass, fat mass and induced colon shortening in comparison to chow diet fed mice [192]. In general, sucrose is frequently discussed to be the true villain causing the obesity epidemic [193], as the amount of sugar consumption had been paralleling the obesity prevalence approximately until the early 2000s [194]. Moreover, consumption of high-fat, but very low-carbohydrate diets was associated with health benefits such as a reduction in body weight, triglycerides levels and diastolic blood pressure in humans [195]. Yet, in rodents, short-term ketogenic diet feeding showed weight loss with no alterations in glucose tolerance and insulin secretion in mice, while 20 weeks of feeding the ketogenic diets was associated with a reduction of glucose tolerance and loss of α- and β cell mass [196]. In the present study, 10% kcal from fat and 33%kcal from sucrose control diet was used (Figure 5) and only long-term feeding of the control diet (84 and 140 days) increased body mass and fat mass gain, as well as glucose intolerance in male, but not female C57BL/6N mice. However, as these changes became only significant after long-term feeding, one could also argue that these alterations were age-induced, as it is also known that ageing can impair glucose tolerance in C57BL/6 mice [197].

In general, it has been multiply shown and is common sense that the duration of HFD feeding positively correlates with the level of weight gain, fat mass gain and glucose intolerance [198-200]. Consistent with this, in this present experiment the time-dependent increase in body weight was paralleled with an increase in fat and lean mass as well as an increase in adipose tissue weights (data not shown). Basal glucose levels increased in a time-dependent manner, except for the 56 days cohorts, where basal glucose levels were lower than in the 14 days cohorts. Yet, hyperinsulinemia only occurred in the 84 days and 140 days cohorts in male and female mice, indicating that the hyperglycemia in the 14 days cohort could be due to nutrient overflow, whereby the hyperglycemia in the long-term feedings was caused by the development of obesity-associated insulin resistance, as it has been proposed in an similar approach by Kless et al. in AKR/J and SWR/J mice [201]. Still, this effect could be also due to inter-cohort-variability combined with effects of seasonal changes. As previously described, the 56 days cohort was started in March and not in autumn, like the other

cohorts were started. Although all mice were housed in the same room of the same conventional animal facility, with controlled ambient temperature, humidity and light/dark cycle, it is imaginable that differences in the housing conditions, for instance difference of mice cohorts housed there at the respective time and respective researchers entering and leaving the room, could also impact the low response to DIO in this cohort. Especially female mice gained comparably low amounts of weight during the 56 days feeding experiment. This might have been caused by higher stress levels. It was for instance shown that the experimenters' odor influenced the stress response in rodents [202] and conventional housing impacted the outcome of DIO studies more than for instance specific-pathogen-free housing [203] and the use of individually ventilated cages. Even the position of the cages in the rack was discussed to explain variations in the outcome of DIO studies [191].

Unlike in the human situation, especially male C57BL/6J mice were proven to be more susceptible to DIO than female mice [112]. In line, in this present work, the development of obesity was more pronounced in male but not female mice during the shorter-term cohorts. Only in the longer-term cohorts, meaning 84 and 140 days of feeding, female mice given the 60% kcal from fat HFD displayed similar body weights and fat mass as male mice on the same diet. Yet, one has to point out, that the 84 days cohort of female mice on the 60% HFD, showed significantly increased body mass at 84 days than the female mice of the 140 days cohort at the same time point. This is again indicating a high inter-study variability, which can be attributed to rather "intrinsic factors" than "extrinsic factors", since the cohorts were running in parallel. Also only in the long-term feeding cohorts, significant hyperinsulinemia was detected in female mice, indicating that they were more protected against insulin resistance in the beginning. The later onset of obesity and hyperinsulinemia is likely due to a variety of factors, but the involvement of sex hormones secretion should be taken into account. It was for instance shown that the absence or decrease in estrogen is paralleled by the induction of obesity and insulin resistance in men and in women [1, 204]. Dakin et al. for instance showed that supplementation with estradiol ameliorated obesity induced glucose intolerance and insulin resistance in male C57BL/6 mice after 5 weeks of HFD feeding [205]. Furthermore, the lipolytic effect of estrogen, mediated through estrogen-related receptor α (ERα) was shown to be associated with decreased accumulation of fat in the visceral tissues and decreased development of insulin resistance [112].

Lastly, the literature research performed, identified 60% kcal from fat HFDs as the most abundantly used diets in DIO research, followed by 45% kcal from fat diets. In the experiments performed here, the development of DIO was compared upon feeding lard-based 45% and 60% HFDs, derived from Ssniff. Thereby, the differences in the outcome between these two experimental feedings were not markedly present, as changes, due to the higher fat content of the diet, in body and fat mass, as well as changes in glucose and insulin levels became only apparent in the long-term feeding

cohorts. Indicating that the increased dietary lipid content HFDs do not necessarily fuel fastened obesity and its related symptoms. A similar finding was also previously presented by Benoit and colleagues, who displayed that feeding a 45% HFD for 12 weeks increased body weights and relevant metabolic parameters in mice, but was not associated with inflammation, whereas feeding a 22% HFD induced the opposite phenotype [206]. Moreover, it was shown that the texture and palatability of the diets influences hyperphagia and the onset of DIO more than the actual lipid content [207].

4.2 Diet-induced weight loss is associated with an inflammatory fingerprint in liver and adipose tissue of formerly obese mice

Using a model of diet-switched mice, we aimed to investigate the molecular alterations inherited from a history of DIO. Changes in diet and exercise are the preferred method of weight loss for the vast majority of the population [208-211]. Yet, weight loss following dietary interventions are not sustainable, as most obese patients re-bounce to a higher body weight than their pre-dieting weight within one year [120, 123]. In 1998, the group of Richard S. Surwit already showed the reversal of a DIO-phenotype by a reduction of dietary fat intake in the C57BL/6 strain [212]. There, mice were fed a 58%kcal HFD for 16 weeks, after which half of the HFD-fed mice were switched to a LFD for further 16 weeks. In line with this study, the diet-switch reversed fat mass, hyperglycemia and hyperinsulinemia within 16 weeks after the diet change [212]. In this present study, body and fat masses were normalized 7 weeks after the diet-switch. At this time point, glucose tolerances of formerly obese mice were congruent to those of the age-matched lean mice [18]. Moreover, here, formerly obese mice showed the same levels of circulating insulin and leptin to lean mice, 7 weeks after the diet-switch [18]. Consistently, Shi et al. reported a normalization of plasma leptin and insulin levels in DIO mice, already two weeks after the diet-switch to the low-fat diet *ad libitum* [213]. Despite the fact that the diet-switched mice retained a greater amount of body and fat mass, HFD-induced glucose intolerance was reversed two weeks after the switch [213], indicating that the restoration of glucose tolerance, insulin and leptin resistance is preceding the restoration of body mass. This was further in accordance with a previous study, where Enriori et al. showed that leptin sensitivity and glycemic control was restored, by decreasing the dietary fat content of the diet, the mice got *ad libitum* [136]. The reduction of leptin in the plasma has been discussed to be the cause for the observed hyperphagia upon weight loss. Previously, it has been shown, that caloric restriction and weight loss, induced by Roux-en-Y gastric bypass can induce browning and energy expenditure in white adipose tissue [175, 214]. However, in the present study, the *ad libitum* switch to a LFD did not induce expression of thermogenic genes in scWAT nor BAT and did not affect BAT respiratory capacity [18], which is also consistent with a newer study showing no browning of subcutaneous

tissue upon caloric restriction [215]. This is indicating that the achieved weight loss was solely due to decreased caloric intake and not increased energy expenditure.

It was previously demonstrated that restricting the caloric intake by at least 50% of the average energy intake of control mice, induces acute and persistent hyperphagia and body weight rebound of formerly obese mice upon *ad libitum* re-feeding of both, low- and high-fat diets [127, 176]. Interestingly, in the current model, in which moderate caloric restriction was caused by an *ad libitum* switch to a LFD, neither accelerated food intake nor body weight gain of formerly obese mice could be observed when they were re-introduced to HFD *ad libitum* [18]. Moreover, no shifts towards an increased orexigenic hypothalamic mRNA expression of *Pomc* and *Leptinr* were assessed, as it was described before upon weight loss and re-feeding [127, 176]. Additionally, hypothalamic inflammation, which has been shown to occur already after one day of HFD feeding [178], was reversed in formerly obese mice, which is in line with what has been reported [127, 216]. Moreover, hypothalamic inflammation was not influenced by a history of DIO when compared to age-matched lean mice, upon 48h of re-feeding [18].

As previously mentioned (1.3.2), NAFLD is considered an important complication of obesity. In the present study, DIO mice showed increased liver weights and triglyceride contents when compared to lean mice. Moreover, 7 weeks after the diet-switch, formerly obese mice exhibited a normalized liver mass and triglyceride content [18]. Kowalski et al. recently showed that reducing dietary intake *ad libitum* normalizes liver mass and triglyceride contents within 9 days after the switch, to such an extent that the diet-switched mice did not differ from the chow-fed control mice [217]. In this experiment, obese mice showed a severe accumulation of macrovesicular fat droplets and portal-to portal as well as pericellular, so-called “chicken-wire fibrosis”, which was in the same range as described before in DIO mice, fed HFD for 24 weeks [200]. Despite the fact that liver weight and triglyceride content were not statistically different from those of lean mice, it was intriguing to find that the livers of formerly obese mice histologically showed elevated signs of fibrosis and fat accumulation than lean mice. Many studies in mice and men have demonstrated that weight loss interventions have beneficial effects on the outcome of NAFLD [218, 219], yet, no significant reduction in liver fibrosis were detected in formerly obese mice. Consistent with this, Myrononovych et al. previously reported that caloric restriction was not as potent in reducing obesity associated hepatic steatosis as vertical sleeve gastrectomy in DIO mice [220]. In line, increased mRNA levels of inflammatory cytokine *Il1β* discovered in the livers of formerly obese mice, when compared to those of lean mice, further indicating that the obesity-related hepatic inflammation was not fully recovered upon weight loss [18]. Moreover, mRNA levels of *Srebp2* and *Ldlr* were persistently down-regulated upon obesity and in formerly obese mice [18]. Suggesting, that the livers of formerly obese mice were still saturated with cholesterol, despite a (tissue) weight normalization. In line with this, transcriptional

profiling of the livers from formerly obese and lean mice revealed 199 genes to be up- and 123 to be significantly down-regulated in the direct comparison between formerly obese and lean mice (FC >1.2, p< 0.01, Av>8). One of the top down-regulated gene was elongation of very long chain fatty acids –like *Elovl3* (FC -1.527), an enzyme that controls the rate-limiting step in the long chain fatty-acid elongation cycles and its hepatic expression has been described to be regulated by steroid hormones following a diurnal rhythm exclusively in male mature mice [221].

Moreover, the top-associated pathways with the differentially regulated genes was "inflammatory response" in the livers of formerly obese vs. lean mice. Moreover, the hepatic cholestasis pathway was also enriched (data not shown). However, it remains elusive whether prolonged maintenance on a LFD would ameliorate or fully recover observed hepatic alterations in formerly obese mice.

The most striking finding was that scWAT and gWAT showed a remarkable heterogeneity concerning their response to weight loss. In detail, an opposing mRNA expression of *Leptin* and *Adiponectin* in scWAT and gWAT was identified during obese and formerly obese conditions. Consistently, as previously mentioned in the introduction, it was already known that leptin is higher expressed in subcutaneous than visceral adipose tissue in lean and obese subjects [46, 47], whereas adiponectin expression has been shown to be oppositely regulated [222, 223]. Moreover, in this present experiment, adipocyte cell expansion was only reversed in the subcutaneous but not perigonadal depot of the formerly obese mice upon weight loss [18]. Previous studies indicate that the fat cell volume positively correlates with fat mass in lean and obese conditions, regarding the visceral and subcutaneous depot [128]. Here, tissue weights of both, scWAT and gWAT from formerly obese mice were not different to lean mice. Yet, a depot-specific hypertrophy was found in pergionadal adipocytes from formerly obese mice [18]. It was shown that scWAT cell sizes correlate inversely with insulin sensitivity and the rate of weight loss in formerly obese patients [63, 64]. Moreover we know that visceral adipocytes have a limited capacity to expand. Upon reaching this limitation, M1 type macrophage infiltration and subsequent CLS formation takes place, inducing a higher rate of fat cell turnover [58, 62, 224]. Transferring this to the present study, one could argue that here, the reduction of gWAT weight upon weight loss in formerly obese mice was mainly caused by a higher fat cell turnover, rather than a reduction of hypertrophy. The notion that subcutaneous fat is less metabolically harmful is supported by transplantation studies in mice where transplantation of subcutaneous adipose tissue from lean mice into the visceral cavity have beneficial effects on body weight, glucose metabolism and improve insulin sensitivity [39] in lean [225] and obese [226, 227] subjects. In contrast, transplantation of visceral adipose tissue to subcutaneous sites was associated with transient reduction of adipose tissue mass [39] or no beneficial metabolic effects [225, 228] while few studies show metabolic advantages [39, 229]. Therefore, epidemiological studies on 'obese but metabolically healthy' and 'lean but metabolically obese' individuals, as well as transplantation

studies suggest that visceral adiposity is more harmful than peripheral, subcutaneous obesity, and is therefore for considered a risk factor for the development of NAFLD and type 2 diabetes [230] [18].

As mentioned before, it has been reported that weight loss, induced by caloric restriction or bariatric surgery, improves the metabolic phenotype but not white adipose tissue inflammation in mice and obese patients respectively, one year post-intervention [176]. Consistently, deep transcriptional profiling confirmed that also in the current experiment, a history of obesity induced differential gene expression of in total 309 genes in gWAT of formerly obese mice vs. lean mice, which were related to networks regarding innate immunity, inflammation and cell death and survival. Together with the increased CLS formation found, this is further strengthening the hypothesis that weight-loss induced visceral adipose tissue reduction is rather caused by a higher fat call turnover and remodeling of the tissue than a reduction of hypertrophy [18]. However, the exact mechanisms of tissue remodeling remains to be addressed in future studies, especially assessing the putative influence of identified differentially regulated genes.

4.3. BAT-derived ATF3 does not impact the development of DIO in mice

In the previous chapter, Activating Transcription Factor 3 (ATF3) was identified to be up-regulated in WAT and BAT of obese and formerly obese mice when compared to lean mice. This was considered particularly interesting, since the role of ATF3 was not described in murine BAT so far, except for a recent finding from our group, proposing ATF3 as a noradrenergic response gene in BAT [165]. Multiple functions of the transcriptional regulator ATF3 have been attributed to various cell types. To elucidate the importance of ATF3 in BAT metabolism, a UCP1- specific ATF3 loss-of function model was applied. In the experimental set-up, no phenotypic or molecular changes of male and female mice carrying the UCP1-specifc ATF3 depletion were identified, when compared to their floxed littermates at basal conditions. Only gender-specific differences within the genotypes were found, as male mice had increased body mass when compared to female mice. Consistent with what was presented before (3.1.4), this sex-difference in body weight has been numerously reported in wildtype animals [111, 191]. Yet, somewhat surprising was the fact that *Atf3* expression was not different between the two genotypes, first proposing a problem within the experimental procedure and the generation of a knockout line. However, previous reports show that ATF3 is barely detectable in basal, un-stressed or un-stimulated cells [231]. In line, the depletion of ATF3 became only detectable in isoproterenol-stimulated adipocytes. Previously, it was shown that *Atf3* is highly expressed in perigonadal adipose tissue of (diet-induced) obese animals [157, 232], which we could also confirm [18]. Since *Atf3* was also expressed in BAT of male obese and formerly obese mice, it was aimed to elucidate the specific role of ATF3 in BAT from DIO mice, by applying a HFD-challenge to the created UCP1-specific conditional knockout mice. Thereby, no differences were found in the DIO

phenotype of UCP1-specific ATF3 depleted mice, as no differences in weight gain, glucose tolerance or hyperinsulinemia were detected, when compared to the gender-matched floxed littermates. In line, whole body ATF3ko mice, which experienced a metabolic stress in form of a HFD feeding, were shown to display the same onset of obesity as their floxed littermates regarding the increase of body mass, hyperphagia and hyperglycemia [153]. Yet, whole body ATF3ko mice on HFD exhibited impaired glucose tolerance, when compared to wildtype mice, despite no difference in basal glucose levels or insulin clearance [153]. Indicating that BAT-derived ATF3 does not contribute to the previously described impaired glucose tolerance of ATF3 whole body knockout. NAFLD is considered a hallmark for obesity [20]. Here, no differences in liver weights nor triglyceride contents could be identified in the livers of female and male $Atf3^{fl/fl}$;$Ucp1^{cre+}$ versus $Atf3^{fl/fl}$ mice, indicating that the onset of NAFLD was not impaired by the presence of ATF3 in brown adipocytes. Before, it was shown that ATF3 overexpression in β-cells was associated with a decrease of hepatic gluconeogenic genes [148]. Here, neither the expression of hepatic gluconeogenesis markers, nor lipolysis or lipogenesis markers were altered between the genotypes, regarding both genders.

Surprisingly, despite a trend to a down-regulation of ATF3 mRNA expression in BAT of $Atf3^{fl/fl}$;$Ucp1^{cre+}$ mice, no significant reduction of *Atf3* could be detected, neither in male nor female obese mice. This can most likely be explained by the fact, that ATF3 is also induced under HFD in other cell types from the stromal vascular fraction (SVF), such as macrophages or pre-adipocytes [233]. Therefore, the down-regulation of ATF3 in this conditional knockout model might have been overwritten by the increased expression of ATF3 in adipose tissue macrophages. To confirm this theory, isolation of brown adipocytes and SVF/ or macrophages from lean and obese $Atf3^{fl/fl}$ and $Atf3^{fl/fl}$;$Ucp1^{cre+}$ mice will be mandatory. Unfortunately, these determinations have not been completed during my PhD-project. Moreover, in our hands, it was unfortunately not possible to detect ATF3 protein levels via Western Blot, neither in un-stressed nor stressed tissues of wildtype and $Atf3^{fl/fl}$;$Ucp1^{cre+}$ animals, though various attempts were made, using different kinds of mono- or polyclonal ATF3-antibodies in whole cell lysates as well as nuclear fractions (data not shown). Therefore, to gain knowledge to this experiment, detection of protein contents will be necessary. In humans, BAT activity and mass negatively correlate with body-, fat mass and circulating glucose levels [86]. Here, no significant differences in BAT weight were identified between $Atf3^{fl/fl}$ and $Atf3^{fl/fl}$;$Ucp1^{cre+}$ mice. In the present study, expression levels of BAT specific markers, such as *Ucp1* were not impacted by the ablation of ATF3 in brown adipocytes. Previously, it has been shown by Jang et al. that overexpression of ATF3, e.g, due to hypoxia, was associated with decreased expression of adipogenesis markers PPARy and decreased differentiation of 3T3L1 adipocytes [159, 160]. By implication, ablation of ATF3 could induce enhanced differentiation and increased expression of adipogenesis markers PPARY, GLUT4 and Adiponectin in brown adipocytes. Here, *Ppary*, *Glut4* and

Adiponectin were however not altered in obese BAT of this transgenic model (Figure 43). Of note, in isolated primary subcutaneous pre-adipocytes from lean $Atf3^{fl/fl}$;$Ucp1^{cre+}$ mice, a trend to an up-regulation of UCP1 mRNA expression was identified upon rosiglitazone stimulated differentiation (Figure 38B). Indicating that the absence of ATF3 could enhance *Ucp1* expression in subcutaneous adipocytes, consistent with the just mentioned finding of Jang et al. [159], showing that ATF3 expression diminishes differentiation and adipogenesis in 3T3L1 cells.

Studies performed in rodents have shown that UCP1 expression was diminished in BAT from *ob/ob* mice [234]. Consistently, the transition from the typical brown fat morphology to a white fat - like morphology, including the loss of multilocular lipid droplets, vascularization, UCP1 and β-adrenergic receptors expressions, cumulating in mitochondrial dysfunction and BAT inactivity, was already described in brown adipocytes from HFD-fed rodents [182]. Here, a whitening of BAT tissue was detected in DIO- $Atf3^{fl/fl}$;$Ucp1^{cre+}$ male and female mice, compared to $Atf3^{fl/fl}$ mice. Indicating that the loss of ATF3 could be involved in increased triglyceride accumulation and lipogenesis upon HFD-feeding. Interestingly, it has been reported that ATF3 expression was augmented upon lipolysis in adipose tissue macrophages and endothelial cells [233, 235]. To validate whether the loss of ATF3 was indeed involved in lipogenesis, quantification of adipocyte sizes and assessment of lipogenesis and lipolysis markers remain to be determined.

Similarly to the whitening of BAT, a hypertrophy in WAT of male and especially female $Atf3^{fl/fl}$;$Ucp1^{cre+}$ mice was observed, despite only a trend to a significant difference in tissue weight. Adipogenesis and activation of beige adipocytes in the scWAT can be induced by various signals, e.g rosiglitazone treatment, and has been shown to contribute to an overall increase of energy expenditure, fueling the protection against DIO in rodents [236, 237]. Strikingly, we identified a significant down-regulation of *Ucp1* in scWAT of HFD-fed female $Atf3^{fl/fl}$;$Ucp1^{cre+}$ mice compared to floxed littermates. This was in contrast to the above-mentioned *in vitro* trend of increased *Ucp1* expression in rosiglitazone-differentiated subcutaneous adipocytes from lean $Atf3^{fl/fl}$;$Ucp1^{cre+}$. However, the result from the *in vitro* experiment was not statistically significant and performed in isolated and differentiated pre-adipocytes from lean male and female mice. Due to low n-sizes, these data could not be separated by gender. Thus it is hard to draw conclusions from there. The fact that females have a higher amount of beige adipocytes in the subcutaneous fat than male mice [238] in basal states is known. Moreover, it has been reported that females are more susceptible to noradrenergic- induced browning of white fat [239]. This might explain why the overall levels of UCP1 expression were higher in HFD-female than in HFD-male mice of both genotypes in this experiment. The transition from beige adipocytes back to "normal" white adipocytes takes place already after a short adaptation in thermoneutral conditions [240], by inhibition of the beta-adrenergic pathway [241] and by HFD-feeding. Here, HFD-fed female $Atf3^{fl/fl}$;$Ucp1^{cre+}$ mice gained slightly more weight and expressed less

brown like cells in scWAT than floxed females. We know that UCP1-expressing subcutaneous adipocytes can adopt distinct anabolic or catabolic functions, depending on the duration of adrenergic stimulation [92] and metabolic demands [85]. Thus, it is not clear whether the HFD-induced down-regulation of *Ucp1* was responsible for the increase in body mass in ATF3-lacking females, or whether the ablation of ATF3 was actually responsible for the loss of beige adipocytes in HFD-conditions. Therefore, the exact hierarchy of events remains to be elucidated. In sum, these data provide first indications that BAT-ATF3 does not affect HFD-induced weight gain and glucose intolerance, but could be involved in the regulation of lipogenesis and adipogenesis.

5. Conclusion and perspectives

Summing up, the work of this thesis has extended the knowledge on experimental conditions, which impact the outcome of DIO in C57BL/6 mice and further revealed some of the molecular alterations following a history of DIO. In detail, in this current work, the common knowledge that C57BL/6J mice are more susceptible to DIO was contradicted, as C57BL/6N mice were identified to be more susceptible to HFD-induced weight gain. As expected, the duration of feeding was positively correlated with the level of weight gain. However, glucose intolerance was already detected after 14 days of HFD feeding in male and female C57BL/6N mice, whereas hyperinsulinemia only manifested in the 84 days and 140 days cohorts. Suggesting that when aiming to study effects on obesity-associated insulin resistance, HFD-experiments should be performed in longer feeding experiments. In addition, the level of body and fat mass gain was not instantly affected by increased amount of dietary fat content in the HFDs, but only emerged after longer feeding durations. Importantly, in these experiments, male control diet-fed male mice also gained a substantial amount of body weight and showed an impairment in glucose tolerance after long term feeding. Indicating that the decrease in glucose tolerance was not only fueled by an excess intake of dietary fat, but also an excess of sucrose. Therefore, special care has to be taken when using HFD-matched control diets, rich in sucrose. In addition, it must be noticed that a high inter-study variability was detected, which was particularly present in female mice and might have been caused by intrinsic factors, e.g. mice "non-responding" to a HFD or extrinsic factors, e.g. due to changes in the onset time of feeding. Previously, female C57BL/6N mice were discussed to be resistant to DIO. Here, also female C57BL/6N mice gained a substantial amount of body weight in the 84 and 140 days cohort, indicating that the onset of DIO in female C57BL/6N mice might only be shifted in time, rather than being actually absent. Of course, one has to keep in mind that these present findings result from experiments performed with relatively low statistical power, as used n-sizes were ranging between 6 and 18 animals per group. Therefore, to confirm these findings, a repetition of these experimental feeding studies will be necessary. However, one can conclude that, in order to guarantee comparability between DIO studies, experimental set-ups should be well thought-through and adapted to the respective outcome of interest (e.g. hyperglycemia or hyperinsulinemia).

In the context of this dissertation, it was moreover shown that DIO in male C57BL/6J mice can be reversed with a simple switch from a HFD to a LFD *ad libitum*. Thereby, the achieved weight loss was paralleled by a reduction of fat mass, glucose intolerance and circulating metabolic parameters, within 7 weeks after the switch [18]. Furthermore, it was demonstrated that a switch to a low-fat diet *ad libitum,* in contrast to severe caloric restriction as previously shown, did not induce orexigenic hypothalamic alterations, which facilitated body mass rebound within 48h of hypercaloric (re-)

feeding. Therefore, one can speculate that hyperphagia in formerly obese mice can be influenced by the level of caloric restriction, the mice have undergone [126]. Of note, it remains elusive whether prolonged HFD re-feeding would impact body weight rebound in this model of formerly obese mice. To answer this, further studies will be necessary. Importantly, it was identified that a history of obesity was associated with specific inflammatory fingerprints in the liver and adipose tissue of formerly obese mice. This was shown by signs of liver inflammation and fibrosis as well as adipocyte hypertrophy in gWAT, which were not completely recovered in formerly obese mice [18]. Suggesting that these pro-inflammatory molecular alterations could set the stage for the recurring weight gain observed in formerly obese patients. Thus, it will be necessary to study the impact of in liver and gWAT of obese and formerly obese mice identified up-regulated genes on the development of DIO, in more detail. Therefore, also other researchers might profit from the detailed description of the differentially regulated genes in gWAT and livers of formerly obese and lean mice.

Within the scope of this dissertation, ATF3 was identified as an interesting candidate gene, as its mRNA expression was up-regulated in BAT and gWAT of obese and formerly obese mice. Therefore, the impact of BAT-derived ATF3 was assessed on the development of DIO, by applying an UCP1-specific conditional knockout mouse line. While hardly detectable at basal states, the UCP1-specific ablation of ATF3 became apparent in isoproterenol-activated brown adipocytes. Confirming the previously in our group identified finding that ATF3 was an adrenergic response gene in BAT. Yet, the UCP1-specific ablation of ATF3 did not impact the susceptibility to DIO in male or female C57BL/6N mice, regarding the onset of body weight and fat mass gain, glucose intolerance and hyperinsulinemia. Only a slight trend to a hypertrophy of adipocytes was observed in BAT and scWAT from $Atf3^{fl/fl}$;$Ucp1^{cre+}$ mice, when compared to floxed littermates. This “whitening” phenotype was further paralleled by a reduction of *Ucp1* and *Glut4* expression in subcutaneous white adipocytes from female $Atf3^{fl/fl}$;$Ucp1^{cre+}$ mice. Of note, an overall significant reduction of *Atf3* in BAT could not be detected, which might be caused by a compensatory expression of ATF3 in the SVF of the BAT. Therefore, further studies will be necessary, dissecting the expression of ATF3 in brown adipocytes from the expression of ATF3 in the SVF in lean and obese $Atf3^{fl/fl}$;$Ucp1^{cre+}$animals. Thereby, also ER-stress and mitochondrial-stress pathways will be interesting to assess, in the context of obesity-induced hypoxia. Additionally, the whitening of BAT and scWAT in HFD-fed $Atf3^{fl/fl}$;$Ucp1^{cre+}$ mice needs to be further addressed by quantification of adipocyte cell sizes and lipogenesis markers. Moreover, in order to fully understand the function of ATF3 in BAT thermogenesis, $Atf3^{fl/fl}$;$Ucp1^{cre+}$ mice will have to be exposed to a noradrenergic stimulus and energy expenditure will have to be monitored subsequently. Yet, this present work is the first to describe the up-regulation of ATF3 in BAT of obese and formerly obese mice. Taken together, the present work exhibits novel insights on the interplay between dietary interventions and selected metabolic and genetic parameters.

References

1. Schoettl, T., I.P. Fischer, and S. Ussar, Heterogeneity of adipose tissue in development and metabolic function. J Exp Biol, 2018. 221(Pt Suppl 1).

2. WHO, Obesity and overweight. Fact Sheet N°311. http://www.who.int/mediacentre/factsheets/fs311/en/, 2016.

3. Collaborators, G.B.D.O., et al., Health Effects of Overweight and Obesity in 195 Countries over 25 Years. N Engl J Med, 2017. 377(1): p. 13-27.

4. Kusminski, C.M., P.E. Bickel, and P.E. Scherer, Targeting adipose tissue in the treatment of obesity-associated diabetes. Nat Rev Drug Discov, 2016. 15(9): p. 639-60.

5. Huszar, D., et al., Targeted disruption of the melanocortin-4 receptor results in obesity in mice. Cell, 1997. 88(1): p. 131-41.

6. Farooqi, I.S., et al., Dominant and recessive inheritance of morbid obesity associated with melanocortin 4 receptor deficiency. J Clin Invest, 2000. 106(2): p. 271-9.

7. Zhang, Y.P., R.; Maffei, M.; Barone, M.; Leopold, L. and Friedman, J., Positional cloning of the mouse obese gene and its human homologue. Nature, 1994. 372: p. 425-432.

8. Clement, K., et al., A mutation in the human leptin receptor gene causes obesity and pituitary dysfunction. Nature, 1998. 392(6674): p. 398-401.

9. Frayling, T.M., et al., A common variant in the FTO gene is associated with body mass index and predisposes to childhood and adult obesity. Science, 2007. 316(5826): p. 889-94.

10. Dina, C., et al., Variation in FTO contributes to childhood obesity and severe adult obesity. Nat Genet, 2007. 39(6): p. 724-6.

11. Smemo, S., et al., Obesity-associated variants within FTO form long-range functional connections with IRX3. Nature, 2014. 507(7492): p. 371-5.

12. Stratigopoulos, G., et al., Hypomorphism for RPGRIP1L, a ciliary gene vicinal to the FTO locus, causes increased adiposity in mice. Cell Metab, 2014. 19(5): p. 767-79.

13. Tung, Y.C.L., et al., Obesity and FTO: Changing Focus at a Complex Locus. Cell Metab, 2014. 20(5): p. 710-718.

14. Barsh, G.S., I.S. Farooqi, and S. O'Rahilly, Genetics of body-weight regulation. Nature, 2000. 404(6778): p. 644-51.

15. Farooqi, I.S. and S. O'Rahilly, The Genetics of Obesity in Humans, in Endotext, L.J. De Groot, et al., Editors. 2000: South Dartmouth (MA).

16. Huypens, P.S., S.; Wu, M.; Dyckhoff, D.; Tschöp, M.H.; Theis, F.; Marschall, S.; Hrabe de Angelis, M. and Beckers, J., Epigenetic germline inheritance of diet-induced obesity and insulin resistance. Nat Gen, 2016. 48: p. 497-499.

17. Ussar, S., S. Fujisaka, and C.R. Kahn, Interactions between host genetics and gut microbiome in diabetes and metabolic syndrome. Mol Metab, 2016. 5(9): p. 795-803.

18. Fischer, I.P., et al., A history of obesity leaves an inflammatory fingerprint in liver and adipose tissue. Int J Obes (Lond), 2018. 42: p. 507-517.

19. Younossi, Z.M., et al., Global epidemiology of nonalcoholic fatty liver disease-Meta-analytic assessment of prevalence, incidence, and outcomes. Hepatology, 2016. 64(1): p. 73-84.

20. Anstee, Q.M., G. Targher, and C.P. Day, Progression of NAFLD to diabetes mellitus, cardiovascular disease or cirrhosis. Nat Rev Gastroenterol Hepatol, 2013. 10(6): p. 330-44.

21. Hebbard, L. and J. George, Animal models of nonalcoholic fatty liver disease. Nat Rev Gastroenterol Hepatol, 2011. 8(1): p. 35-44.

22. Baffy, G., E.M. Brunt, and S.H. Caldwell, Hepatocellular carcinoma in non-alcoholic fatty liver disease: an emerging menace. J Hepatol, 2012. 56(6): p. 1384-91.

23. Farrell, G.C., et al., NASH is an Inflammatory Disorder: Pathogenic, Prognostic and Therapeutic Implications. Gut Liver, 2012. 6(2): p. 149-71.

24. Hallsworth, K., L. Avery, and M.I. Trenell, Targeting Lifestyle Behavior Change in Adults with NAFLD During a 20-min Consultation: Summary of the Dietary and Exercise Literature. Curr Gastroenterol Rep, 2016. 18(3): p. 11.

25. Kerner, W., J. Bruckel, and A. German Diabetes, Definition, classification and diagnosis of diabetes mellitus. Exp Clin Endocrinol Diabetes, 2014. 122(7): p. 384-6.

26. Mathers, C.D. and D. Loncar, Projections of global mortality and burden of disease from 2002 to 2030. PLoS Med, 2006. 3(11): p. e442.

27. Chen, L., D.J. Magliano, and P.Z. Zimmet, The worldwide epidemiology of type 2 diabetes mellitus--present and future perspectives. Nat Rev Endocrinol, 2011. 8(4): p. 228-36.

28. Atkinson, M.A., The pathogenesis and natural history of type 1 diabetes. Cold Spring Harb Perspect Med, 2012. 2(11).

29. Atkinson, M.A., G.S. Eisenbarth, and A.W. Michels, Type 1 diabetes. Lancet, 2014. 383(9911): p. 69-82.

30. Kahn, S.E., M.E. Cooper, and S. Del Prato, Pathophysiology and treatment of type 2 diabetes: perspectives on the past, present, and future. Lancet, 2014. 383(9922): p. 1068-83.

31. Morris, A.P., et al., Large-scale association analysis provides insights into the genetic architecture and pathophysiology of type 2 diabetes. Nat Genet, 2012. 44(9): p. 981-90.

32. Ndiaye, F.K., et al., Expression and functional assessment of candidate type 2 diabetes susceptibility genes identify four new genes contributing to human insulin secretion. Mol Metab, 2017. 6(6): p. 459-470.

33. Groop, L., Pathogenesis of type 2 diabetes: the relative contribution of insulin resistance and impaired insulin secretion. Int J Clin Pract Suppl, 2000(113): p. 3-13.

34. Pond, C.M., An evolutionary and functional view of mammalian adipose tissue. Proc. Nut. Soc, 1992. 51: p. 367-377.

35. Cinti, S., The Adipose Organ. Nutrition and Health: Adipose Tissue and Adipokines in Health adn Disease, 2000: p. 3-19.

36. Bjorndal, B., et al., Different adipose depots: their role in the development of metabolic syndrome and mitochondrial response to hypolipidemic agents. J Obes, 2011. 2011: p. 490650.

37. Wajchenberg, B.L.G.-N., D.; da Silva, M.E.R.; Santos, R.F., Depot-specific Hormonal Characteristics of Subcutaneous and Visceral Adipose Tissue and their Relation to the Metabolic Syndrome. Horm Metab Res 2002. 34: p. 616-621.

38. Schleinitz, D., et al., The genetics of fat distribution. Diabetologia, 2014. 57(7): p. 1276-86.

39. Tran, T.T. and C.R. Kahn, Transplantation of adipose tissue and stem cells: role in metabolism and disease. Nat Rev Endocrinol, 2010. 6(4): p. 195-213.

40. de Jong, J.M.A.L., O.; Cannon, B. and Nedergaard, J., A stringent validation of mouse adipose tissue identity markers. Am J Physiol Endocrinol Metab, 2015. 308: p. 1085-1105.

41. Fawcett, D.W., Differences in Physiological Activity in Brown and White Fat as Revealed by Histochemical Reactions. Science, 1947. 105(2718): p. 123.

42. Suomalainen, P. and A.M. Herlevi, The alarm reaction and the hibernating gland. Science, 1951. 114(2960): p. 300.

43. Halaas, J.L.G., K. S.; Maffei, M.; Cohen, S. L.; Chait, B. T.; Rabinowitz, D.; Lallone, R. L.; Burley, S. K. ; Friedman, J. M., Weight-Reducing Effects of the Plasma Protein Encoded by the obese Gene. Science, 1995. 269(5223): p. 543-546.

44. Ouchi, N., et al., Adipokines in inflammation and metabolic disease. Nat Rev Immunol, 2011. 11(2): p. 85-97.

45. Sell, H., C. Habich, and J. Eckel, Adaptive immunity in obesity and insulin resistance. Nat Rev Endocrinol, 2012. 8(12): p. 709-16.

46. Hube, F.L., U.; Igel, M.; Jensen, P.B.; Tornqvist, H.; Joost, H.-G. and Hauner, H., Difference in Leptin mRNA Levels Between Omental and Subcutaneous Abdominal Adipose Tissue From Obese Humans. Horm. Metab. Res., 1996. 28: p. 690-693.

47. Lefebvre, A.-M.L., M.; Vega, N.; Riou, J. P.; van Gaak, L.; Auwerx, J.; Vidal, H., Depot-Specific Differences in Adipose Tissue Gene Expression in Lean and Obese Subjects. Diabetes, 1998. 47: p. 98-103.

48. Santos-Alvarez J, G.R., Sánchez-Margalet V., Human leptin stimulates proliferation and activation of human circulating monocytes. Cell Immunol., 1999. 194(1): p. 6-11.

49. Kiguchi, N., et al., Leptin enhances CC-chemokine ligand expression in cultured murine macrophage. Biochem Biophys Res Commun, 2009. 384(3): p. 311-5.

50. Qi, Y., et al., Adiponectin acts in the brain to decrease body weight. Nat Med, 2004. 10(5): p. 524-9.

51. Berg, A.H. and P.E. Scherer, Adipose tissue, inflammation, and cardiovascular disease. Circ Res, 2005. 96(9): p. 939-49.

52. Bouskila, M., U.B. Pajvani, and P.E. Scherer, Adiponectin: a relevant player in PPARgamma-agonist-mediated improvements in hepatic insulin sensitivity? Int J Obes (Lond), 2005. 29 Suppl 1: p. S17-23.

53. Ouchi N, K.S., Funahashi T, Matsuzawa Y, Walsh K., Obesity, adiponectin and vascular inflammatory disease. Curr Opin Lipidol, 2003. 14(6): p. 561-566.

54. Björntorp, P., "Portal" adipose tissue as a generator of risk factors for cardiovascular disease and diabetes. Arterioscler Thromb Vasc Biol., 1990. 10: p. 493-496.

55. Martinsson, A., Hypertrophy and hyperplasia of human adipose tissue in obesity. Pol Arch Med Wewn, 1969. 42(3): p. 481-486.

56. Ochner, C.N., et al., Biological mechanisms that promote weight regain following weight loss in obese humans. Physiol Behav, 2013. 120: p. 106-13.

57. Singh, P., et al., Effects of weight gain and weight loss on regional fat distribution. Am J Clin Nutr, 2012. 96(2): p. 229-33.

58. Wang, Q.A., et al., Tracking adipogenesis during white adipose tissue development, expansion and regeneration. Nat Med, 2013. 19(10): p. 1338-44.

59. Sackmann-Sala, L., et al., Heterogeneity among white adipose tissue depots in male C57BL/6J mice. Obesity (Silver Spring), 2012. 20(1): p. 101-11.

60. Tchkonia, T., et al., Mechanisms and metabolic implications of regional differences among fat depots. Cell Metab, 2013. 17(5): p. 644-56.

61. Pellegrinelli, V., S. Carobbio, and A. Vidal-Puig, Adipose tissue plasticity: how fat depots respond differently to pathophysiological cues. Diabetologia, 2016. 59(6): p. 1075-88.

62. van Beek, L., et al., The limited storage capacity of gonadal adipose tissue directs the development of metabolic disorders in male C57Bl/6J mice. Diabetologia, 2015. 58(7): p. 1601-9.

63. Andersson, D.P., et al., Changes in subcutaneous fat cell volume and insulin sensitivity after weight loss. Diabetes Care, 2014. 37(7): p. 1831-6.

64. Eriksson-Hogling, D., et al., Adipose tissue morphology predicts improved insulin sensitivity following moderate or pronounced weight loss. Int J Obes (Lond), 2015. 39(6): p. 893-8.

65. Sun, K., C.M. Kusminski, and P.E. Scherer, Adipose tissue remodeling and obesity. J Clin Invest, 2011. 121(6): p. 2094-101.

66. Sun, K., et al., Fibrosis and adipose tissue dysfunction. Cell Metab, 2013. 18(4): p. 470-7.

67. Halberg, N., et al., Hypoxia-inducible factor 1alpha induces fibrosis and insulin resistance in white adipose tissue. Mol Cell Biol, 2009. 29(16): p. 4467-83.

68. Grandl, G., et al., Depot specific differences in the adipogenic potential of precursors are mediated by collagenous extracellular matrix and Flotillin 2 dependent signaling. Mol Metab, 2016. 5(10): p. 937-47.

69. Sun, K.H., N.; Khan, M.; Magalang, U.J.; Scherer, P.E., Selective Inhibition of Hypoxia-Inducible Factor 1a Ameliorates Adipose Tissue Dysfunction. Mol Cell Biol, 2013. 33(5): p. 904-917.

70. Zhang, X., et al., Adipose tissue-specific inhibition of hypoxia-inducible factor 1{alpha} induces obesity and glucose intolerance by impeding energy expenditure in mice. J Biol Chem, 2010. 285(43): p. 32869-77.

71. Rosen, E.D. and B.M. Spiegelman, Adipocytes as regulators of energy balance and glucose homeostasis. Nature, 2006. 444(7121): p. 847-53.

72. Kahn, B.B., Lilly lecture 1995: Glucose Transport: Pivotal Step in Insulin Action. Diabetes, 1996. 45.

73. Festuccia, W.T., et al., Depot-specific effects of the PPARgamma agonist rosiglitazone on adipose tissue glucose uptake and metabolism. J Lipid Res, 2009. 50(6): p. 1185-94.

74. Huang, S. and M.P. Czech, The GLUT4 glucose transporter. Cell Metab, 2007. 5(4): p. 237-52.

75. Engfeldt, P.A., P., Lipolysis in human adipocytes, effects of cell size, age and of regional differences. Horm Metab Res Suppl, 1988. 19.

76. Gastaldelli, A., et al., Metabolic effects of visceral fat accumulation in type 2 diabetes. J Clin Endocrinol Metab, 2002. 87(11): p. 5098-103.

77. Cinti, S., et al., Adipocyte death defines macrophage localization and function in adipose tissue of obese mice and humans. J Lipid Res, 2005. 46(11): p. 2347-55.

78. Shimobayashi, M., et al., Insulin resistance causes inflammation in adipose tissue. J Clin Invest, 2018. 128(4): p. 1538-1550.

79. Giordano, A., A. Frontini, and S. Cinti, Convertible visceral fat as a therapeutic target to curb obesity. Nat Rev Drug Discov, 2016. 15(6): p. 405-24.

80. Migliorini, R.H.G., M. A. R; Kettelhut, I.C., Increased sympathetic activity in rat white adipose tissue during prolonged fasting. The American journal of physiology, 1997. 272: p. 656-661.

81. Lean, M.E.J., Brown adipose tissue in humans. Proc. Nut. Soc, 1989. 48: p. 243-256.

82. Cypess, A.M., et al., Identification and importance of brown adipose tissue in adult humans. N Engl J Med, 2009. 360(15): p. 1509-17.

83. Virtanen, K.M.L., M.E.; Orava, J.; Heglind, M.; Westergren, R.; Niemi, T.; Taittonen, M.; Laine, J.; Savisto, N.-J.; Enerbäck, S. and Nuutila, P., Functional Brown Adipose Tissue in Healthy Adults. N Engl J Med, 2009. 360: p. 1518-25.

84. Van Marken Lichtenbelt, V.D.V., J.W.; Smulders, N.M.; Drossaerts, J.M.A.F.L.; Kemerink, G.J.; Bouvy, N.D.; Schrauwen, P. and Teule, G.J., Cold-activated brown adipose tissue in healthy men. N Engl J Med, 2009. 360(15): p. 1500-1508.

85. Wang, Q., et al., Brown adipose tissue activation is inversely related to central obesity and metabolic parameters in adult human. PLoS One, 2015. 10(4): p. e0123795.

86. Lee, P.G., J.R.; Ho, K.K.y. and Fulham, M.J., A critical appraisal of the prevalence and metabolic significance of brown adipose tissue in adult humans. Am J Physiol Endocrinol Metab, 2010. 299: p. 601-606.

87. Harms, M. and P. Seale, Brown and beige fat: development, function and therapeutic potential. Nat Med, 2013. 19(10): p. 1252-63.

88. Wu, J., et al., Beige adipocytes are a distinct type of thermogenic fat cell in mouse and human. Cell, 2012. 150(2): p. 366-76.

89. Seale, P., et al., PRDM16 controls a brown fat/skeletal muscle switch. Nature, 2008. 454(7207): p. 961-7.

90. Ussar, S., et al., ASC-1, PAT2, and P2RX5 are cell surface markers for white, beige, and brown adipocytes. Sci Transl Med, 2014. 6(247): p. 247ra103.

91. Xue, B., et al., Genetic variability affects the development of brown adipocytes in white fat but not in interscapular brown fat. J Lipid Res, 2007. 48(1): p. 41-51.

92. Lee, Y.H., et al., Metabolic heterogeneity of activated beige/brite adipocytes in inguinal adipose tissue. Sci Rep, 2017. 7: p. 39794.

93. Kajimura, S., B.M. Spiegelman, and P. Seale, Brown and Beige Fat: Physiological Roles beyond Heat Generation. Cell Metab, 2015. 22(4): p. 546-59.

94. van der Lans, A.A., et al., Cold-activated brown adipose tissue in human adults: methodological issues. Am J Physiol Regul Integr Comp Physiol, 2014. 307(2): p. R103-13.

95. Mukherjee, J., A. Baranwal, and K.N. Schade, Classification of Therapeutic and Experimental Drugs for Brown Adipose Tissue Activation: Potential Treatment Strategies for Diabetes and Obesity. Curr Diabetes Rev, 2016. 12(4): p. 414-428.

96. Boquist, L., et al., Influence of the mutation "diabetes" on insulin release and islet morphology in mice of different genetic backgrounds. J Cell Biol, 1974. 62(1): p. 77-89.

97. Hariri, N. and L. Thibault, High-fat diet-induced obesity in animal models. Nutr Res Rev, 2010. 23(2): p. 270-99.

98. Buettner, R., J. Scholmerich, and L.C. Bollheimer, High-fat diets: modeling the metabolic disorders of human obesity in rodents. Obesity (Silver Spring), 2007. 15(4): p. 798-808.

99. Ayala, J.E., et al., Standard operating procedures for describing and performing metabolic tests of glucose homeostasis in mice. Dis Model Mech, 2010. 3(9-10): p. 525-34.

100. Montgomery, M.K., et al., Mouse strain-dependent variation in obesity and glucose homeostasis in response to high-fat feeding. Diabetologia, 2013. 56(5): p. 1129-39.

101. Fontaine, D.A. and D.B. Davis, Attention to Background Strain Is Essential for Metabolic Research: C57BL/6 and the International Knockout Mouse Consortium. Diabetes, 2016. 65(1): p. 25-33.

102. Mekada, K., et al., Genetic differences among C57BL/6 substrains. Exp Anim, 2009. 58(2): p. 141-9.

103. Pettitt, S.J., et al., Agouti C57BL/6N embryonic stem cells for mouse genetic resources. Nat Methods, 2009. 6(7): p. 493-5.

104. Toye, A.A., et al., A genetic and physiological study of impaired glucose homeostasis control in C57BL/6J mice. Diabetologia, 2005. 48: p. 675-686.

105. Jackson, J.B., et al., Review and Hypothesis. New insights into the reaction mechanism of transhydrogenase: Swivelling the dIII component may gate the proton channel. FEBS Lett, 2015. 589(16): p. 2027-33.

106. Ronchi, J.A., et al., A spontaneous mutation in the nicotinamide nucleotide transhydrogenase gene of C57BL/6J mice results in mitochondrial redox abnormalities. Free Radic Biol Med, 2013. 63: p. 446-56.

107. Freeman, H.C., et al., Deletion of nicotinamide nucleotide transhydrogenase: a new quantitive trait locus accounting for glucose intolerance in C57BL/6J mice. Diabetes, 2006. 55(7): p. 2153-6.

108. Simon, M.M., et al., A comparative phenotypic and genomic analysis of C57BL/6J and C57BL/6N mouse strains. Genome Biol, 2013. 14(7): p. R82.

109. Nicholson, A., et al., Diet-induced obesity in two C57BL/6 substrains with intact or mutant nicotinamide nucleotide transhydrogenase (Nnt) gene. Obesity (Silver Spring), 2010. 18(10): p. 1902-5.

110. Macotela, Y., et al., Sex and depot differences in adipocyte insulin sensitivity and glucose metabolism. Diabetes, 2009. 58(4): p. 803-12.

111. Medrikova, D., et al., Sex differences during the course of diet-induced obesity in mice: adipose tissue expandability and glycemic control. Int J Obes (Lond), 2012. 36(2): p. 262-72.

112. Palmer, B.F. and D.J. Clegg, The sexual dimorphism of obesity. Mol Cell Endocrinol, 2015. 402: p. 113-9.

113. Pettersson, U.S., et al., Female mice are protected against high-fat diet induced metabolic syndrome and increase the regulatory T cell population in adipose tissue. PLoS One, 2012. 7(9): p. e46057.

114. Riant, E., et al., Estrogens protect against high-fat diet-induced insulin resistance and glucose intolerance in mice. Endocrinology, 2009. 150(5): p. 2109-17.

115. Miras, A.D. and C.W. le Roux, Mechanisms underlying weight loss after bariatric surgery. Nat Rev Gastroenterol Hepatol, 2013. 10(10): p. 575-84.

116. Buchwald H., A.Y., Braunwald E., Jensen M.D., Pories W., Fahrbach K., Schoelles K., Bariatric Surgery: A Systematic Review and Meta-analysis. JAMA, 2004. 292(14): p. 1724-1737.

117. Eldar, S., et al., Bariatric surgery for treatment of obesity. Int J Obes (Lond), 2011. 35 Suppl 3: p. S16-21.

118. Flum D.R., B.S.H., King W.C., Wahed A.S., Berk P., Chapman W., Perioperative safety in the longitudinal assessment of bariatric surgery. N Engl J Med, 2009. 361: p. 445-454.

119. Buchwald H., E.R., Fahrbach K., Banel D., Sledge I., Trends in mortality in bariatric surgery: a systematic review and meta-analysis. Surgery, 2007. 142: p. 621-632.

120. Johnson D.; Drenick, E.J., Therapeutic fasting in morbid obesity: Long-term follow-up. Archives of Internal Medicine, 1977. 137: p. 1381-1382.

121. Pietilainen, K.H., et al., Does dieting make you fat? A twin study. Int J Obes (Lond), 2012. 36(3): p. 456-64.

122. Leibel, R.L., Molecular physiology of weight regulation in mice and humans. Int J Obes (Lond), 2008. 32 Suppl 7: p. S98-108.

123. Leibel, R.L.R., M.; Hirsch, J., Changes in energy expenditure resulting from altered body weight. The New England Journal of Medicine, 1995. 332(10): p. 621-628.

124. Wing, R.R.a.H., J. O., Successful weight loss maintenance. Annu. Rev. Nutr., 2001. 21: p. 323-41.

125. Pankevich, D.E., et al., Caloric restriction experience reprograms stress and orexigenic pathways and promotes binge eating. J Neurosci, 2010. 30(48): p. 16399-407.

126. Hambly, C. and J.R. Speakman, Mice that gorged during dietary restriction increased foraging related behaviors and differed in their macronutrient preference when released from restriction. PeerJ, 2015. 3: p. e1091.

127. Kirchner, H.H., S. M.; Fischer-Rosinsky, A.; Hembree, J.; Abplanalp, W.; Ottaway, N.; Donelan, E.; Krishna, R.; Woods, S.C.; Müller, T. D.; Spranger, J.; Perez-Tilve, D.; Pfluger, P. T.; Tschöp, M. H.; and Habegger, K. M., Caloric Restriction Chronically Impairs Metabolic Programming in Mice. Diabetes, 2012. 61: p. 2734-2742.

128. Spalding, K.L., et al., Dynamics of fat cell turnover in humans. Nature, 2008. 453(7196): p. 783-7.

129. Lofgren, P., et al., Long-term prospective and controlled studies demonstrate adipose tissue hypercellularity and relative leptin deficiency in the postobese state. J Clin Endocrinol Metab, 2005. 90(11): p. 6207-13.

130. Pelleymounter, M.A.C., M. J.; Baker, M. B.; Hecht, R.; Winters, D.; Boone, T.; Collins, F., Effects of the obese Gene Product on Body Weight Regulation in ob/ob mice. Science, 1995. 269(5223): p. 540-543.

131. Campfield, L.A.S., F. J.; Guisez, Y.; Devos, R.; Burn, P., Recombinant Mouse OB Protein: Evidence for a Peripheral Signal Linking Adiposity and Central Neural Networks. Science, 1995. 269(5223): p. 546-549.

132. Della-Fera, M.A.Q., H. and Baile, A., Adipocyte apoptosis in the regulation of body fat mass by leptin. Diabetes, Obesity and Metabolism, 2001. 3: p. 299-310.

133. Rosenbaum, M.L., R. L., Leptin: A Molecule Integrating Somatic Energy Stores, Energy Expenditure and Fertility. Trends in Endocrinology & Metabolism, 1998. 9(3): p. 117-124.

134. Ryan, K.K., S.C. Woods, and R.J. Seeley, Central nervous system mechanisms linking the consumption of palatable high-fat diets to the defense of greater adiposity. Cell Metab, 2012. 15(2): p. 137-49.

135. Seeley, R.J.V.D., G.; Campfield, L. A.; Smith, F. J.; Burn, P.; Nelligan, J.A.; Bell, S. M.; Baskin, D.G.; Woods, S. C.; Schwartz M. W., Intraventricular Leptin Reduces Food Intake and Body Weight of Lean Rats but Not Obese Zucker Rats. Horm. Metab. Res., 1996. 28: p. 664-668.

136. Enriori, P.J., et al., Diet-induced obesity causes severe but reversible leptin resistance in arcuate melanocortin neurons. Cell Metab, 2007. 5(3): p. 181-94.

137. Chhabra, K.H., et al., Reprogramming the body weight set point by a reciprocal interaction of hypothalamic leptin sensitivity and Pomc gene expression reverts extreme obesity. Molecular Metabolism, 2016. 5(10): p. 869-881.

138. Kissileff, H.R., et al., Leptin reverses declines in satiation in weight-reduced obese humans. Am J Clin Nutr, 2012. 95(2): p. 309-17.

139. Ravussin, Y., et al., Effects of chronic leptin infusion on subsequent body weight and composition in mice: Can body weight set point be reset? Mol Metab, 2014. 3(4): p. 432-40.

140. Hai, T.H., M. G., The molecular biology and nomenclature of the activating transcription factor/cAMP responsive element binding family of transcription factors: activating transcription factor proteins and homeostasis. Gene 2001. 273: p. 1-11.

141. Celli, J. and R.M. Tsolis, Bacteria, the endoplasmic reticulum and the unfolded protein response: friends or foes? Nat Rev Microbiol, 2015. 13(2): p. 71-82.

142. Rozpedek, W., et al., The Role of the PERK/eIF2alpha/ATF4/CHOP Signaling Pathway in Tumor Progression During Endoplasmic Reticulum Stress. Curr Mol Med, 2016. 16(6): p. 533-44.

143. de Franca, S.A., et al., A Low-Protein, High-Carbohydrate Diet Stimulates Thermogenesis in the Brown Adipose Tissue of Rats via ATF-2. Lipids, 2016. 51(3): p. 303-10.

144. Muller, T.D., et al., p62 links beta-adrenergic input to mitochondrial function and thermogenesis. J Clin Invest, 2013. 123(1): p. 469-78.

145. Ku, C.H., H.; Lin, CS.; Tsai, MH.; Wuputra, K.; Eckner, R.; Yamaguchi, N.; Yokoyama, KK., Control of the cell cycle and mitosis by phosphorylated activating transcription factor 2 and its homologue. Journal of Nature and Science, 2015. 1(4): p. e74.

146. Kim, J.Y., et al., Activating transcription factor 3 is a target molecule linking hepatic steatosis to impaired glucose homeostasis. J Hepatol, 2017. 67(2): p. 349-359.

147. Allen-Jennings, A.E., et al., The roles of ATF3 in glucose homeostasis. A transgenic mouse model with liver dysfunction and defects in endocrine pancreas. J Biol Chem, 2001. 276(31): p. 29507-14.

148. Hartman, M.G., et al., Role for activating transcription factor 3 in stress-induced beta-cell apoptosis. Mol Cell Biol, 2004. 24(13): p. 5721-32.

149. Nawa, T., et al., Expression of transcriptional repressor ATF3/LRF1 in human atherosclerosis: colocalization and possible involvement in cell death of vascular endothelial cells. Atherosclerosis, 2002. 161(2): p. 281-91.

150. Chen, S.C., et al., Acute hypoxia to endothelial cells induces activating transcription factor 3 (ATF3) expression that is mediated via nitric oxide. Atherosclerosis, 2008. 201(2): p. 281-8.

151. Kool, J., et al., Induction of ATF3 by ionizing radiation is mediated via a signaling pathway that includes ATM, Nibrin1, stress-induced MAPkinases and ATF-2. Oncogene, 2003. 22(27): p. 4235-42.

152. Brooks, A.C., et al., Endoplasmic reticulum stress-dependent activation of ATF3 mediates the late phase of ischemic preconditioning. J Mol Cell Cardiol, 2014. 76: p. 138-47.

153. Zmuda, E.J., et al., The roles of ATF3, an adaptive-response gene, in high-fat-diet-induced diabetes and pancreatic beta-cell dysfunction. Mol Endocrinol, 2010. 24(7): p. 1423-33.

154. Lee, Y.-S.K., M.; Kikuchi, O.; Sasaki, T.; Yokota-Hashimoto, H.; Susanti, V.Y.; Kitamura, Y.I.; Kitamura, T., ATF3 expression is induced by low glucose in pancreatic α and β cells and regulates glucagon but not insulin gene transcription. Endocrine Journal, 2014. 61(1): p. 85-90.

155. Lee, Y.S., et al., Hypothalamic ATF3 is involved in regulating glucose and energy metabolism in mice. Diabetologia, 2013. 56(6): p. 1383-93.

156. Jang, M.K., Y. Son, and M.H. Jung, ATF3 plays a role in adipocyte hypoxia-mediated mitochondria dysfunction in obesity. Biochem Biophys Res Commun, 2013. 431(3): p. 421-7.

157. Kim, H.B., et al., NFATc4 and ATF3 negatively regulate adiponectin gene expression in 3T3-L1 adipocytes. Diabetes, 2006. 55(5): p. 1342-52.

158. Koh, E.H., et al., Essential role of mitochondrial function in adiponectin synthesis in adipocytes. Diabetes, 2007. 56(12): p. 2973-81.

159. Jang, M.K., et al., ATF3 inhibits adipocyte differentiation of 3T3-L1 cells. Biochem Biophys Res Commun, 2012. 421(1): p. 38-43.

160. Jang, M.K. and M.H. Jung, ATF3 represses PPARgamma expression and inhibits adipocyte differentiation. Biochem Biophys Res Commun, 2014. 454(1): p. 58-64.

161. Jang, M.K. and M.H. Jung, ATF3 inhibits PPARgamma-stimulated transactivation in adipocyte cells. Biochem Biophys Res Commun, 2015. 456(1): p. 80-5.

162. Jadhav, K. and Y. Zhang, Activating transcription factor 3 in immune response and metabolic regulation. Liver Res, 2017. 1(2): p. 96-102.

163. Hasin, T., et al., Angiotensin II signaling up-regulates the immediate early transcription factor ATF3 in the left but not the right atrium. Basic Res Cardiol, 2011. 106(2): p. 175-87.

164. Li, Y., et al., Cardiac Fibroblast-Specific Activating Transcription Factor 3 Protects Against Heart Failure by Suppressing MAP2K3-p38 Signaling. Circulation, 2017. 135(21): p. 2041-2057.

165. Schäfer, J., Elucidating the role of Atf3 as beta-adrenergic response gene in brown adipocytes. 2016.

166. Wolford, C.C., et al., Transcription factor ATF3 links host adaptive response to breast cancer metastasis. J Clin Invest, 2013. 123(7): p. 2893-906.

167. Guerra, C., et al., Brown adipose tissue-specific insulin receptor knockout shows diabetic phenotype without insulin resistance. J Clin Invest, 2001. 108(8): p. 1205-13.

168. Selman, C.K., N. D.; Cooray, A.; Piper, M. D. W.; Lingard, S. J.; Barton, R. H.; Schuster, E. F.; Blanc, E.; Gems, D.; Micholson, J. K.; Thornton, J. M.; Partridge, L.; Withers, D. J., Coordinated multitissue transcriptional and plasma metabonomic profiles following actue caloric restriction in mice. Physiol Genomics, 2006. 27: p. 187-200.

169. Meyer, C.W., et al., Adaptive thermogenesis and thermal conductance in wild-type and UCP1-KO mice. Am J Physiol Regul Integr Comp Physiol, 2010. 299(5): p. R1396-406.

170. Mendler, M.H., G. Kanel, and S. Govindarajan, Proposal for a histological scoring and grading system for non-alcoholic fatty liver disease. Liver International, 2005. 25(2): p. 294-304.

171. Pfaffl, M.W., A new mathematical model for relative quantification in real-time RT-PCR. Nucleic Acids Research, 2001. 29(9).

172. Love, M.I., W. Huber, and S. Anders, Moderated estimation of fold change and dispersion for RNA-seq data with DESeq2. Genome Biol, 2014. 15(12): p. 550.

173. Team, D.C., R: A language and environment for statistical computing. 2005: R Foundation for Statistical Computing, Vienna, Austria.

174. Rainer, J., et al., CARMAweb: comprehensive R- and bioconductor-based web service for microarray data analysis. Nucleic Acids Res, 2006. 34(Web Server issue): p. W498-503.

175. Fabbiano, S., et al., Caloric Restriction Leads to Browning of White Adipose Tissue through Type 2 Immune Signaling. Cell Metab, 2016. 24(3): p. 434-46.

176. Schmitz, J., et al., Obesogenic memory can confer long-term increases in adipose tissue but not liver inflammation and insulin resistance after weight loss. Mol Metab, 2016. 5(5): p. 328-39.

177. Schwartz, M.W., et al., Central nervous system control of food intake. Nature, 2000. 404(6778): p. 661-71.

178. Thaler, J.P., et al., Obesity is associated with hypothalamic injury in rodents and humans. J Clin Invest, 2012. 122(1): p. 153-62.

179. Ishak, K.B., A.; Bianchi, L.; Callea, F.; De Groote, J.; Gudat, F.; Denk, H.; Desmet, V.; Korb, G.; MacSween, R. N.M.,; Phillips, M.J.; Portman, B.G.; Poulsen,H.; Scheuer, P.J.; Schmid, M.; Thaler, H., Histological grading and staging of chronic hepatitis. Journal of Hepatology, 1995.

180. Lago, F., et al., Adipokines as emerging mediators of immune response and inflammation. Nat Clin Pract Rheumatol, 2007. 3(12): p. 716-24.

181. Swarbrick, M.M. and P.J. Havel, Physiological, pharmacological, and nutritional regulation of circulating adiponectin concentrations in humans. Metab Syndr Relat Disord, 2008. 6(2): p. 87-102.

182. Shimizu, I., et al., Vascular rarefaction mediates whitening of brown fat in obesity. J Clin Invest, 2014. 124(5): p. 2099-112.

183. Lusis, A.J., A.D. Attie, and K. Reue, Metabolic syndrome: from epidemiology to systems biology. Nat Rev Genet, 2008. 9(11): p. 819-30.

184. Rodgers, R.J., M.H. Tschop, and J.P. Wilding, Anti-obesity drugs: past, present and future. Dis Model Mech, 2012. 5(5): p. 621-6.

185. Sanchez-Garrido, M.A., et al., GLP-1/glucagon receptor co-agonism for treatment of obesity. Diabetologia, 2017. 60(10): p. 1851-1861.

186. Finan, B., et al., A rationally designed monomeric peptide triagonist corrects obesity and diabetes in rodents. Nat Med, 2015. 21(1): p. 27-36.

187. Fruhbeck, G., D.N. Kiortsis, and V. Catalan, Precision medicine: diagnosis and management of obesity. Lancet Diabetes Endocrinol, 2018. 6(3): p. 164-166.

188. K., M., et al., Genetic Differences among C57BL/6 Substrains. Experimental Animals, 2009. 58(2): p. 141-149.

189. Liu, Y., et al., Accumulation and Changes in Composition of Collagens in Subcutaneous Adipose Tissue After Bariatric Surgery. J Clin Endocrinol Metab, 2016. 101(1): p. 293-304.

190. Kahle, M., et al., Phenotypic comparison of common mouse strains developing high-fat diet-induced hepatosteatosis. Mol Metab, 2013. 2(4): p. 435-46.

191. Kleinert, M., et al., Animal models of obesity and diabetes mellitus. Nat Rev Endocrinol, 2018. 14(3): p. 140-162.

192. Chassaing, B., et al., Lack of soluble fiber drives diet-induced adiposity in mice. Am J Physiol Gastrointest Liver Physiol, 2015. 309(7): p. G528-41.

193. Bray, G.A., S.J. Nielsen, and B.M. Popkin, Consumption of high-fructose corn syrup in beverages may play a role in the epidemic of obesity. Am J Clin Nutr, 2004. 79(4): p. 537-43.

194. Siervo, M., et al., Sugar consumption and global prevalence of obesity and hypertension: an ecological analysis. Public Health Nutr, 2014. 17(3): p. 587-96.

195. Bueno, N.B., et al., Very-low-carbohydrate ketogenic diet v. low-fat diet for long-term weight loss: a meta-analysis of randomised controlled trials. Br J Nutr, 2013. 110(7): p. 1178-87.

196. Ellenbroek, J.H., et al., Long-term ketogenic diet causes glucose intolerance and reduced beta- and alpha-cell mass but no weight loss in mice. Am J Physiol Endocrinol Metab, 2014. 306(5): p. E552-8.

197. Shimokata, H., et al., Age as independent determinant of glucose tolerance. Diabetes, 1991. 40(1): p. 44-51.

198. Yang, Y., et al., Variations in body weight, food intake and body composition after long-term high-fat diet feeding in C57BL/6J mice. Obesity (Silver Spring), 2014. 22(10): p. 2147-55.

199. McGregor, R.A., et al., Time-course microarrays reveal modulation of developmental, lipid metabolism and immune gene networks in intrascapular brown adipose tissue during the development of diet-induced obesity. Int J Obes (Lond), 2013. 37(12): p. 1524-31.

200. Oh, H.Y., et al., Time-dependent network analysis reveals molecular targets underlying the development of diet-induced obesity and non-alcoholic steatohepatitis. Genes Nutr, 2013. 8(3): p. 301-16.

201. Kless, C., et al., Diet-induced obesity causes metabolic impairment independent of alterations in gut barrier integrity. Mol Nutr Food Res, 2015. 59(5): p. 968-78.

202. Sorge, R.E., et al., Olfactory exposure to males, including men, causes stress and related analgesia in rodents. Nat Methods, 2014. 11(6): p. 629-32.

203. Muller, V.M., et al., Gut barrier impairment by high-fat diet in mice depends on housing conditions. Mol Nutr Food Res, 2016. 60(4): p. 897-908.

204. Geer, E.B. and W. Shen, Gender differences in insulin resistance, body composition, and energy balance. Gend Med, 2009. 6 Suppl 1: p. 60-75.

205. Dakin, R.S., et al., Estrogens protect male mice from obesity complications and influence glucocorticoid metabolism. Int J Obes (Lond), 2015. 39(10): p. 1539-47.

206. Benoit, B., et al., Increasing fat content from 20 to 45 wt% in a complex diet induces lower endotoxemia in parallel with an increased number of intestinal goblet cells in mice. Nutr Res, 2015. 35(4): p. 346-56.

207. Desmarchelier, C., et al., Diet-induced obesity in ad libitum-fed mice: food texture overrides the effect of macronutrient composition. Br J Nutr, 2013. 109(8): p. 1518-27.

208. Middlemiss, J.E. and C.M. McEniery, Feeling the pressure: (patho) physiological mechanisms of weight gain and weight loss in humans. Hypertens Res, 2016.

209. Clifton, P.M., Dietary treatment for obesity. Nat Clin Pract Gastroenterol Hepatol, 2008. 5(12): p. 672-81.

210. Dixon, J.B., et al., Surgical approaches to the treatment of obesity. Nat Rev Gastroenterol Hepatol, 2011. 8(8): p. 429-37.

211. Makris, A. and G.D. Foster, Dietary approaches to the treatment of obesity. Psychiatr Clin North Am, 2011. 34(4): p. 813-27.

212. Parekh, P.I.P., A. E., Tiller, J. M., Feinglos, M. N., and Surwit, R. S., Reversal of Diet-Induced Obesity and Diabetes in C57BL/6J Mice. Metabolism, 1998. 47(9): p. 1089-1096.

213. Shi, H., et al., Diet-induced obese mice are leptin insufficient after weight reduction. Obesity (Silver Spring), 2009. 17(9): p. 1702-9.

214. Neinast, M.D., et al., Activation of natriuretic peptides and the sympathetic nervous system following Roux-en-Y gastric bypass is associated with gonadal adipose tissues browning. Mol Metab, 2015. 4(5): p. 427-36.

215. Barquissau, V., et al., Caloric Restriction and Diet-Induced Weight Loss Do Not Induce Browning of Human Subcutaneous White Adipose Tissue in Women and Men with Obesity. Cell Rep, 2018. 22(4): p. 1079-1089.

216. Berkseth, K.E., et al., Hypothalamic gliosis associated with high-fat diet feeding is reversible in mice: a combined immunohistochemical and magnetic resonance imaging study. Endocrinology, 2014. 155(8): p. 2858-67.

217. Kowalski, G.M., et al., Reversing diet-induced metabolic dysregulation by diet switching leads to altered hepatic de novo lipogenesis and glycerolipid synthesis. Sci Rep, 2016. 6: p. 27541.

218. Yamamoto, M., et al., Restriction of dietary calories, fat and iron improves non-alcoholic fatty liver disease. J Gastroenterol Hepatol, 2007. 22(4): p. 498-503.

219. Jordy, A.B., et al., Analysis of the liver lipidome reveals insights into the protective effect of excercise on high-fat diet-induced hepatosteatosis in mice. Am J Physiol Endocrinol Metab, 2015. 308: p. 778-791.

220. Myronovych, A., et al., Vertical sleeve gastrectomy reduces hepatic steatosis while increasing serum bile acids in a weight-loss-independent manner. Obesity (Silver Spring), 2014. 22(2): p. 390-400.

221. Brolinson, A., et al., Steroid hormones control circadian Elovl3 expression in mouse liver. Endocrinology, 2008. 149(6): p. 3158-66.

222. Perrini, S., et al., Fat depot-related differences in gene expression, adiponectin secretion, and insulin action and signalling in human adipocytes differentiated in vitro from precursor stromal cells. Diabetologia, 2008. 51(1): p. 155-64.

223. Bueno, A.A., et al., Effects of different fatty acids and dietary lipids on adiponectin gene expression in 3T3-L1 cells and C57BL/6J mice adipose tissue. Pflugers Arch, 2008. 455(4): p. 701-9.

224. Arner, P., et al., Variations in the size of the major omentum are primarily determined by fat cell number. J Clin Endocrinol Metab, 2013. 98(5): p. E897-901.

225. Tran, T.T., et al., Beneficial effects of subcutaneous fat transplantation on metabolism. Cell Metab, 2008. 7(5): p. 410-20.

226. Foster, M.T., et al., Subcutaneous Adipose Tissue Transplantation in Diet-Induced Obese Mice Attenuates Metabolic Dysregulation While Removal Exacerbates It. Physiol Rep, 2013. 1(2).

227. Hocking, S.L., et al., Subcutaneous fat transplantation alleviates diet-induced glucose intolerance and inflammation in mice. Diabetologia, 2015. 58(7): p. 1587-600.

228. Barrera, C.g., A. and Morgan, C., Obese visceral adipose tissue grafted in lean mice can alter glucose homeostasis and energy efficiency. J Biol Regul Homeost Agents, 2012. 26(3): p. 411-417.

229. Satoor, S.N., et al., Location, location, location: Beneficial effects of autologous fat transplantation. Sci Rep, 2011. 1: p. 81.

230. Fox, C.S., et al., Abdominal visceral and subcutaneous adipose tissue compartments: association with metabolic risk factors in the Framingham Heart Study. Circulation, 2007. 116(1): p. 39-48.

231. Hai, T., et al., ATF3 and stress responses. Gene Expr, 1999. 7(4-6): p. 321-35.

232. Qi, L., et al., Adipocyte CREB promotes insulin resistance in obesity. Cell Metab, 2009. 9(3): p. 277-86.

233. Suganami, T., et al., Activating transcription factor 3 constitutes a negative feedback mechanism that attenuates saturated Fatty acid/toll-like receptor 4 signaling and macrophage activation in obese adipose tissue. Circ Res, 2009. 105(1): p. 25-32.

234. Commins, S.P., et al., Induction of uncoupling protein expression in brown and white adipose tissue by leptin. Endocrinology, 1999. 140(1): p. 292-300.

235. Eiselein, L., et al., TGRL Lipolysis Products Induce Stress Protein ATF3 via the TGF-beta Receptor Pathway in Human Aortic Endothelial Cells. PLoS One, 2015. 10(12): p. e0145523.

236. Seale, P., et al., Prdm16 determines the thermogenic program of subcutaneous white adipose tissue in mice. J Clin Invest, 2011. 121(1): p. 96-105.

237. Ohyama, K., et al., A Synergistic Antiobesity Effect by a Combination of Capsinoids and Cold Temperature Through Promoting Beige Adipocyte Biogenesis. Diabetes, 2016. 65(5): p. 1410-23.

238. Valencak, T.G., A. Osterrieder, and T.J. Schulz, Sex matters: The effects of biological sex on adipose tissue biology and energy metabolism. Redox Biol, 2017. 12: p. 806-813.

239. Kim, S.N., et al., Sex differences in sympathetic innervation and browning of white adipose tissue of mice. Biol Sex Differ, 2016. 7: p. 67.

240. Rosenwald, M., et al., Bi-directional interconversion of brite and white adipocytes. Nat Cell Biol, 2013. 15(6): p. 659-67.

241. Altshuler-Keylin, S., et al., Beige Adipocyte Maintenance Is Regulated by Autophagy-Induced Mitochondrial Clearance. Cell Metab, 2016. 24(3): p. 402-419

Acknowledgements

First of all, I would like to thank Prof. Dr. Matthias Tschöp for giving me the opportunity to work on my PhD project at the Institute for Diabetes and Obesity at the Helmholtz Zentrum München as well as supervising and financing my doctoral project, through the Helmholtz ICEMED Alliance backbone funds and the Alexander von Humboldt foundation. Secondly, I am very thankful to Prof. Dr. Johannes Beckers for co-supervision of the doctoral thesis and productive discussions in the frame of the Helmholtz ICEMED Alliance Focus Group on DIO mouse models.

Moreover, I would like to thank Dr. Carola Meyer for providing me with this interesting topic and mentoring the first half of my PhD project. Importantly, I am very thankful to Dr. Siegfried Ussar for "adopting" me into his group, mentoring the second half of my PhD project and very valuable scientific discussions, all along.

Next, I would like to thank all my collaborators who contributed to my publications, specifically Dr. Martin Irmler for performing and evaluating the microarray analysis, Dr. Frauke Neff for performing the liver fibrosis staining and guidance during the hepatosteatosis grading, Dr. Elisabeth Graf and Thomas Schwarzmayr for performing and Dr. Dominik Lutter for analyzing the RNA-Sequencing as well as Prof. Dr. Susanna Hofmann for valuable scientific input.

A good friend of mine once compared a PhD project to a sine-wave, indicating that there's a high after every low during a PhD project. Acknowledging this, I am specifically thankful to my "lab-friends" Marina Wimmer, Jana Schäfer, Dr. Ellen Walheim, Ines Pramme-Steinwachs, Katrin Pfuhlmann, Lisa Suwandhi, Ruth Karlina, Dr. Simone Hausmann and Dr. Theresa Schöttl as well as all my other fellow- PhD students for their scientific input, support and for enduring various "ups" and "downs" together with me. I further specifically thank Dr. Theresa Schöttl for valuable scientific discussions and proof reading of this thesis.

I am deeply thankful to my parents for their love and unconditional support throughout every step of my life and hope that my achievements can be seen, even beyond the grave.

Last but definitely not least, I am more than thankful to my husband Stefan, who always encouraged and motivated me. Thank you for your unwavering love and being my tower of strength.

Publications and presentations

Publications:

Fischer, I.P., et al. *A history of obesity leaves an inflammatory fingerprint in liver and adipose tissue.* International Journal of Obesity (London) 2018 42, 507-517. DOI: 10.1038/ijo.2017.224

Schöttl, T.*, **Fischer, I.P.***. and Ussar, S. *Heterogeneity of adipose tissue in development and metabolic function.* Journal of Experimental Biology 2018, 221. DOI: 10.1242/jeb.162958

*Equal contribution

Oral presentation:

Fischer, I.P. et al. *A history of obesity leaves an inflammatory fingerprint in liver and adipose tissue,* ICEMED Final Joint Meeting, Leipzig Germany, November 7-8, 2017

Poster presentations:

Fischer, I.P., et al. *A guide to induction of diet-induced obesity (DIO) in male and female C57BL/6N mice*, ICEMED Midterm Evaluation, Garching November 17-18, 2015

Fischer, I.P., Irmler, M., Meyer, C.W. Tschöp, M.H., Ussar, S, Beckers, J. & Hofmann, S.M. *Depot-specific adipocyte plasticity after a history of diet-induced obesity,* Miami Winter Symposium 2017-DIABETS: today's research, tomorrow's therapies, January 22-25, 2017

Appendix

Title	PMID	Authors	Journal	IF> 10	strain	HFD	HFD company	fat (%kcal from fat)	Ctrl	Ctrl company	fat (%kcal from fat)	sex	age start (weeks)	duration feeding (days)
MicroRNA-33 regulates sterol regulatory element-binding protein 1 expression in mice.	24300912	Horie T, Nishino T, Baba O et al.	Nat Commun	y		D12451	Research Diets	45%	chow		4.5%	male		84
A closed-loop synthetic gene circuit for the treatment of diet-induced obesity in mice.	24281397	Rössger K, Charpin-El-Hamri G, Fussenegger M.	Nat Commun	y	C57BL/6J	D12492i	Research Diets	60%	D12450Bi	Research Diets	10%	female	14	
High-density lipoprotein maintains skeletal muscle function by modulating cellular respiration in mice.	24170386	Lehti M, Donelan E, Abplanalp W et al.	Circulation	y	C57BL/6J	D12330	Research Diets	58%	D12328	Research Diets	10.5%	male		84
Mitochondrial dynamics controlled by mitofusins regulate Agrp neuronal activity and diet-induced obesity.	24074868	Dietrich MO, Liu ZW, Horvath TL.	Cell	y		D12451	Research Diets	45%	no					105
Microbiome remodelling leads to inhibition of intestinal farnesoid X receptor signalling and decreased obesity.	24064762	Li F, Jiang C, Krausz KW et al.	Nat Commun	y	C57BL/6N		Bio Serv Frenchtown	60%	chow	NIH-31		both	6	119
Ecscr regulates insulin sensitivity and predisposition to obesity by modulating endothelial cell functions.	24022200	Akakabe Y, Koide M, Kitamura Y et al.	Nat Commun	y		HFD	Oriental Bio, Japan	60%	chow			both		98

K(ATP)-channel-dependent regulation of catecholaminergic neurons controls BAT sympathetic nerve activity and energy homeostasis.	24011078	Tovar S, Paeger L, Hess S et al.	Cell Metab	y		C1057	Altromin	55.2%	control diet	Harlan Teklad	12%		3	119
Hepatic menin recruits SIRT1 to control liver steatosis through histone deacetylation.	23867312	Cao Y, Xue Y, Xue L et al.	J Hepatol	y	C57BL/6J	HFD	Research Diets		chow				8	98
Tribbles 3 mediates endoplasmic reticulum stress-induced insulin resistance in skeletal muscle.	23695665	Koh HJ, Toyoda T, Didesch MM et al.	Nat Commun	y	C57BL/6J	D12492	Research Diets	60%	5020	Lab Diet	20%		6	56
Prolyl hydroxylase domain protein 2 plays a critical role in diet-induced obesity and glucose intolerance.	23630130	Matsuura H, Ichiki T, Inoue E et al.	Circulation	y		HFD 32	Clea Japan	60%					12	42
Endothelial mineralocorticoid receptor activation mediates endothelial dysfunction in diet-induced obesity.	23594590	Schäfer N, Lohmann C, Winnik S et al.	Eur Heart J	y	C57BL/6J	D07123 05	Research Diets	60%	normal diet D0712130 4	Research Diets	10%	male	6	98
Interferon regulatory factor 9 protects against hepatic insulin resistance and steatosis in male mice.	23471885	Wang XA, Zhang R, Jiang D et al.	Hepatology	y	C57BL/6	D12492	Research Diets	60%	D12450B	Research Diets	10%	male	8	182
Muscle lipogenesis balances insulin sensitivity and strength through calcium signaling.	23376793	Funai K, Song H, Yin L et al.	J Clin Invest	y	C57BL/6	TD 88137	Harlan Teklad	42.7%	4043	Purina		male	8	28

Central role of E3 ubiquitin ligase MG53 in insulin resistance and metabolic disorders.	23354051	Song R, Peng W, Zhang Y et al.	Nature	y		D12492	Research Diets	60%	chow	Academy Military Medical Sciences	11.4%	male	3	245
Leptin is key to peroxynitrite-mediated oxidative stress and Kupffer cell activation in experimental non-alcoholic steatohepatitis.	23207144	Chatterjee S, Ganini D, Tokar EJ et al.	J Hepatol	y	C57BL/6J	HFD		60%	chow		10%	male	6	70
Mouse KLF11 regulates hepatic lipid metabolism.	23183531	Zhang H, Chen Q, Yang M et al.	J Hepatol	y	C57BL/6	HFD	Research Diets	45%	normal diet	Lab Diet	9%	male	8	112
Weight-independent effects of roux-en-Y gastric bypass on glucose homeostasis via melanocortin-4 receptors in mice and humans.	23159449	Zechner JF, Mirshahi UL, Satapati S et al.	Gastroenterology	y	C57BL/6	D12492	Research Diets	60%	chow	Teklad Harlan		male	6	84-98
					C57BL/6	D12492	Research Diets	60%				male	8	8
					C57BL/6	D12492	Research Diets	60%				male	8	21
Pharmacological inhibition of adipocyte fatty acid binding protein alleviates both acute liver injury and non-alcoholic steatohepatitis in mice.	23108115	Hoo RL, Lee IP, Zhou M, Wong JY, Hui X, Xu A, Lam KS.	J Hepatol	y	C57BL/6J	D12079 B	Research Diets	41%				male	4	28
Divergent metabolic outcomes arising from targeted manipulation of the gut microbiota in diet-induced obesity.	22345653	Murphy EF, Cotter PD, Hogan A et al.	Gut	y	C57BL/6J	D12451	Research Diets	45%	D12450B	Research Diets	10%	male	7	140